NTNU
Innovation and Creativity

30 kW Power Boost System for Drive Trains for Electric Vehicles Based on Supercapacitor Technologies

Frode Lium

Master of Science in Energy and Environment
Submission date: June 2007
Supervisor: Tore Marvin Undeland, ELKRAFT

Norwegian University of Science and Technology
Department of Electrical Power Engineering

Problem Description

In electric and fuel cell vehicles there is a need to boost the battery power during fast changes in power demand.

The goal is to design, dimension and construct a power boost system for the drive trains in electric vehicles, by utilizing supercapacitor technology. The system should consist of a supercapacitor bank and a converter, and be designed for use in the new Think electric vehicle. Each part of the converter should be dimensioned according to information provided by Think Technology.

The master thesis will be limited to the design, dimensioning and construction of the power boost system, while the implementation, interfacing and control of power sharing will not been dealt with.

Assignment given: 15. January 2007
Supervisor: Tore Marvin Undeland, ELKRAFT

Preface

This master thesis is conducted in order to achieve a master degree in the field of energy and environmental engineering. On a personal level I have an interest in working with technology that can help the environment. In my studies I have specialised in electrical engineering, and the master thesis combines both my personal and educational interests, which has motivated me to work in this field.

The thesis is based on a preliminary project concerning the electrical behaviour of supercapacitors that was completed the fall, 2006. This project provided up to date information about automotive projects that utilizes supercapacitor technology around the world. The thesis is also a part of the Ph.D. project of Giuseppe Guidi. This project will be a part of his work and he will implement the power boost system in a commercial EV.

Several companies have supported this master thesis. The supercapacitor bank has been generously funded by Think Technology AS, Fuji electronic has supplied the IGBTs and EFD Induction has generously supplied the foil for the inductors. All other components have been funded by NTNU.

This master thesis report describes the design, dimensioning, construction and preliminary testing of a power boost system based on supercapacitor technology. A literature study has been performed in order to build an up to date system, and to get extensive knowledge about the converter topology. The electrical behaviour of the system has been thoroughly analysed in order to make an optimal system. In connection to this I want to urge anybody who intend to build a converter to start early with the selection and ordering of components, and keep in mind that spare parts might be necessary.

There are several persons that have helped me through this master thesis and I would like to give my thanks for their help and support. First, I would like to mention my supervisors at NTNU. Ph.D student Giuseppe Guidi has helped me a lot through all the stages of this thesis; His experience and knowledge has eased the workload considerably. Prof. Tore Undeland has also helped through this master thesis; His experience and connections has been vital for this master thesis to be possible. I also want to thank all my friends and co-students at the energy conversion group for their help through the stages of this master thesis. It has made my work easier.

Trondheim, 12.06.07 Frode Lium

Table of contents

Index of figures

Index of tables

Abstract

The goal of the master thesis is to design, dimension and construct a power boost system for the drive trains in electric vehicles, utilizing supercapacitor technology. In order to build the system a supercapacitor bank and a converter has been constructed. The system has been designed to be used in the new Think electric vehicle, and each part of the converter has been dimensioned according to information provided by Think Technology.

The master thesis is limited to the design and construction of the power boost system, and the implementation, interfacing and control of power sharing have not been dealt with. The supercapacitor bank and the converter are built based on analytical computations and simulations.

The supercapacitor bank can store up to 100 Wh and is built from 90 series connected cells rated 1500 F each. The bidirectional DC –DC converter is based on a standard intelligent power module with three legs in a bridge configuration and three inductors. An interleaved switching sequence is selected for the operation of the legs and each IGBT is capable of switching 150 A at 600 V. The thermal management of this module is solved with the use of a heat sink with fans for forced air flow. The inductors are made from amorphous alloys and copper foil, achieving an inductance of 0.25 mH and a maximum current rating of 100 A. Voltage smoothing capacitors and measuring devices have also been implemented in the converter design.

The results presented are held to be accurate, all though measurements gathered are affected to a certain degree by noise in the system.

Based on tests of the various components, it is concluded that the power boost system is an up to date system and has achieved the design goals of delivering 30 kW for 12 seconds. Some tests are yet to be completed in order to make sure that the system works in continuous operation.

Further work based on this master thesis should include more extensive testing on the system, and perform an optimization of the supercapacitor bank and the inductors. The intelligence for optimized load sharing must be created, and a communication interface with the power control unit in the Think electric vehicle must be made.

1 Introduction

The natural resources in the world are being consumed at a fast rate. These resources are mainly fossil fuels, which creates large amounts of pollution when exploited. This trend needs to be limited in order to achieve a sustainable development. The cars today are mainly powered by fossil fuels and it would be a large step in the right direction if a viable alternative was produced. However, EV and HEVs (electric and hybrid electric vehicles) are the only commercially available alternative to the ICE (Internal combustion engine) cars, and in terms of cost and performance the ICEs are the best option. Therefore, systems that can improve the performance and cost of the EV and HEVs should be researched. A large limitation for the EVs is the battery, because of the cost, maintenance needs and limited lifetime. The power demand profile for city driving is characterised by repeated acceleration and deceleration, which will deteriorate the battery, especially when the battery charge is low. Supercapacitors are well suited to handle such a power load. They have low losses, long lifetime and are maintenance free compared to the batteries. This makes it worthwhile to research a hybrid power system based on a combination of supercapacitors and batteries.

This master thesis will contribute to this research and the goal can be formulated as follows:

The master thesis aims to build a power boost system for a Think EV based on supercapacitor technology. The system will be constructed from a supercapacitor bank and a converter. These parts should be designed to achieve low weight and volume, high efficiency and good dependability.

The thesis will deal with the design, dimensioning, construction and preliminary testing of the power boost system and each part will be presented. The overall design and converter topology of the system is presented first. This is mostly based on a literature study, but it is also related to the dimensioning. The design of the supercapacitor bank has been limited to the dimensioning and construction for testing purposes. The bank will be rebuilt in order to fit into a car, when a car is available for testing.

The dimensioning part covers the sizing of the supercapacitor bank, dimensioning the inductors, switches and capacitors. The bank is dimensioned in order to operate in the acceleration time range, and limited to the maximum power handling of the power train. The dimensioning of the inductors, switches and capacitors are closely related and in order to be able to do a component selection, a thorough analysis of the electrical behaviour of the system has been completed.

The converter has been constructed and preliminary tests have been performed. The selection of components done in this part is dependant on the availability of them. A cost estimate for such a system is also presented, based on the components selection.

2 Literature Studies

This master thesis is based on a good understanding of power electronics and electric behaviour of different components. With this background it is possible to do a literature study of previous supercapacitor power systems and converters in general, which is vital in order to choose one that will be well suited for this application. A lot of research has been conducted in this field, and in order to build an up to date and functional system this research has been studied. The most relevant publications for this application are presented in this chapter.

Chapter 2.1 and 2.2
A Ph.D. thesis which deals with a power boost system based on supercapacitors was studied. This gave an idea about the challenges with such a project and will be presented first. The Think will be using a Zebra battery, and therefore a paper from the same author that deals with the combination of zebra batteries and supercapacitors will also be presented.

Chapter 2.3
The preliminary project about the supercapacitors electrical behaviour will be presented. This project provides a good understanding of how supercapacitors work and which properties that needs to be taken into consideration when utilizing them.

Chapter 2.4
A paper that shows the advantages of using converters in an interleaved manner is presented. This converter has been tested in real life applications and this ensures that this topology works at higher power levels.

Chapter 2.5
A paper that presents the effects and limits that are necessary to be aware of when constructing dc-dc converters with interleaved modules. Most papers dealing with interleaved converters for automotive applications are considering topologies for power ratings less than a few kW, intended for the electrical system in ordinary cars. Care must be taken when utilizing the results from these papers in a propulsion system with a lot higher power rating.

Chapter 2.6
A book that provides step – by – step orientation and design consideration for construction high frequency inductors are presented.

2.1 Ph.D. Thesis: Design, implementation and evaluation of an auxiliary energy system for electric vehicles, based in ultracapacitors and buck-boost converter

This Ph.D. deals with several of the tasks that will be addressed in this master thesis. The Ph.D. is divided into six parts:

1. Introduction
2. Static converter design and implementation
3. Monitoring and control system
4. Urban circuit tests
5. Results analysis
6. Conclusions

For this master thesis, chapter 1, 2 and 3 will be the most vital, but the other chapters will also be presented.

2.1.1 Introduction

The introduction deals with why there is a need for studies of electrical power trains, why supercapacitors are suitable as auxiliary energy devices and how they work.

The thesis states that there is a need for an auxiliary power supply in EVs and HEVs. For the EVs, this is due to the low specific power of the battery; therefore it needs to be dimensioned for power and not energy. For the HEVs, the engine needs to run steadily at its optimum power output, in order to increase efficiency and emissions. Therefore, the auxiliary energy supply should handle the fast changes in the power demand and contribute with regenerative braking, which is not possible with conventional ICEs. The electric and hybrid cars are not able to compete with conventional ICE cars in terms of performance and cost. This is due to the lower energy density of batteries compared to gasoline, and the need for complex gear or generator systems required on EVs and HEVs. “Therefore, all new technologies that could offer improvements in terms of cost, weight and power should be explored and tested by researchers.” The thesis continues with a description about how the supercapacitors work and compares them with other energy sources. This is described in the next chapter, and will not be displayed here. A literature study in the field of supercapacitors and applications before project start in 2002 is presented. The result of this study was that “by incorporating an ultracapacitor-based auxiliary energy system to EVs, in addition to battery life extension and a better acceleration response, overall increase in vehicle efficiency could be achieved if improvements where performed on static-converter design and energy-management algorithm structure.” This increase in efficiency is what the Ph.D. will prove for urban driving

conditions compared to an EV without a supercapacitor bank. The system consists of a 32 kW brushless DC traction motor, a 54 kW inverter, 26 lead-acid batteries connected in series with a voltage 356 Vdc, a 20 F, 300 Vdc, 200 A supercapacitor bank which is connected to the DC link through a 45 kW buck - boost converter with a 1.6 mH inductor. The control and monitoring system was designed using a DSP from Texas instruments.

2.1.2 Static converter design and implementation

The first element to consider when building a converter is the system in which it will be installed. It must be constructed in such a way that the original, where the addition of the converter do not force alterations in the original design. The supercapacitors are connected as shown in Figure 2.1. The reasons for this are:

1. The voltage on the DC – link is relatively constant compared to the supercapacitors, so in order to use most of the energy stored in the supercapacitors a voltage interface is required.
2. In order to test different power management strategies, control over the power flow and state of charge is necessary.
3. If no converter is applied the supercapacitor bank will only contribute power during transients and not for longer high power demands.

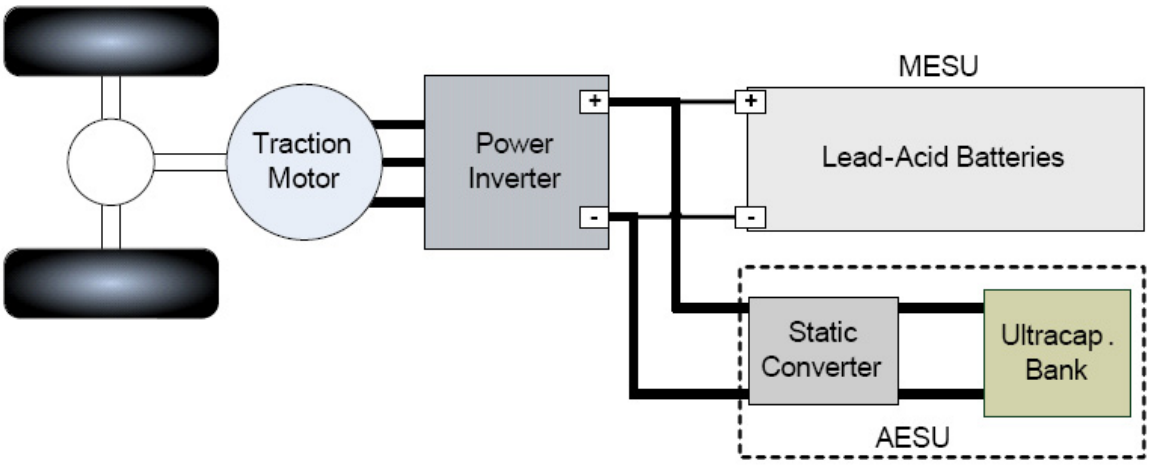

Figure 2.1: Static converter connection

The battery and supercapacitor bank should be dimensioned according to a driving pattern, but there are large variations in these, which makes the dimensioning difficult. In this case, a power profile obtained from experiments is used, with a mean power demand of 10 kW. Since the inverter is capable of handling 54 kW, a converter larger than 40 kW is desirable for the power boost system. The supercapacitor bank will be dimensioned for providing the energy needed to accelerate from 0 – 60 km/h, and to cover a hill climb of 30 m height. This plus

losses is the energy that the supercapacitor bank needs to be able to store and summarizes to 255 Wh.

The static converter is a bidirectional buck – boost converter and presented in Figure 2.2.

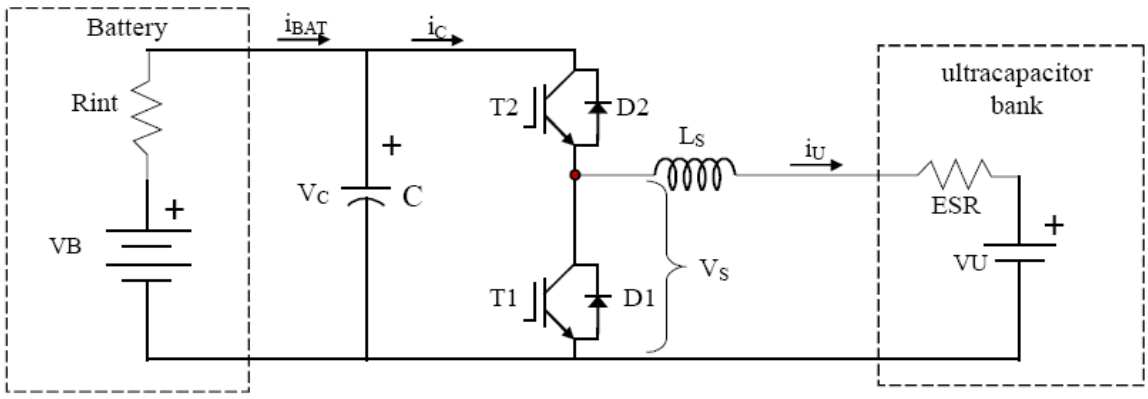

Figure 2.2: Buck - boost converter equivalent circuit

The converter is designed for delivering a peak power of 45 kW. At a DC link potential the current will be 150 A, therefore components rated 400 V and 200 A is used. The battery voltage is kept above 300 V with the AES – support, because the AES will supply the large currents necessary during high power demand periods. Therefore the voltage on the supercapacitor bank is limited to 295 V. The bank is built from 132 series connected 2700 F ultracapacitors form Epcos, with switched resistors as equalizing circuit.

To dimension the inductor shown in Figure 2.2, a maximum of 5 A was allowed. With a switching frequency of 12 kHz and a battery voltage of 360 V this will result in an inductance of 1.5 mH. An air core design was chosen in order to keep the inductance from saturation, and more turns were applied in order to compensate for the high reluctance. The windings were made from 0.5 mm thick laminated aluminium foil in order to cope with the skin effect. The result was a 22 kg, 1.6 mH inductance.

The capacitor is dimensioned to cope with voltage surges du to stray inductance and to filter the current from the converter. Because of good simulation results, a 3300 µF electrolytic capacitor was chosen.

The semiconductor device chosen in this Ph.D. was a 600 V, 400 A IGBT modules with an integrated gate drive and over-voltage protection. Completed with snubber circuits and safety features like fuses were implemented in the design.

Thermal conditions in the converter are analysed by means of an equivalent circuit, shown in Figure 2.3. This circuit contains both switches and both diodes, and it is from the junction of the switch/diode to the ambient.

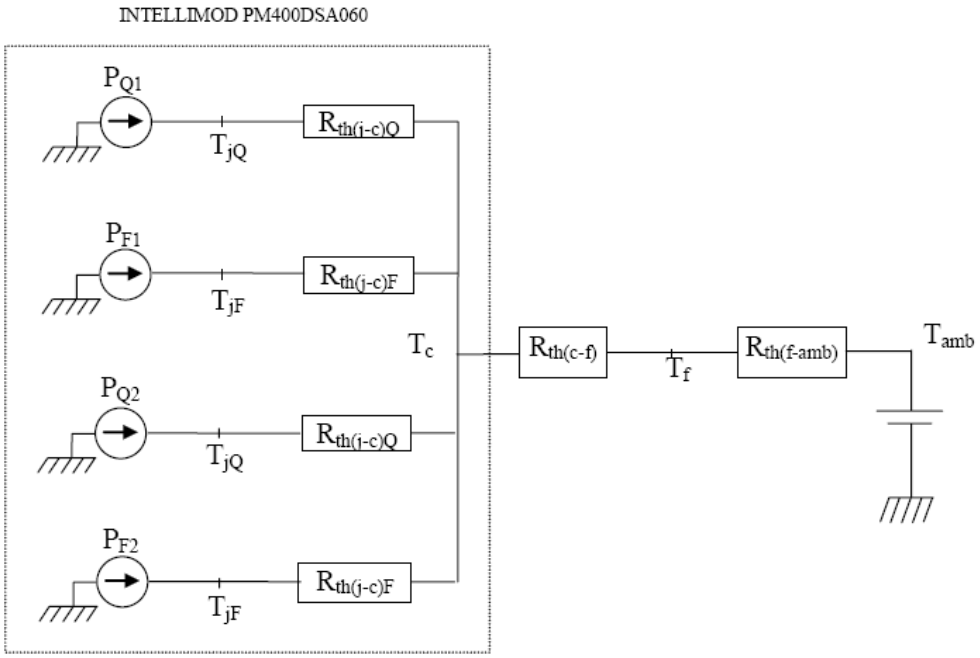

Figure 2.3: Thermal equivalent circuit

The heat produced origins from switching losses, reverse recovery losses and conduction losses. These losses are dependant on the current, voltage drop over the switches/diodes, the switching frequency and the duty cycle. The worst case scenario used in the calculations is a charge and discharge cycle with maximum current of 150 A every minute. Based on the fact that the duty cycle follows an almost linear path for the discharge and charge, an average duty cycle is found using interpolation. Equation (1.1) shows how the duty ratio changes during discharge.

$$D = 1 - \frac{V_{SC}}{V_{Batt}} \tag{1.1}$$

The calculations results in a heat sink with a thermal resistance of maximum 0.107 °C/W. Because no commercially available sufficient heat sink was found, one was made in a workshop. The heat sink was constructed with water cooling, and a thermal resistance of 0.01023 °C/W was achieved.

All this needed to fit into the car, and mounted in such way that the dependability was ensured. To achieve this, the whole static converter system was designed and tested in order to meet the highest standards.

2.1.3 Monitoring and control system

The Ph.D. presents two different control systems for the supercapacitor bank. Figure 2.4 presents the first system. In this case the supercapacitor bank state of charge is being determined by the speed and the battery state of charge. This is active when the power need is low, and the battery is able to charge the supercapacitors. The state of charge reference to the supercapacitor bank is based on the next most probable situation, i.e. deliver power at low speed and receive power at high speed. In high power demand situations a maximum battery current limit was established, and the supercapacitors supplied the remainder of the power need. The current limit was only active when the supercapacitors were charged.

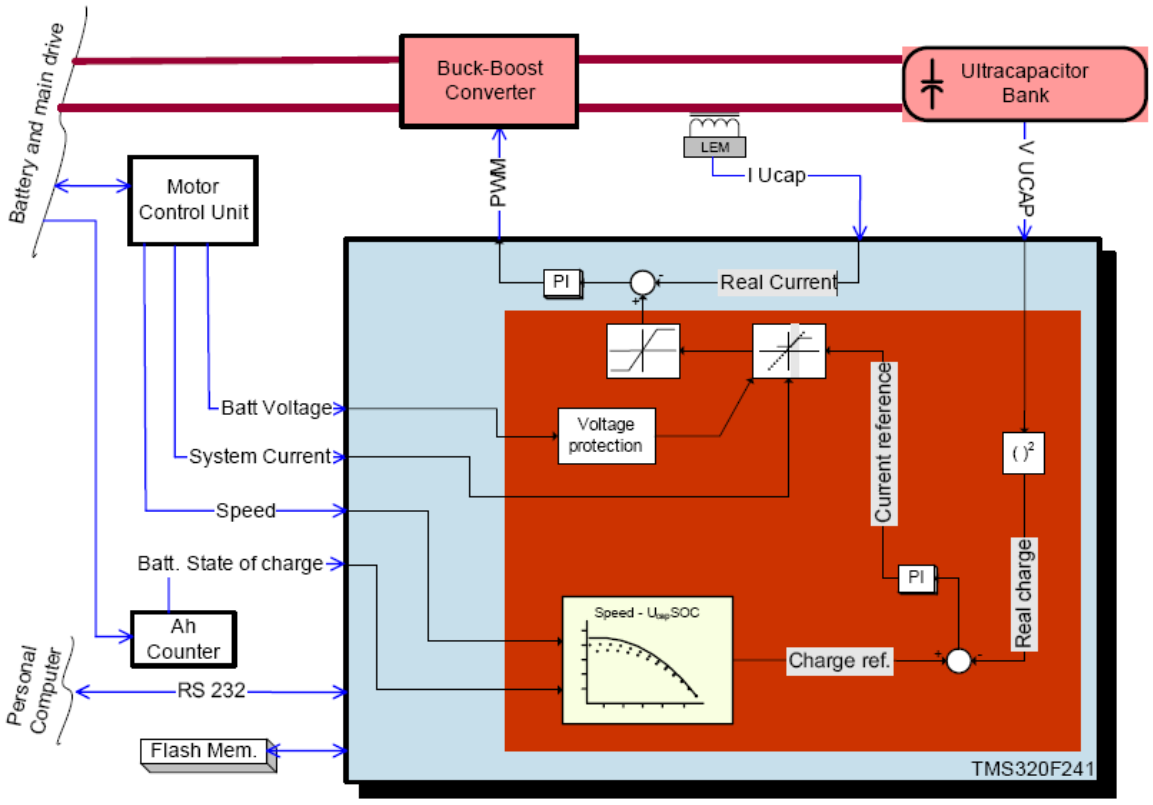

Figure 2.4: State of charge control algorithm

The second control algorithm presented is based on the training of a neural network. This neural network finds the optimal state of charge for different drive cycles. In order to get good results, ten power demand cycles was used to train the neural network, and 20 power demand cycles were used for validation. This system had a 5 % mean calculated efficiency increase compared to the state of charge control algorithm.

2.1.4 Urban circuit tests

In order to test this system, the Ph.D. uses an urban test course, presented in Figure 2.5, which is 14 km long, with a maximum speed of 60 km/h and a mean speed of 18 km/h. Most of the tests were performed measuring the total energy used, for the four different conditions;

Battery only
Battery with regenerative braking,
Auxiliary energy system using both algorithms

In addition to the energy, the speed, voltages, currents, power and state of charge was logged.

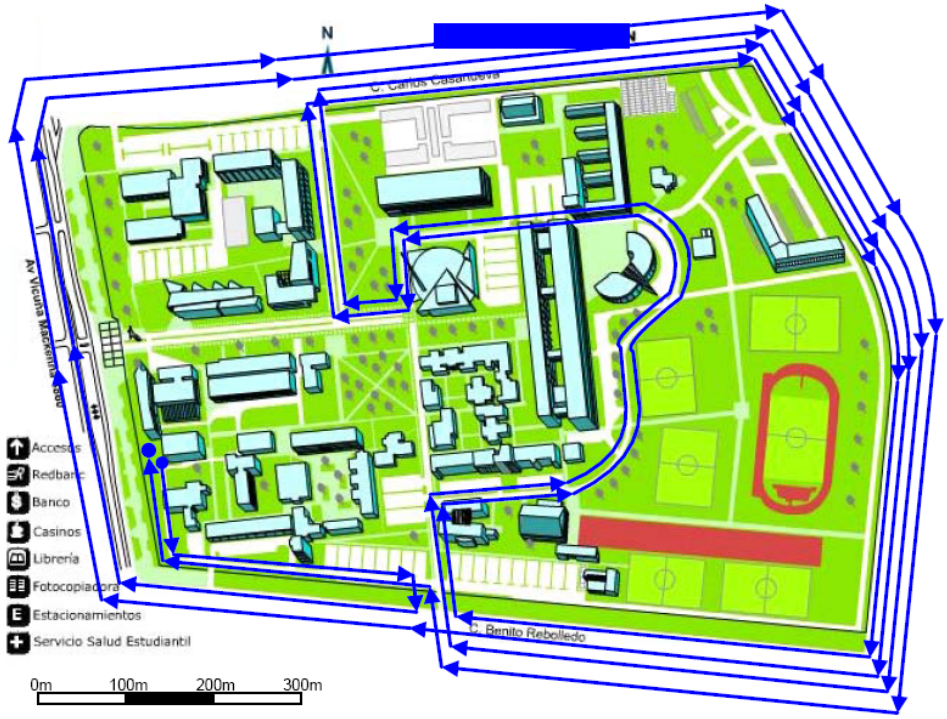

Figure 2.5: Urban circuit test course

The test results are presented in Table 1. The tests were conducted in one month, with simulated stops and slow driving parts in order to obtain fairly identical driving conditions.

Table 1: Urban test results

	Drive City Circuit (km)	kWh Used	Ah Used	km/kWh	km/kWh Improvement
Batteries without Regeneration	14.2	5.45	13.90	2.61	-
Batteries with Regeneration	14.2	4.61	11.23	3.09	-
Batteries with AES (SOC Control)	14.2	4.36	10.55	3.25	**5.2%**
Batteries with AES (Optimal Neural Network Control)	14.2	4.24	10.58	3.36	**8.9%**

2.1.5 Results analysis

This part of the Ph.D. introduces an economical analysis of the test results. The results are presented in Table 2. If the supercapacitors improve the lifetime of the batteries with more than 50 %, the supercapacitor bank is commercially viable, but if improvement is less, the increased performance of the vehicle must justify the supercapacitor bank.

Table 2: Economical cost comparison with batteries as energy source

Component	Batteries Only	Batteries (50%+) + Ucaps	Batteries (20%+) + Ucaps
Vehicle[1]	$ 8,000	$ 8,000	$ 8,000
Bateries[2]	$ 16,181	$ 11,595	$ 13,897
Ucaps[3] + static converter[4]	$ 0	$ 5,160	$ 5,160
Total cost of energy[5]	$ 3,288	$ 3,024	$ 3,024
Maintenance[6]	$ 2,856	$ 2,856	$ 2,856
Residual value[7]	-$ 450	-$ 724	-$ 578
PV of total costs[8]	$ 29,874	$ 29,910	$ 32,358
Total average cost ($/km)	**$ 0.191**	**$ 0.192**	**$ 0.207**
Cost change percentage	-	0.1%	8.3%

The trend in EV development covers the use of fuel cells. An economical comparison of fuel cells with supercapacitors and fuel cells with batteries is also conducted in this Ph.D., which are displayed in Table 3.

Table 3: Economical comparison with fuel cells as main energy source

Component	FuelCell Only	FuelCell + Batteries	FuelCell + Ucaps
Vehicle[1]	$ 8,000	$ 8,000	$ 8,000
Bateries[9]	$ 0	$ 5,706	$ 0
Fuel Cell[10]	$ 20,000	$ 4,000	$ 4,000
Ucaps[3] + static converter[4]	$ 0	$ 0	$ 5,160
Total cost of energy[5]	$ 3,670	$ 3,110	$ 2,960
Maintenance[6]	$ 2,856	$ 2,856	$ 2,856
Residual value[7]	-$ 238	-$ 238	-$ 238
PV of total costs[8]	$ 34,287	$ 23,433	$ 22,737
Total average cost ($/km)	**$ 0.220**	**$ 0.150**	**$ 0.146**
Cost change percentage	-	-31.7%	-33.7%

This shows that fuel cells applications gains most from the introduction of supercapacitors in EVs. In this case the yield was increased with 18 % using batteries and 24 % using supercapacitors. The drawback in these cases is that the vehicle cannot be used for sustained hill climb or high speeds, due to the reduced size of the fuel cell.

Micah E. Ortúzar, Design, implementation and evaluation of an auxiliary energy system for electric vehicles, based in ultracapacitors and buck-boost converter. Ph.D. Catholic University of Chile, 2005

2.2 Zebra plus ultracapacitors: A good match for energy efficient EVs

This paper presents many of the results described in the Ph.D., but replacing the lead – acid batteries with a zebra battery. Zebra batteries have high specific energy but low specific power, and a lot can be gained by building a hybrid of zebra batteries and supercapacitors. The zebra battery has a long lifetime with more than 1000 cycles, good efficiency and temperature stability and can be almost fully discharged. The battery operates at a temperature between 270 °C and 350 °C.

The paper provides a simulation of the EV during acceleration from 40 km/h to 60 km/h in 4 seconds at 80 % DOD (Depth Of Discharge). The behaviour of the system was almost identical at 10 % and 50 % DOD. The system is simulated with and without the supercapacitor – zebra hybrid solution. The current from the zebra battery is limited to 150 A without the supercapacitor system and 70 A with the supercapacitor system.

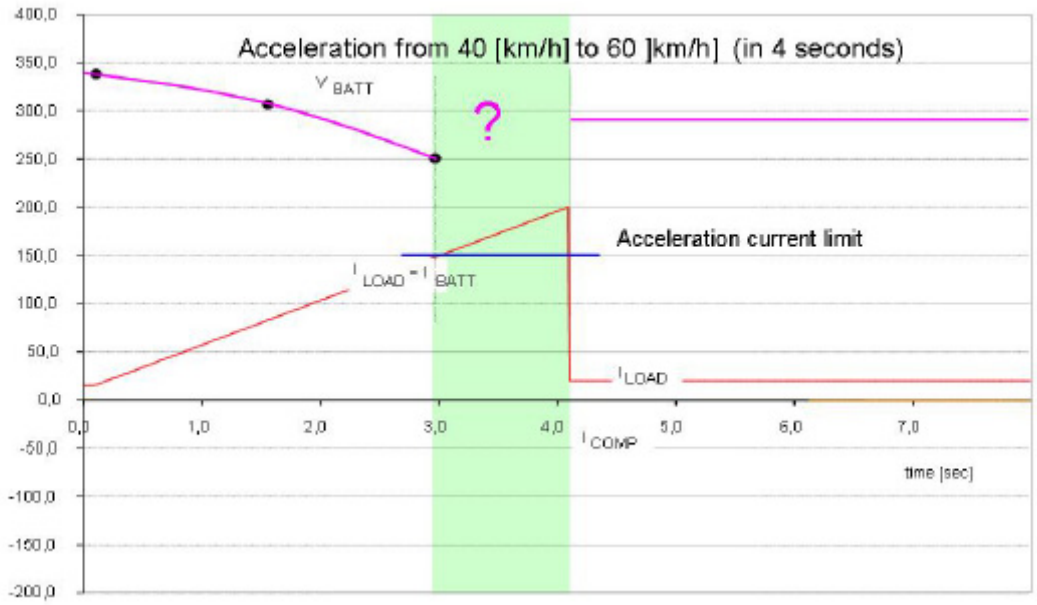

Figure 2.6: Acceleration simulation for a zebra battery

In the green area in Figure 2.6, there is no data from the voltage in this application, because at this point the converter stops due to low voltage alarm. The current needed for the acceleration is shown, but the vehicle will not be able to operate under these conditions.

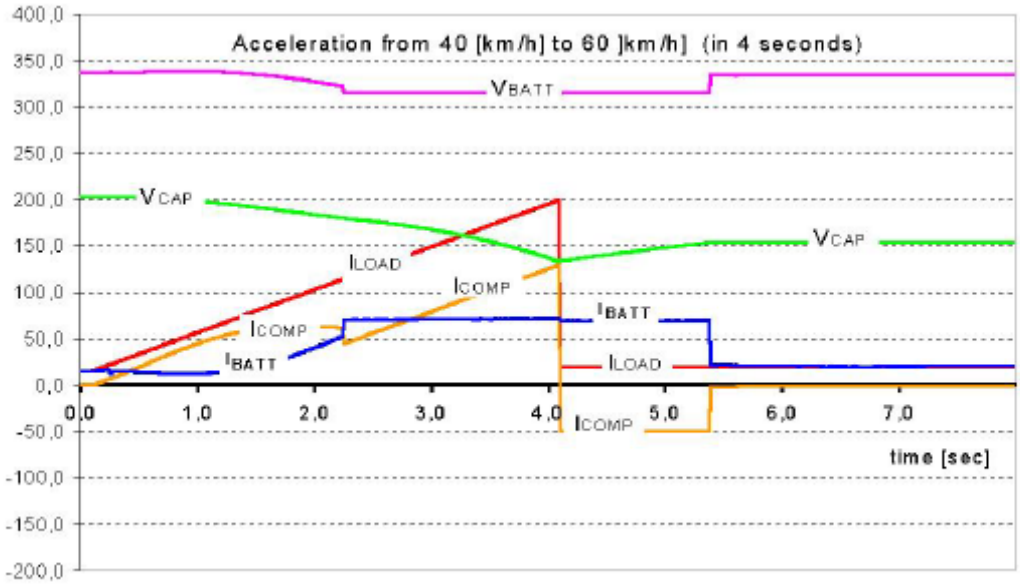

Figure 2.7: Acceleration simulation with zebra battery and supercapacitor bank

Figure 2.7 displays the system behaviour with the supercapacitor bank implemented in the system. In this case the DC – link voltage is fairly stable, with a small reduction due to the acceleration and a period with lower voltage due to recharging of the supercapacitor bank. However, this is only simulations, and results from real life testing with the EV, is yet to be presented.

Juan Dixon, Miach Ortúzar, Eduardo Arcos, Ian Nakashima, "*Zebra plus ultracapacitors: A good match for energy efficient EVs*",

2.3 Preliminary project to the master thesis: Supercapacitors as energy storage devices

This project [3] was conducted in order to acquire knowledge about supercapacitors, their behaviour and challenges using them. The required knowledge was gained from a literature study, attendance to the second European symposium on supercapacitors and applications several tests on supercapacitors were conducted.

2.3.6 Literature study

The electrochemical double layer, which is the basis of the supercapacitors, was discovered in 1853 by Helmholz. The first supercapacitors were produced in 1967, but the development progress has been slow, because few people believed that the supercapacitors had a future [4]. [4] The last ten years there have been substantial development of supercapacitors and applications that utilizes them. Supercapacitors are characterized high energy density and power density. A comparison between supercapacitors and other energy storage devices is presented in Figure 2.8. In terms of charging cycles, supercapacitors have a much better lifetime than batteries, capable of at least 500000 cycles.

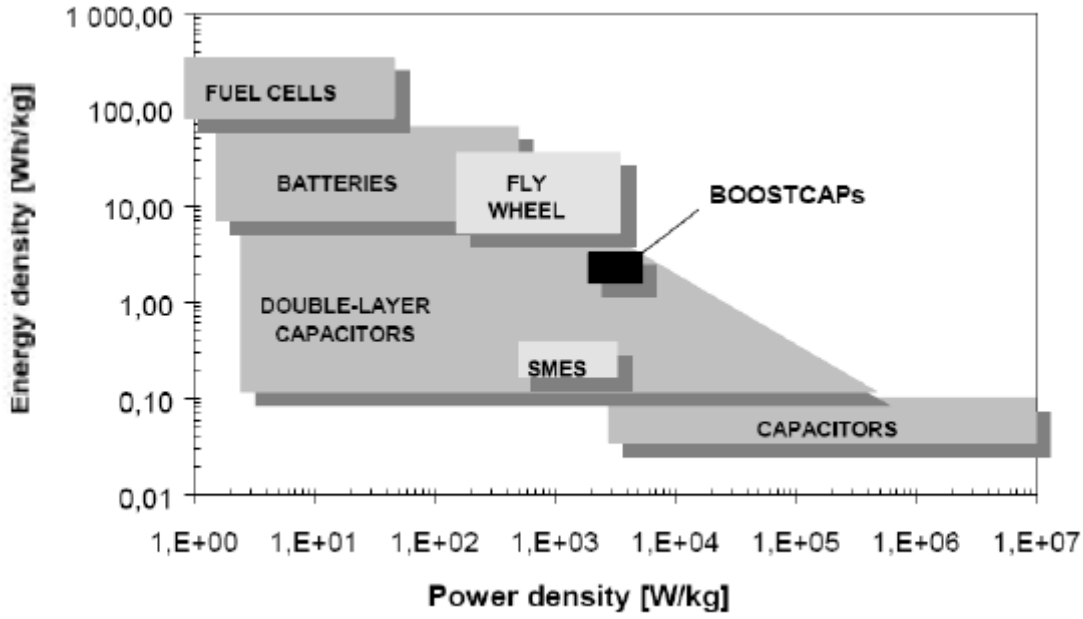

Figure 2.8: Energy and power density of various energy storage devices [4]

The electrochemical double layer, which gives the supercapacitors their unique characteristics, is a layer of electrons and ions that emerges between the electrolyte and the electrode. When a charge enters the electrode, it will pull on an ion in the electrolyte. Then there is a case of two charges separated by a non-conducting substance, which qualitatively describes a capacitor. The capacitance can be calculated with (1.2).

$$C=\frac{\varepsilon A}{\delta} \tag{1.2}$$

The δ is the distance between the charges, and is in the range of 10^{-10} m, and can be seen to the right in Figure 2.9.

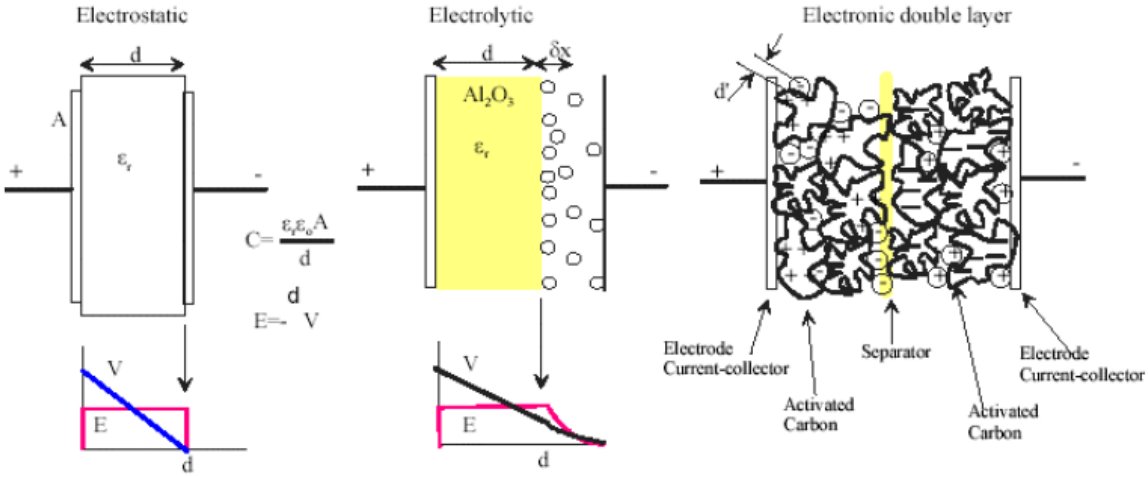

Figure 2.9: Supercapacitors compared to ordinary capacitor technology [5]

Another clue to the large capacitance of the supercapacitors is the area A of the electrode. The electrode is created by coating the current collector with a layer of activated carbon. The activated carbon has a surface area of between 1500 and 2500 m^2/g. A combination of these facts results in products with very high capacitance. Products in the range of 3000 F are commercially available.

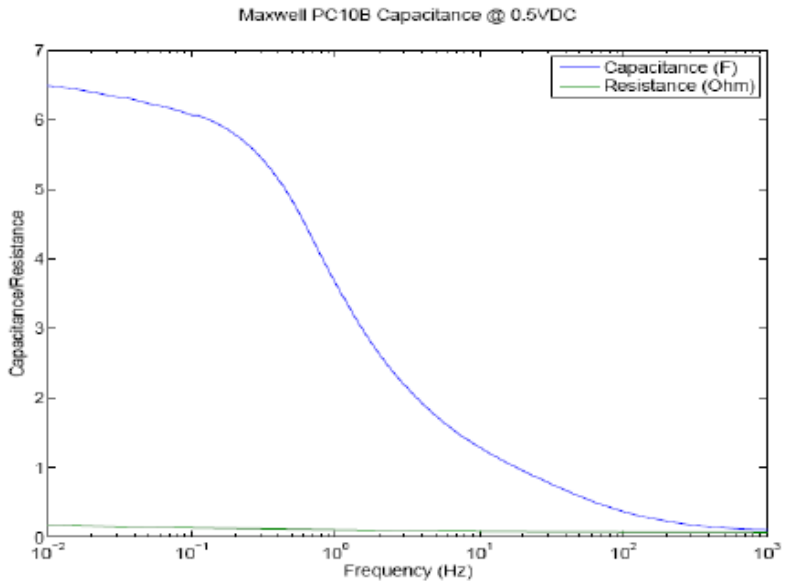

Figure 2.10: Capacitance dependence on frequency [6]

Figure 2.10 displays how the capacitance changes with frequency. This is a characteristic of the supercapacitor which makes them unusable for filtering purposes.

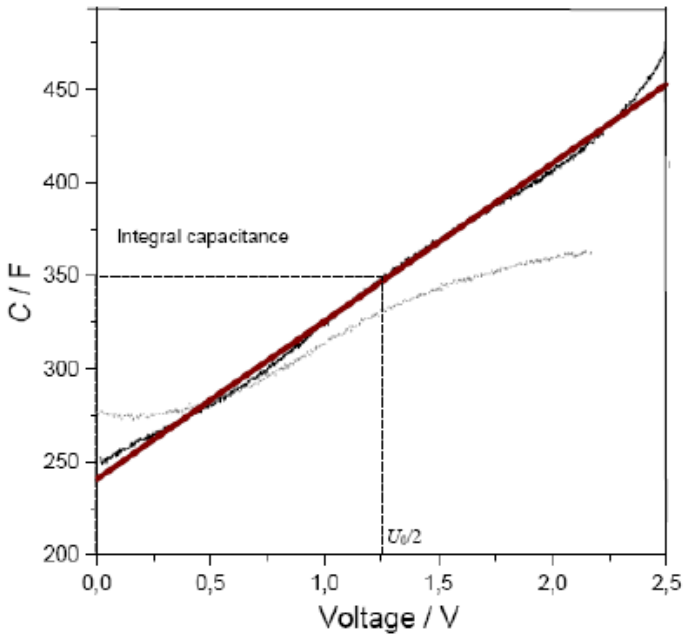

Figure 2.11: Capacitance dependence on voltage [7]

Figure 2.11 displays the change of capacitance due to voltage changes. The rated capacitance is measured at 2.7 V. If the supercapacitors are operated at a lower voltage level, a drop of capacitance must be expected.

Based on the unique characteristics of the supercapacitors, a lot of different models have been proposed. However if the characteristics mentioned above is kept in mind it is possible to work with a simple equivalent circuit, where only the ESR (Equivalent Series Resistance) and the EPR (Equivalent Parallel Resistance) is take into account.

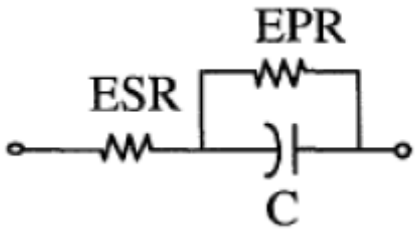

Figure 2.12: Equivalent supercapacitor circuit [8]

The main drawback of the supercapacitors is the limited voltage that they can be charged with. Due to the dissociation of the electrolyte the voltage is limited to about 3 V for organic electrolytes. Aqueous electrolytes has a maximum voltage of 1.23 V, typically 0.9 V. When higher voltages are applied the electrolyte will produce gasses, and this will substantially decrease the lifetime of the supercapacitor.

The supercapacitors needs to be series connected in order to increase the voltage. This is a challenge due to the tolerances in the supercapacitor, which is normally 20 %. This tolerance will result in an uneven distribution of the voltage, which can lead to over voltages. There are several ways of solving this problem. The most efficient and fastest solution is to connect a buck boost converter in parallel with each pair of supercapacitors as displayed in Figure 2.13. For N supercapacitors, N - 1 converters are needed. This topology can reach a global efficiency of 97 %, but is too complex to use when large supercapacitor banks are needed, because the cost of the converter will be substantial compared to the supercapacitor.

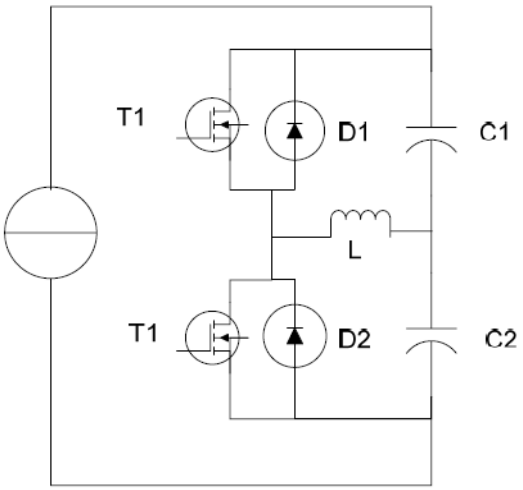

Figure 2.13: Converters in parallel topology [9]

The best solution for series connection of large numbers of capacitors is the switched resistor topology which is shown in Figure 2.14. This is a much simpler configuration and hence much cheaper. The efficiency of this circuit is less than the converter configuration, because it is based on power dissipation. In addition the circuit will not equalize the voltages as fast as the more complex topology, and care must be taken during the initial charging of the supercapacitors.

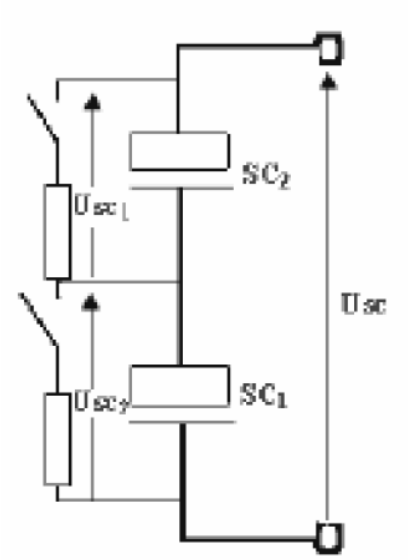

Figure 2.14: Switched resistor topology [10]

Utilizing a voltage equalization circuit will substantially increase the lifetime of the supercapacitors.

2.3.7 2nd European Symposium on Super Capacitors and Application

The project included attendance to the ESSCAP conference in Switzerland, and the most interesting of them are presented in the project report. The first paper introduced is: Hyheels [11], a project that intended to build several cars utilizing supercapacitors and fuel cells. It is a large EU funded project where several universities and companies are cooperating. The project has until now been concerned with supercapacitor technology and building a controller. They intend to implement the controller and supercapacitor bank in a commercial electric vehicle.

The second paper introduced is "Energy storage onboard railway vehicles" [12]. This paper shows a project done by Bombardier, about how an onboard supercapacitor bank decreases the energy demand of light railway vehicles, diesel electric railway vehicles and metros. In addition to decreased energy demand, the system reduces the peak power needed and makes the railway vehicles able to move up to 500 m without connection to the energy grid.

Table 4: Energy reduction with the Energy Saver [12]

		Metro 600 & 750V system		LRV Tram	Diesel Multiple Unit
		infrastructure coupled through	infrastructure not coupled through	Typically	typically
Energy split in System	Infrastructure Energy losses	15…20%	10…15%	5…10%	
	Regeneration	20…25%	10…15%	10…20%	
	Energy wasted in Brake Resistor	15…20%	20…30%	25…35%	30…45%
ES Savings	Infrast. Savings with Energy Saver	7…10%	5…8%	2…6%	
	Brake R Savings with Energy Saver	10…15%	15…25%	20…30%	27…40%
	Losses in Energy Saver	-3…-4%	-3…-4%	-4…-5%	-3…-5%
Savings with Energy Saver		**14…21%**	**17…29%**	**18…31%**	**24…35%**

Table 4 shows the energy saving possibilities using an energy saver. The energy is not only saved through regenerative braking, but also in the power lines, where the losses are greatly reduced.

The next presented paper from the ESSCAP conference is "Role and utilization of voltage balancing of EDLC stacks"[13]. It presents a simpler circuitry for balancing supercapacitors, than commonly used. The goal of this circuit is to reduce the price of the voltage balancing. The paper also addresses the necessity for a voltage balancing circuit.

The last paper presented is "Comparison of the Different Circuits Used for Balancing the Voltage of Supercapacitors: Studying Performance and Lifetime of Supercapacitors" [10] As the title states, the paper is concerned with the reason for and solution to the voltage balancing. Figure 2.15 displays a how the lifetime of supercapacitors decreases as a function of voltage and temperature. This is important to know when constructing systems that utilize supercapacitors.

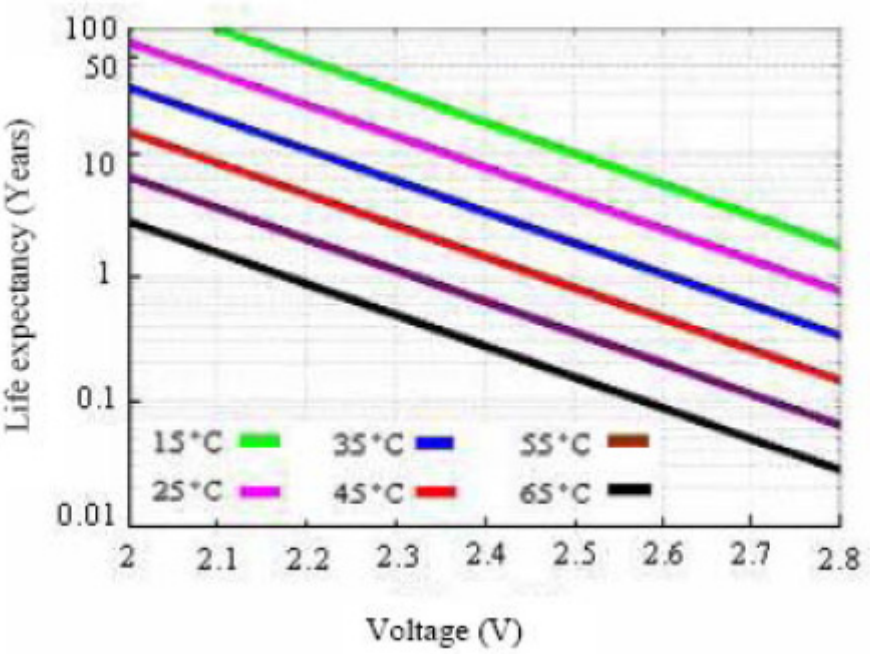

Figure 2.15: Lifetime of the supercapacitors as a function of temperature and voltage [10]

The paper also provides a good comparison of the different balancing circuits. The simulations are done with the assumption that the second capacitor has 20 % lower capacitance. The results are displayed in Table 5.

Table 5: Comparison of different voltage equalization circuits [10]

Balancing circuit	Without balancing circuits		Passive Balancing circuits with R=50Ω		Switched –resistor balancing circuits with R=1Ω		DC/DC converters balancing circuits	
Component	SC_1	SC_2	SC_1	SC_2	SC_1	SC_2	SC_1	SC_2
Average life expectancy (years)	17	1.4	37	3.5	16	6.0	6..2	6.0
Average life expectancy of module (years)	1.4		3.5		6.0		6.0	
η %	100	100	79	76	100	83		
η module %	100		77		91		93	

Notice that the switched resistor balancing circuit has only 2 % lower efficiency than the one utilizing DC/DC converters.

2.3.8 Lab tests and driver construction

A large part of this project was different lab tests. These tests gave a lot of knowledge about the electrical behaviour of the supercapacitors. Three tests were done. First a preliminary test was conducted in order to investigate the how the supercapacitors behaved during charging.

Based on voltage and current measurements the capacitance, ESR and shearing of voltage for two supercapacitors were determined. The test verified that the capacitance of the supercapacitors varied with the voltage.

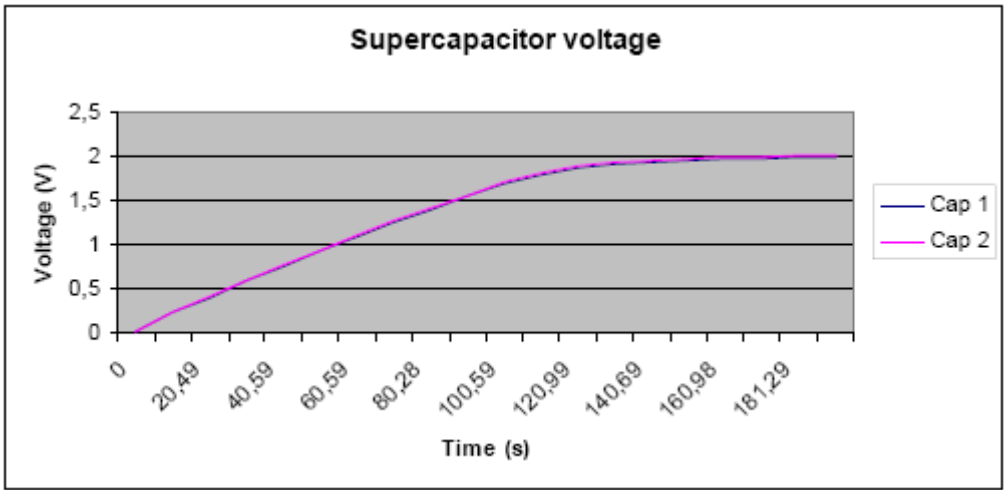

Figure 2.16: Charging of the supercapacitors

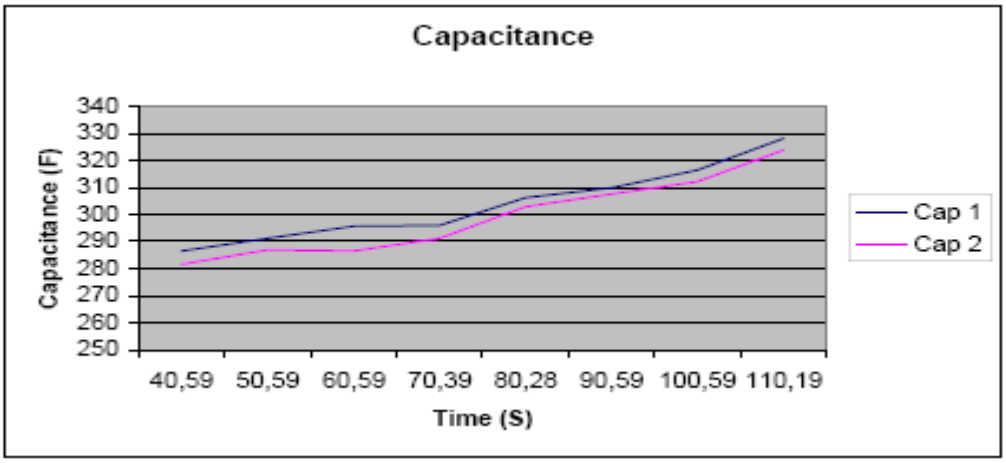

Figure 2.17: Capacitance and voltage during charging

Figure 2.17 displays how the capacitance changes through a charge cycle. Note that the capacitance was only calculated for the linear voltage increase.

A discharge test was also conducted in this project, in order to calculate the EPR, and a difference in EPR of 45 % was measured. Over time this can lead to serious over-voltages on the supercapacitors.

The second test investigated how resistors in parallel affected the performance of the supercapacitors. The first observation was that if the resistor used is large, it will not affect the charging/discharging of the supercapacitors much. This will keep the supercapacitors from getting over-voltages when they are kept charged, but will not prevent over-voltages due to tolerances in the capacitors. If the resistor is small (less than 1 Ω depending on the system),

the dynamics of the equalization circuit is fast enough to keep over-voltages from appearing. However, the losses in the resistors increase in inverse ratio with the size of the resistors, and for 1 Ω resistor the losses would be unacceptably high in almost any application.

The third laboratory experiment dealt with the construction of a mosfet driver for an active equalization circuit. The whole process of drawing, building and testing the circuit is described in the report. The test shows that the active equalization circuit is capable of equalizing the voltage much faster than the resistors in parallel.

Frode Lium, Supercapacitors as energy storage devices, project 2006

2.4 Control of Rubber Tyred Gantry Crane With Energy Storage Based on Supercapacitor Bank

This paper presents a solution for performance improvement of a gantry crane. It is not used for the same automotive application that this master thesis deals with, but it is a high power application that utilizes supercapacitors. In that effect it provides a useful converter topology that is useful in automotive applications.

The gantry crane in this paper is used to move large containers onto trucks. A system that lowers the fuel consumption and emissions from the crane is presented. The crane uses a diesel generator set to produce energy. The tasks performed by the crane are hoist up, move and hoist down. The average power need is a lot lower than the peak power need for such an application, thus a supercapacitor set can provide peak power shaving and the possibility for capturing energy during hoist down.

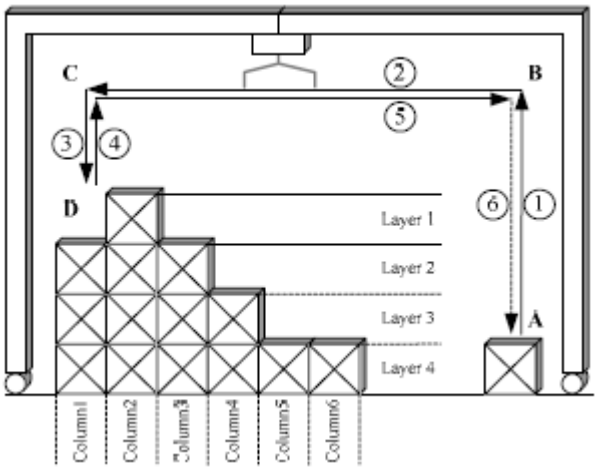

Figure 2.18: Operation of rubber tyred gantry crane

The maximum power and energy rating of this application is 290 kW and 3.4 MJ. Because of the power input from the generator set, the maximum needed energy from the supercapacitor bank is 2.9 MJ. The supercapacitors have a maximum voltage of 2.3 V and a minimum voltage of 0.76 V.

A prototype has been constructed with a supercapacitor bank which weighs about 400 kg. The supercapacitor bank covered the peak power demands from the system; the generator set needed only to provide the mean power and could be reduced to on third of the initial size. In order to use the supercapacitor bank a converter topology is proposed. A lot of different topologies can be used to build such a bidirectional dc – dc converter, but the paper decides on the topology shown in Figure 2.19.

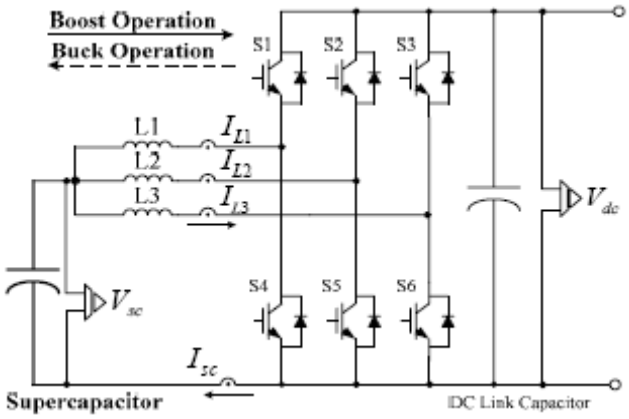

Figure 2.19: Gantry crane converter topology

The advantages with such a converter are numerous. Reduced size and ripple when operating in an interleaved manner, increased dependability and availability are factors which are touched upon.

Further in the article a control strategy for power sharing between the generator set and supercapacitor bank is proposed. The control has two loops. One loop is based on the frequency/power characteristics and the other is to obtain voltage control through regulating the field currents.

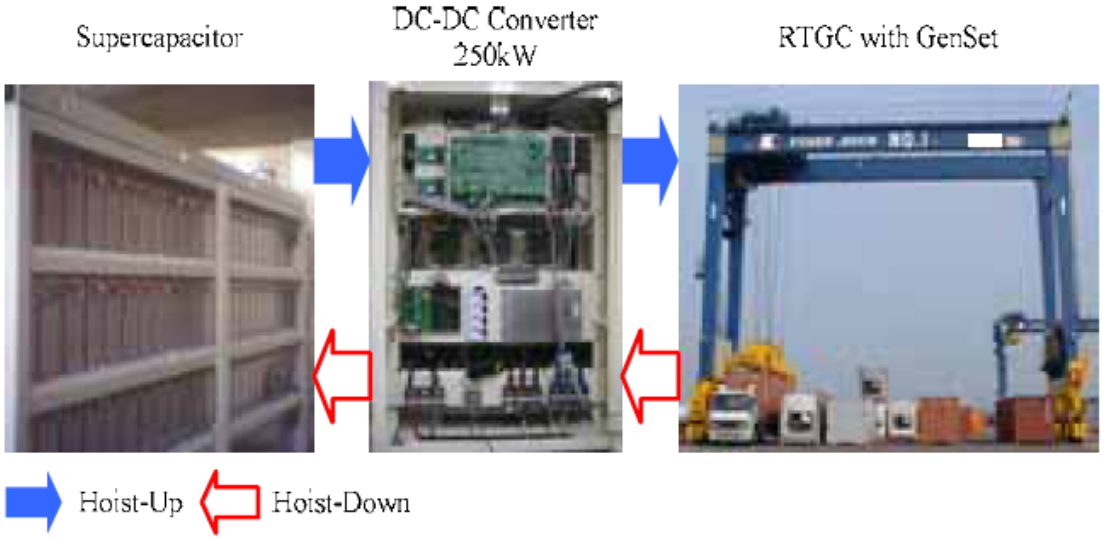

.

Figure 2.20: Supercapacitor gantry crane prototype

A prototype of the system has been constructed and tested The tests show more than 30 % decrease in fuel consumption and a 15 % decrease size compared to the original system.

Kim, Sang-Min, Sul, Seung-Ki, "*Control of rubber tyred gantry crane with energy storage based on supercapacitor bank",* IEEE Transactions on power electronics, vol. 21, No. 5, September 2006

2.5 Passive component analysis in interleaved buck converters

This paper displays how size and losses of passive components are reduced when utilizing interleaved converters. The converter they analyse is an interleaved buck converter 42/14 V with an output current of 100 A. The main question this paper intends to solve is: "How many phases is the optimum number for a given specification and what is the optimal inductance per phase?"

In order to analyse the inductors a program called PExprt made by Ansoft has been used. It has a library that contains several cores, materials and windings. In order to get higher resolution in the simulations, more cores have been added to the library by scaling commercial cores. The frequency they operate with are 100 kHz, the ripple current is 5 , 10 and 20 A and the average current is varied from 100 A to 100 mA.

Through analysis and experiments it is stated that for a given temperature the volume is proportional to the stored energy in the inductor.

$$Vol \propto \frac{1}{2} L i_{Max}^2 \tag{1.3}$$

When analysing this equation it can be shown that the minimum volume for given specifications is not dependant on the number of phases, if they work at their optimum operating point. Figure 2.21 shows this relation.

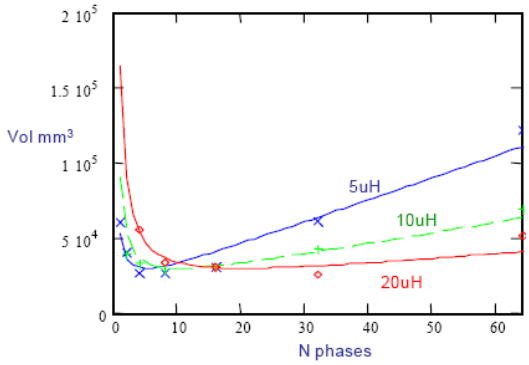

Figure 2.21: Volume per number of phases, calculated and actual

It should be noted that the volume increases linearly with the number of phases after a certain point. This is because the volume of the inductor is determined by the ripple and not the average current.

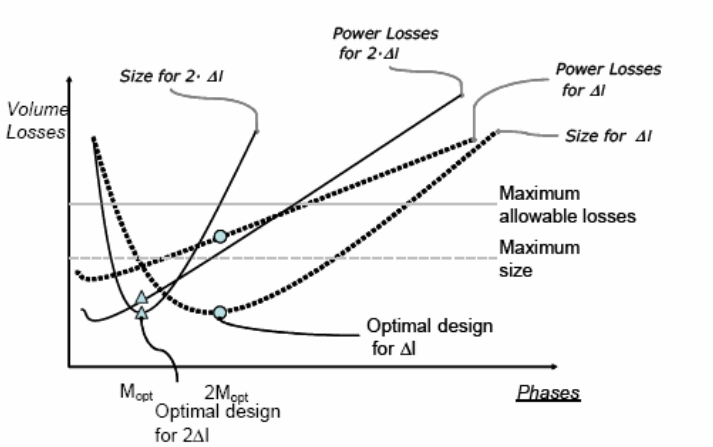

Figure 2.22: Two different inductors comparison

Figure 2.22 displays how the total losses and size of the converter for two different inductors are. If the converter is designed for low losses, the size of the inductors should be large and the number of phases should be low

The next chapter in the paper deals with the capacitance. Analyses are performed and they show that when the number of phases is increased, the ripple is reduced according to equation(1.4).

$$\Delta V_{out} = \frac{\Delta I_{1ph}}{C * M} * Fc(M) * (\frac{1}{8Fs} + M * C * R_{ESR}) \tag{1.4}$$

Fc is the cancellation factor of the output current ripple calculated from Figure 2.23.

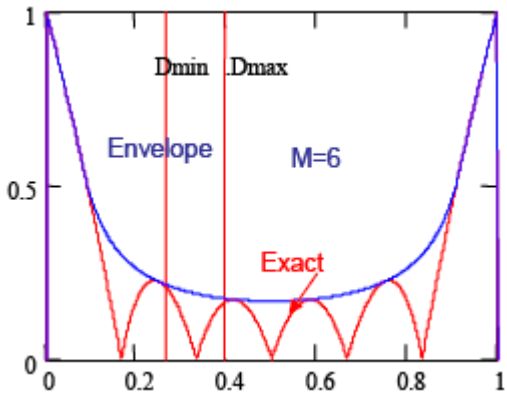

Figure 2.23: Cancellation factor for the ripple current

From this equation it is easy to see that the capacitance can be reduced by increasing the number of phases. If enough phases are added, a change in capacitor technology is possible, thus decreasing the losses in capacitor substantially.

Interleaving has advantages regarding EMI filtering. Under ideal conditions the current ripple is cancelled out, except for the multiples of the number of phases. If 6 phases are used at 100 kHz, all harmonics up to 500 kHz are cancelled and the first harmonics appears at 600 kHz.

The paper presents an output filter optimization next, by regarding the L*C product. This optimization shows how much the capacitance is reduced when adding phases. It also considers the load current step response of the converter. However, this optimization is severely affected by tolerances in the inductors.

The tolerances in the inductors will produce harmonics at the switching frequency that needs to be filtered by the output capacitor. The paper presents an equation for obtaining the number of phases that can be used before the harmonics generated by the tolerances are larger then the ripple caused by the converter if the inductors were equal. The model is based on the case that all but one has the same inductance. The equation is presented in (1.5).

$$M=\frac{1}{2}\sqrt{\frac{1}{D(1-D)}*\frac{100}{\Delta L_{ph}(\%)}} \tag{1.5}$$

For this application, where the duty cycle is 33 % and using a 5 % tolerance in the inductor, the number of phases where ripple cancellation is no longer effective is 4. The paper also suggest solutions where the applications demand that the output voltage changes.

J. A. Oliver, P. Zumel, O. García, J.A. Cobos, J. Uceda, *"Passive component analysis in interleaved buck converters"*, Applied Power Electronics Conference and Exposition, 2004

2.6 Magnetic core selection for transformers and inductors

This book is written by Colonel Wm. T. McLyman for aerospace applications. It is written in 1982, but still it gives a lot of valuable information about designing inductors and transformers. It is meant to complement another book called transformer and inductor design handbook, by collecting data from various manufacturers and present them in this book. That way the engineer can evaluate the configuration with a standard unit of measurement. This book starts by explaining all the symbols used in inductor and transformer design, with their notation. Next all the equations needed for specification are listed. This is very useful in order to quickly go through the steps of inductor and transformer design.

The book then gives a scientific approach to the general challenges of transformer and inductor design. Since transformer design is not a part of this master thesis, the focus will be on the inductor part. The design of a linear dc reactor is dependant on four conditions given by the system:

1. Desired inductance
2. Direct current
3. Alternating current
4. Power loss and temperature rise

These values the designer needs to know before the design of inductor can be conducted. Following, the book explains how to use the different equations and what simplifications that is possible to make. This part is written in such a way that the designer can do the design following the book step-by-step.

In the next chapters the book presents several design examples for both transformers and inductors. These design examples consider different techniques for approaching the design problem. The examples also show how different converter topologies affect the inductor design.

The next chapter address the trade offs regarding cores, and core loss considerations. The rest of the book is basically tables of different core properties. This information is outdated and new data must be gathered by the designer.

Colonel Wm. T. McLyman, *Magnetic core selection for transformers and inductors*, Marcel Dekker, Inc, 1982

3 Supercapacitor Bank

3.1 Dimensioning the supercapacitor bank

The goal of the supercapacitor bank is to improve the performance of the vehicle, by providing an energy storage that supplies a power boost with low losses and no maintenance. The first step towards constructing a supercapacitor bank is to establish the voltage level of the DC – link and the maximum power the car can operate with.

From the technical specifications provided by Think [17] , the DC – link data can be shown:

Voltage level: 278 V
Maximum power: 30 kW

The operating voltage of the Zebra battery decreases with increasing power demand and with battery SOC [18]. The supercapacitor bank should therefore be dimensioned to a lower voltage than the nominal battery voltage. The minimum voltage of the battery is 186 V, but this happens only when the battery is supplying a large current.

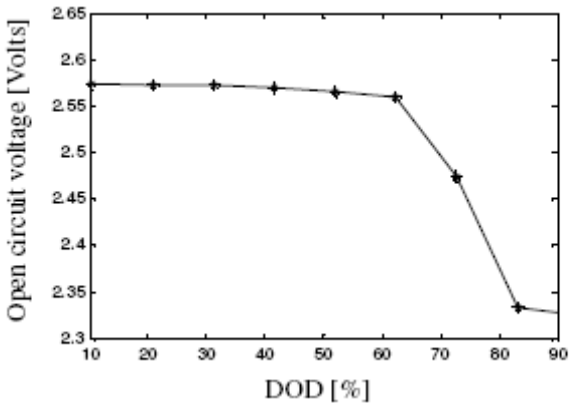

Figure 3.1: Estimated open loop voltage at 295 °C [18]

For acceleration purposes, the supercapacitors will provide the current and the battery will operate at the nominal voltage. For dimensioning purposes the voltage has been selected to be 240 V, as an estimate of the minimum battery voltage with the power boost attached. This voltage can be altered at a later stage, by adding or removing supercapacitors. A more optimized voltage can be found when the battery is available for testing. In order to achieve this voltage, 89 supercapacitors need to be put in series connection. In order to fulfil the power demand, the supercapacitors must be able to provide currents in the range of 125 A @ 240 V (fully charged) and 250 A @ 120 V (completely discharged). The discharge of the supercapacitors is limited to 50 % of the rated voltage [19]. This is in order to limit the VA ratings of the converter and also to avoid excessive losses in the SC due to high discharge

current. 75 % of the total energy stored in the supercapacitor bank will still be available to the DC-link.

The next step is to establish the energy needs during acceleration, which the supercapacitor bank must supply. The supercapacitor bank will work as a peak power assist, therefore the demand will be in the seconds range. The energy stored in the supercapacitors can be calculated with equation(2.1).

$$E = \frac{CV^2}{2} \tag{2.1}$$

Depending on the capacitance, the supercapacitors are able to deliver full power for a limited time span. The time can be calculated by: t = Energy / Power. Four possible products are shown in the table below:

Table 6: Energy available in the supercapacitor bank

Capacitance	Seconds capable of delivering full power
650 F	5.2 s
1200 F	9.7 s
1500 F	12.1 s
2000 F	17.7 s

The car is able to accelerate from 0 – 50 km/h in 6.5 s and 0 – 80 in 16 seconds. The supercapacitor bank should be dimensioned to be able to provide power for acceleration times in that range. Using data from Table 6, the 1500 F alternative or the 1200 F is the best alternatives. However, the 1200 series is going out of production, leaving the 1500 F supercapacitors as the best choice.

3.2 Designing the supercapacitor bank

3.2.1 Series connecting supercapacitors

There are several problems that needs to be addressed when series connecting supercapacitors. The main problem is the voltage balancing between the cells, because of differences between each supercapacitor. They are given with a +20 % tolerance, i.e. the capacitance is between 1500 F and 1800 F. [20] The voltage will not be distributed evenly over the whole bank and could destroy the cells after some time. Another problem is

connected to the EPR (equivalent parallel resistance) of the supercapacitors. If the supercapacitor bank is kept charged for longer periods of time, the voltage will divide itself according to the EPR. This can lead to over-voltages and destruction of the cells. Because of these problems, voltage balancing circuits must be implemented between the supercapacitors. Maxwell provides implementation kits where this voltage balancing is included. The voltage balancing does not require any external power source or control [21].

3.2.2 Capacitors or modules

There are two possibilities to realize the supercapacitor bank. First alternative is to build it from scratch with single capacitors. The second alternative is to utilize modules to construct it.

A few advantages connected to the single supercapacitor solution can be identified. The most important one is the cost. It is cheaper to build the power boost from supercapacitors than from modules. Capacitors are also more flexible in terms of shaping the supercapacitor bank, and obtaining the needed power, voltage and energy. A disadvantage is that the voltage over each capacitor needs to be controlled, or the bank must be oversized. This control circuit can be bought as a part of an implementation kit, but these adds to the cost. The advantages concerning modules are that the voltage equalizing system is integrated. The modules are also easier to operate, and less work needs to be put into the design of the bank. The modules come in aluminium cases, equipped monitoring systems for voltage and temperature.

Because of the reduced price, and good availability of the single capacitors these were selected for the bank.

3.2.3 Building the supercapacitor bank

The final design of the supercapacitor bank needs to be built in a form that will fit in to the available space inside the Think. The supercapacitor bank will have a volume of approximately 30 L. The space occupied by it will be larger, because of empty space between the supercapacitors. There must also be space available for cooling equipment and the converter. Two areas are suggested by Think, and there should be enough space in both of them.

Behind the battery within the battery tray:
- Height: 319 mm
- Width: 997.5 mm
- Length: 234 mm

Total volume: 74.46 L. All of this space is not available. There are some brackets holding the battery which are taking up some space.

Between the battery tray and the rear bumper:
- Height: 290 mm
- Width: 997 mm
- Length: 663 mm
Total volume: 191.69 L.

The final design will be completed when the car is provided, but then it is much easier to build a casing which will fit into the car. For preliminary testing the supercapacitor bank will be placed in a cabinet, which makes it easy and safe to test and control the bank.

3.3 Potential dangers concerning supercapacitors in automotive applications

Supercapacitors are generally very safe and stable components. However, situations can arise where they present a possible danger. There are three main scenarios to consider:

1. Short circuit of the supercapacitor bank
2. Rupture of the supercapacitor can
3. Scenario 1 and 2 simultaneously

3.3.4 Short circuit of the supercapacitor bank

The supercapacitors have a short circuit capacity of 3900 A each. With a voltage of 240 V, this amounts to 936 kW. With the energy stored in the supercapacitors this situation can last for 0.52 seconds. This can be harmful for human beings and equipment; therefore a circuit breaker must be implemented in the circuit in order to reduce the consequences of a short circuit. The supercapacitor bank must be built in such a way that the chances of a short circuit are as low as possible.

3.3.5 Rupture of the supercapacitor can

Supercapacitors are normally built into cans that can withstand 12 bars. However, it can rupture due to over voltages (Figure 3.2), over heating or mechanical stress.

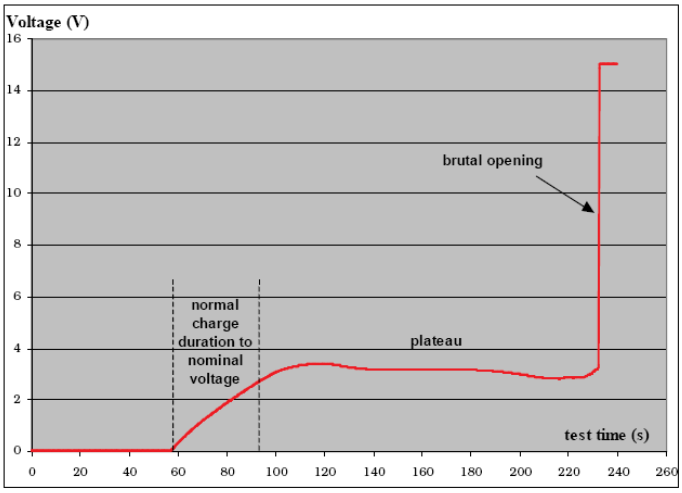

Figure 3.2: Effects of over-voltages on supercapacitors [22]

When the supercapacitors rupture because of over-temperatures or over-voltages, it is due to increased internal pressure. Most supercapacitors are therefore equipped with a valve in order to prevent explosions. However, a blow type flame can emerge under such conditions and must be taken into account by the designer [22]. If a can ruptures because of external mechanical stress, normally no explosion or blow type flame will occur. If a can is ruptured due to mechanical stress, some of the electrolyte can escape the cell, but most of if is absorbed in the cell. The electrolyte consists of organic liquid and is characterised as ignitable, and represents a potential fire hazard.

3.3.6 Short circuit due to ruptured cans

A dangerous situation and possible fire can occur when two supercapacitors in a supercapacitor bank are ruptured. This was discovered during a test drive with an EV with a supercapacitor bank in Chile, where a fire occurred in the bank. The two ruptures lead to a short circuit between supercapacitor number 9 and 78 in the supercapacitor bank, which discharged the supercapacitors in between [23].

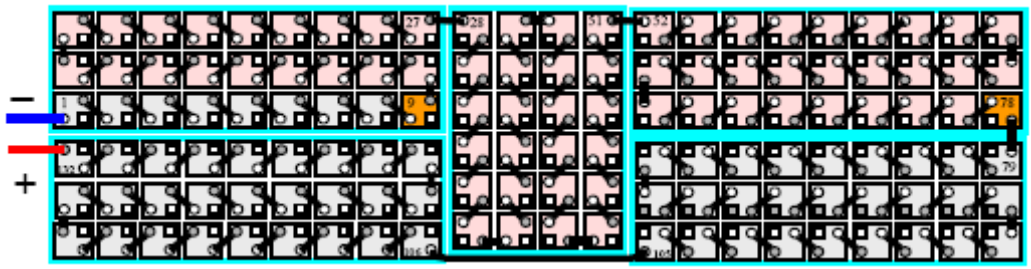

Figure 3.3: Supercapacitor bank showing ruptured and discharged elements [23]

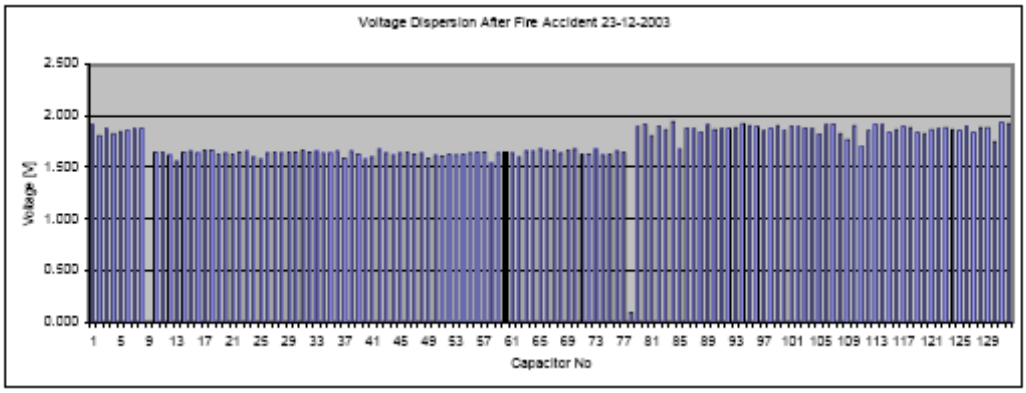

Figure 3.4: Voltage distribution of the supercapacitors after the fire [23]

Figure 3.3 and Figure 3.4 displays clearly how the ruptured cans has no energy stored and the ones in between has reduced voltage. The supercapacitors ruptured because of mechanical stress origination from aluminium bolts in the casing. The discharge of the almost 70 supercapacitors in between created a spark discharge from the electrolyte to the casing, and ignited it. This shows that the designer of supercapacitor banks needs to be careful when designing the casing.

4 Converter

When a supercapacitor bank is connected directly in parallel with a battery, there will be a natural sharing of the load. The supercapacitor will always be charged to the battery voltage, and due to the larger power handling capability of the supercapacitor, the voltage will be more stable. The down side to this direct connection to the DC link is that only a part of the potential of the supercapacitors is used. In order to fully exploit the potential of the supercapacitor a converter must be placed between the supercapacitor and the DC link.

4.1 System identification

The components in the converter must be dimensioned according to the parameters of the surrounding system. Some of the necessary data is presented in Table 7.

Table 7: System parameters [17]

Parameter	Value
Battery voltage, max (VDC)	278
Battery voltage, min (VDC)	186
Supercapacitor voltage, max (VDC)	240
Supercapacitor voltage, min (VDC)	120
Maximum power (kW)	30

The supercapacitor maximum voltage is based on the Zebra battery profile. The open circuit voltage from the battery is 278 V, but during operation the voltage will be reduced. The battery voltage should not decrease to the minimum value when the power boost system is connected to the DC – link. The largest currents will occur during acceleration, and these will be handled by the supercapacitor. Therefore, the battery voltage should be stable at a relatively high voltage. The maximum voltage of the supercapacitor bank is chosen in order to keep the supercapacitor voltage stays below the battery voltage. When the battery is available for testing a more optimal size for the supercapacitor bank and a better profile of the battery can be obtained.

4.2 Converter topology

The converter must be able to charge and discharge the supercapacitor bank. Hence, a bidirectional dc-dc converter is necessary. There are many different solutions that can be used for this purpose, and a lot of literature is available on the subject. The converter will be used in an EV, and properties like weight, volume and dependability are essential to the design. A converter that has several legs for carrying the current has shown promising advantages [14]. First, the current is distributed over several converter legs, thus reducing the current handling demands for the switches and inductors, and reduces the ohmic conductive losses. Second, the converter legs can be used in an interleaved manner, which will reduce the ripple on the supercapacitors, which allows for smaller inductors. This relation is displayed in Figure 4.2 , with different number of legs. Third, since the converter is built from several independent legs, it can still operate if one leg fails. This will improve the dependability of the EV. Fourth, the weight will be in the same range as the ordinary buck-boost converter or less, dependant on the current profile and available inductors. Modules with 2, 4 or 6 integrated switches are commercially available, and special design is not necessary. The converter topology with three legs is shown in Figure 4.1 [14].

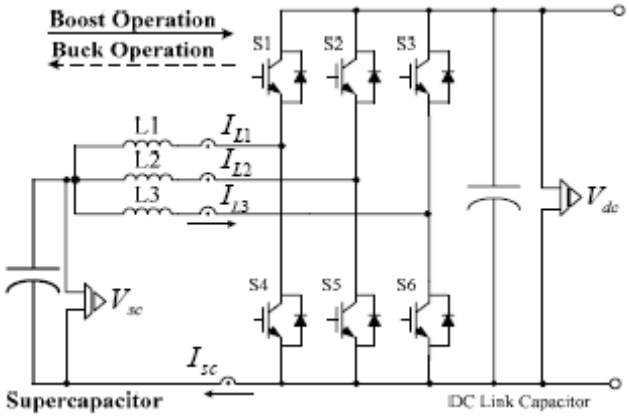

Figure 4.1: Three legged converter [14]

In order to optimize the number of legs, it is necessary to analyse the ripple currents in the converter. This is important in for the dimensioning of the inductors and the capacitors in the system. The ripple current will also contribute a lot of losses, which should be minimized.

The ripple current in each inductor is calculated using (3.1).

$$\Delta i_L = \frac{VscT_s D}{2L} \tag{3.1}$$

The peak to peak values of the ripple current in the supercapacitor bank is given by the equations below:

$$\Delta i_{sc,1converter} = 2\Delta i_L \tag{3.2}$$

$$\Delta i_{SC,2converters} = \Delta i_L * (2 - \frac{1}{1-D}) \tag{3.3}$$

$$\Delta i_{sc,3converters,D<0.33} = (3\Delta i_L - \frac{2\Delta i_L}{1-D}) \tag{3.4}$$

$$\Delta i_{sc,3converters,D>0.33} = \Delta i_L (1 - \frac{2}{3(1-D)} + \frac{2(D-1/3)}{D}) \tag{3.5}$$

$$\Delta i_{SC,4converters,D<0.25} = \Delta i_L * (4 - \frac{3}{1-D}) \tag{3.6}$$

$$\Delta i_{SC,4converters,D>0.25} = \Delta i_L * (4 - \frac{3}{2(1-D)} - \frac{1}{2D}) \tag{3.7}$$

These equations are derived by adding the triangular ripple currents, phase shifted by Ts/N where N is the number of converters. This is done for N between 1 and 4 in order to show the ripple behaviour. A more extensive general derivation of this relation is given in the literature [24].

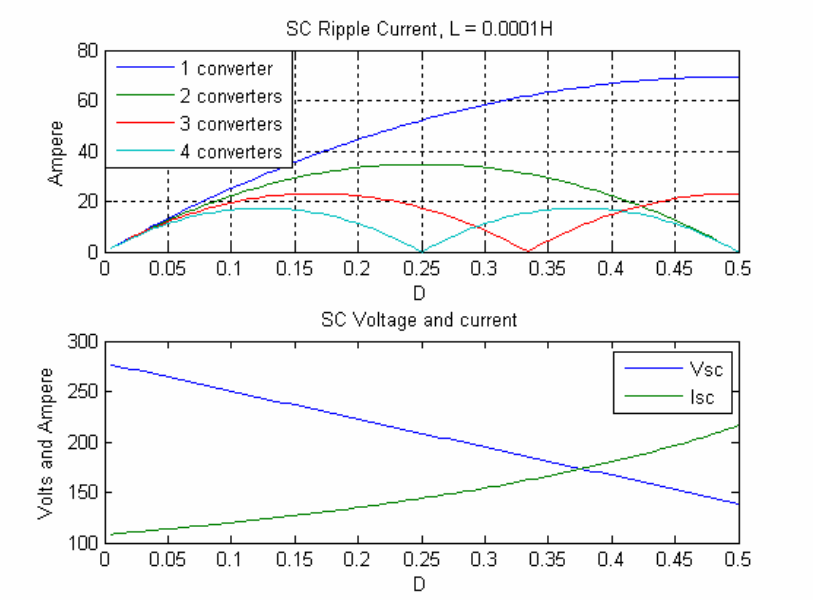

Figure 4.2: Peak to peak ripple and approximate voltage of the supercapacitor bank, for different duty ratios and stiff battery voltage of 278 V

Figure 4.2 displays the peak to peak ripple in the supercapacitor bank for one to four legs in a bridge configuration. The Matlab code is presented in appendix A. As can be seen from the figure, the maximum ripple is in inverse ratio to the number of converters. If the battery voltage is stiff during energy transfer, the duty ratio will vary between 0.15 and 0.5. Examining Figure 4.2, it seems like the best option is to connect as many legs as possible in parallel. There are of course other factors to take into account. The ripple in each inductor is given by equation (3.1), and will produce losses. With increasing number of converter legs the system complexity increases. Each leg needs it own set of switches and each switch needs their own signal. All though the size of the inductors can be reduced, a trade off must be done between the losses in the inductor and the capacitance and the size [15]. Another problem to consider is that the inductors have some tolerance. This limits the effect of interleaving a large number of phases. This effect can be reduced by proper control of the phases, but it still will have a significant effect [25]. Figure 4.3 shows how the necessary capacitance increases with the tolerance limits of the inductor.

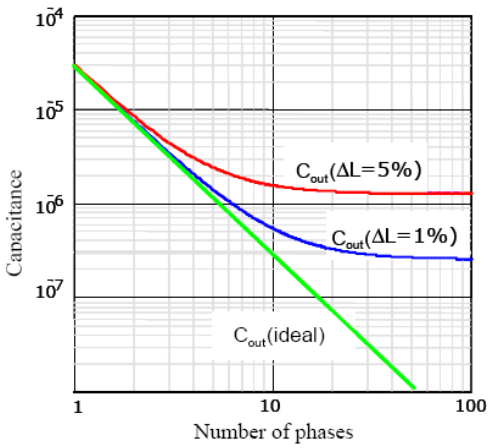

Figure 4.3: Example of capacitance increase as a function of number of phases [25].

The inductor is a large part of the converter, and its design will be crucial to the total converter optimization. Due to relative high ESR compared to capacitors, the supercapacitor bank do not handle ripple well. Therefore in addition to the circuit displayed in Figure 4.1, an ordinary capacitor must be connected in parallel to the supercapacitor bank.

4.3 IGBT selection considerations

In order to decrease the time used for building the power boost system and simplify the construction of the converter, an IPM (Intelligent Power module) will be used. The IPM is a more compact solution than using single switches, and the gate driver is included, thus reducing the work needed for the implementation. The voltage across the switches is the maximum battery voltage. In addition to this is the voltage ripple given by (3.8) [19].

$$\Delta V_0 = \frac{I_0 D T_s}{C} \tag{3.8}$$

This is dependant on the output capacitor, which will have to be dimensioned to limit the ripple to be below the maximum ratings of the DC link and the switches. However, the voltage ripple will be much larger than the value calculated by (3.8), because of inductance in the wire, commutation and harmonics. IPMs come with a recommended maximum DC – link voltage, which is lower than the maximum voltage rating of the switches. I.e. a 600 V IPM has a recommended DC – link voltage of between 200 V and 400 V, which is the voltage that this converter is designed for. There are a limited number of IPM manufacturers, and they do not stock or produce all components at all time. Due to this, the selection of an IPM is based on what can be made available for us that meets the minimum demand set by the system.

The peak current through each switch and diode is equal to the maximum current through each inductor, plus the ripple current. If the peak current exceeds the specifications, there is a danger that the IGBT can go into latch up, and in that state the IGBT can only be turned of due to forced commutation [19]. However, the practical limiting factor for the IGBTs is heat produced by the conduction and switching losses. The average current through the switches is dependant on the number of legs in the converter and the voltage of the supercapacitor bank. The ripple current is dependant on the size of the inductor for each leg of the converter. These have to be estimated in order to get a right selection of the IPM. Losses in the IGBTs will be a substantial part of the overall heat production of the power boost system, and care must be taken when the thermal management is solved. In addition to these criteria it is important to note that the IPM should be certified for automotive applications in the final design.

5 Inductor Design

"Inductor design is an important part of building a converter. There are not commercially available inductors in a vide range of properties, but they are designed for each application" [19]. An inductor is essentially some conducting material wound around a core. The core of the inductor will determine its shape and what kind of winding is the best option.

The inductance is dependant on three factors:

The material and shape of the core
The number and type of windings
The air gap

These factors are related to each other through equation (4.1):

$$L = \frac{N \hat{B} Acore}{\hat{I}} \tag{4.1}$$

The shape and type of material the core is made from decides how many windings it is possible to wind and the maximum flux it is possible to send through the core. The winding must be able to carry the maximum current. The air gap provides a magnetic resistance which will decide how much flux is produced for a given current.

5.1 Inductor core material selection

The purpose of the core is to carry the flux generated by the windings. The losses in the core are dependant on the flux and frequency of the electromagnetic field. This application will be operated in the range of 10 kHz. There are many types of core materials to choose from, but in this frequency range the most suitable core materials are ferrites and amorphous alloys.

The ferrite core has excellent high frequency properties, with almost no hysteresis losses. The drawback for this material is that the flux density is limited to about 0.3 T.

The amorphous core has the ability to carry more flux than the ferrites, with a maximum flux density of 1.56 T. The hysteresis losses are larger than in the ferrite core, and at higher frequencies they will produce more losses.

Figure 5.1 shows the core losers versus flux density for different frequencies.

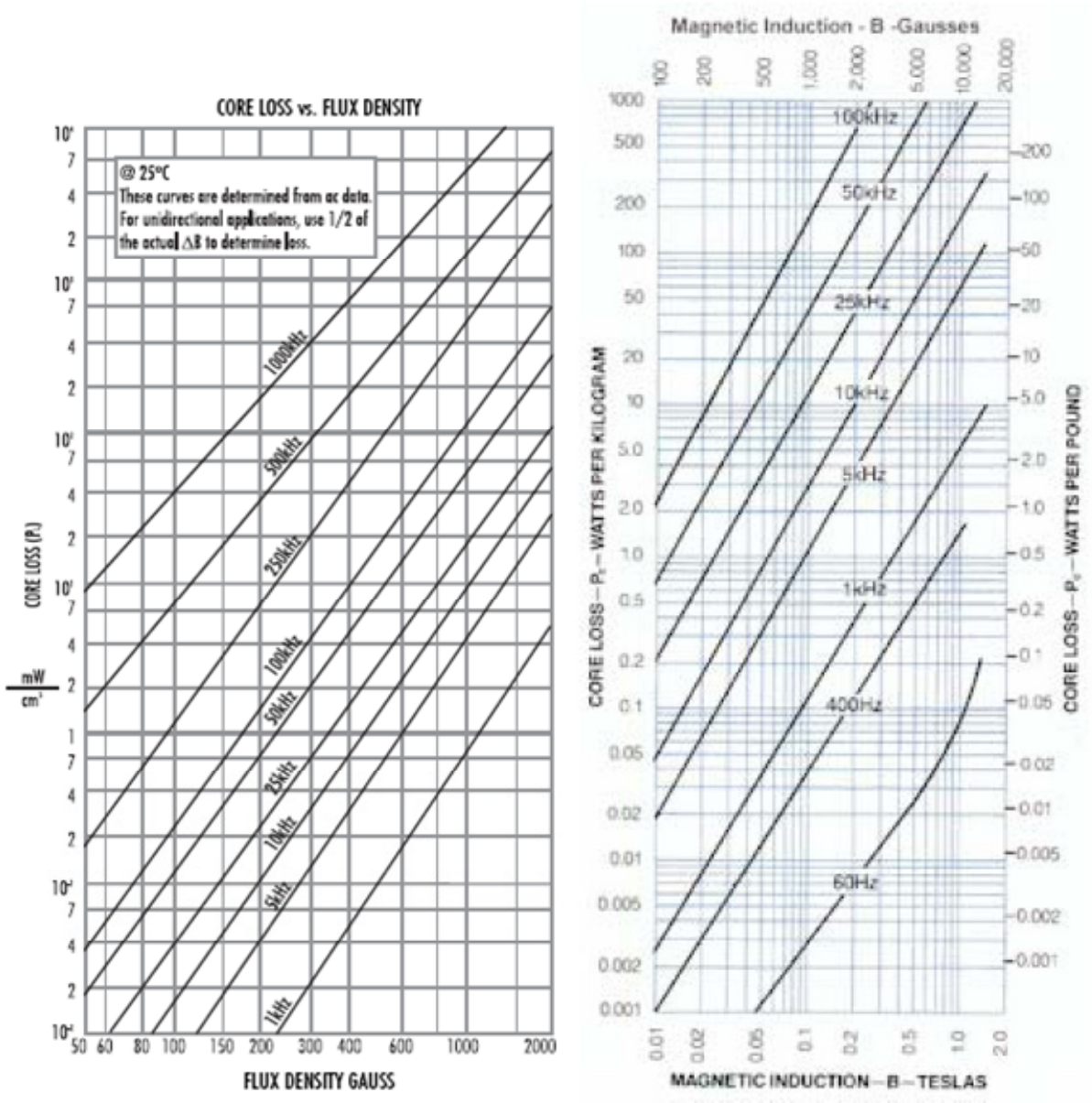

Figure 5.1: Core losses, Left: Magnetics ferrite F, Right: Metglas amorphous cores alloy 2605SA1.

Note that the losses in Figure 5.1 are in mW/cm3 and W/kg respectively. In order to get the amorphous alloy core losses in mW/cm3, multiply by 7.19. For comparison; the highest flux density possible for a maximum loss of 10 mW/cm3 at 10 kHz is:

Ferrite: 0.1 T
Amorphous: 0.06 T

The flux density is dependant on the current in the coil [16].

$$B_{\max} = \frac{0.4\pi N(I_{dc} + \frac{\Delta I_{ac}}{2}) * 10^{-4}}{l_g} \tag{4.2}$$

Bmax is the peak flux density [T], and lg is the length of the air gap [cm]. This is a simplified model, which does not take into account the fringing of the flux in the air gap. This effect will be addressed later, when the air gap is calculated. The peak flux density must be kept below the saturation flux density of the core. If more current is pushed through the inductor, the flux will not increase, thus reducing the inductance. Lower inductance allows more current to flow which will again lower the inductance. This effect can be regarded as a short circuit and will seriously harm the system if not controlled. If the inductor reaches the saturation flux density, the losses will increase, due to a lower effective permeability and resistive losses. In order to avoid this effect, the inductor should be designed to operate below the saturation flux density.

The weight of the inductor is related to the size of the core and windings. Because of the difference in saturation flux density, the ferrite core needs to be approximately six times larger than the amorphous core in order to carry the same flux. Therefore, due to the large difference in weight, the amorphous core is selected for this application.

5.2 Optimization of the inductor

In order to dimension the inductor with a good accuracy, it is important to evaluate the rms current. The average current is calculated from a worst case scenario, where the supercapacitor bank completely discharged at maximum power. The currents and voltages will follow two equations through the discharge:

$$V(t) * I(t) = P \tag{4.3}$$

$$I(t) = C_{SC} \frac{dV(t)}{dt} \tag{4.4}$$

The ripple in the switches is dependant on the inductance according to (3.1). If the inductance is too small, the ripple will be above acceptable levels. Since the ripple is dependant on both Vsc and D, it will change during the discharge. This is possible to achieve by simulating the discharge using iterations in Matlab.

The rms value can be calculated with (4.5) [19]:

$$I_{rms} = \sqrt{\frac{1}{T_{discharge}} \int_0^{T_{discharge}} i_L^2 dt} \tag{4.5}$$

iL in (4.5) must contain both the average and the ripple part of the inductor current. The average current I_L is calculated based on (4.3) and (4.4), and the ripple ΔI_L based on (3.1).

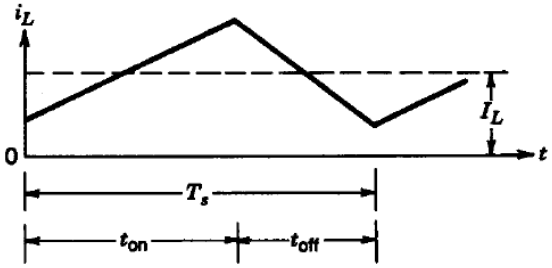

Figure 5.2: Inductor current [19]

Figure 5.2 shows how the current through an inductor behaves in steady state. From this it is possible to find an expression for i_L:

$$\begin{aligned} t_{on} &: i_L = I_L - \Delta I_L + \frac{2\Delta I_L t}{DT_S} \\ t_{off} &: i_L = I_L + \Delta I_L - \frac{2\Delta I_L t}{(1-D)T_S} \end{aligned} \tag{4.6}$$

Using (4.6), the integral in (4.5) can be solved:

$$\begin{aligned} \int {i_L}^2 dt &= \int_0^{DTs} i_{L,t_{on}}^2 dt + \int_{(1-D)Ts}^{Ts} i_{L,t_{off}}^2 dt \\ &= \left(I_L^2 + \frac{1}{3}\Delta I_L^2 \right) * Ts \end{aligned} \tag{4.7}$$

Equation (4.5) is then reduced to:

$$I_{rms} = \sqrt{\frac{\sum_0^N \left(I_L^2 + \frac{1}{3}\Delta I_L^2 \right)}{N}} \tag{4.8}$$

Where N is the number of calculation points for one discharge cycle.

Please not that equation (4.7) returns the integral of i_L^2 for one cycle. In order to reduce the calculation time, the number of measuring points can be reduced from the total number of ripples during one discharge. The Matlab program is presented in appendix A.

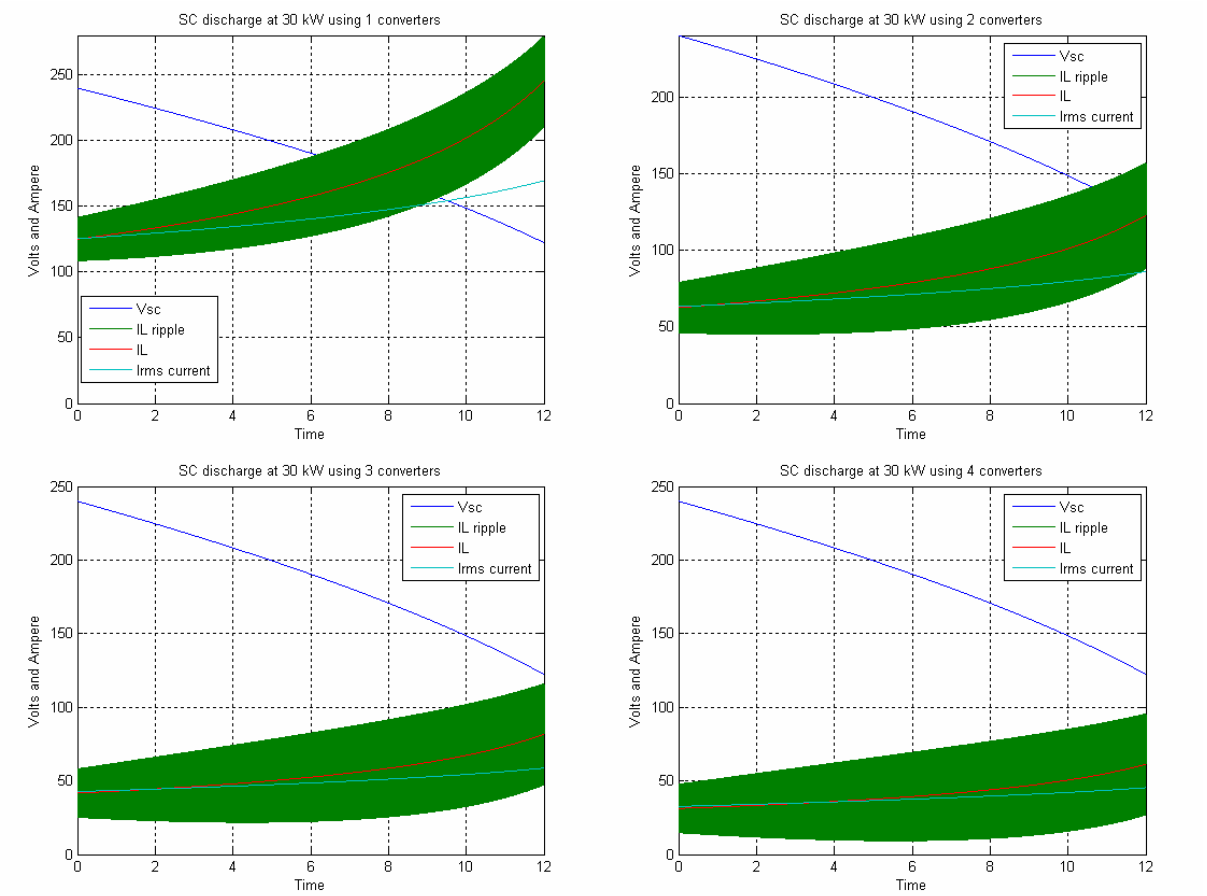

Figure 5.3: Supercapacitor discharge voltage and current simulation at l = 0.1 mH for 1-4 legs in parallel. Note that the Irms current is the integral value.

There are several programs for dimensioning inductors available on the internet. These are usually provided by inductor core manufacturers and will give a solution with their type of core material. Metglas provides a program for dimensioning a dc-reactor on their web pages [26]. Utilizing the numbers calculated in the simulation and for the converter dimensioning, it is possible to evaluate different inductor design.

Table 8: Inductor design results for L = 0.1 mH

Parameter	1 Converter	2 Converters	3 Converters	4 Converters
Max inductor current	279.2	156.7	115.9	95.5
Max ripple current	34.8	34.8	34.8	34.8
RMS inductor current	169.4	86.0	58.6	45.4
Loss (W)	93.0	59.8	63.3	66.0
Loss total (W)	**93.0**	**119.6**	**189.9**	**264.1**
Weight (Kg)	5.01	2.16	1.85	1.38
Weight total (Kg)	**5.01**	**4.32**	**5.55**	**5.52**
Volume (L)	0.66	0.3	0.30	0.28
Volume total (L)	**0.66**	**0.61**	**0.91**	**1.11**
Peak to peak SC current ripple (A)	**70**	**35**	**23.3**	**17.5**

Table 9: Inductor design results, SC ripple = 35 A

Property	1 Converter L = 0.2 mH	2 Converters L = 0.1 mH	3 Converters L = 0.067 mH	4 Converters L = 0.05 mH
Max inductor current	262.0	156.7	132.8	129.7
Max ripple current	17.4	34.8	51.8	69.5
RMS inductor current	169.8	86.0	61.5	53.9
Loss (W)	90.2	59.8	93.3	151.2
Loss total (W)	**90.2**	**119.6**	**279.9**	**604.6**
Weight (Kg)	9.13	2.16	1,99	1.86
Weight total (Kg)	**9.13**	**4.32**	**5.97**	**7.44**
Volume (L)	1.32	0.3	0.44	0.44
Volume total (L)	**1.32**	**0.61**	**1.31**	**1.76**
Peak to peak SC current ripple (A)	35	35	35	35

Table 10: Inductor design results, L = 0.2 mH, SCripple < 35 A

Property	1 Converter L = 0.2 mH	2 Converters L = 0.2 mH	3 Converters L = 0.2 mH	4 Converters L = 0.2 mH
Max inductor current	262.0	139.59	98.77	78.36
RMS inductor current	169.8	84.71	56.82	42.96
Max ripple current	17.37	17.37	17.37	17.37
Loss (W)	90.2	56.8	42.32	38.2
Loss total (W)	**90.2**	**113.6**	**127.0**	**152.7**
Weight (Kg)	9.13	3.25	2.06	1.35
Weight total (Kg)	**9.13**	**6.5**	**6.18**	**5.4**
Volume (L)	1.32			
Volume total (L)	**1.32**			
Peak to peak SC current ripple (A)	35	17.37	11.7	8.8

The data from Table 9 and Table 10, implies that it might be better to design for a larger inductance, if the inductor current ripple is large compared to the dc value of the current. Because of the supercapacitors poor high frequency capabilities the supercapacitor current ripple should be kept low. The maximum efficiency for an inductor is reached when the core losses and the copper losses are equal, but only when the gap loss is zero [16]. Zero air gap length is difficult to achieve due to large currents, but as a design strategy these losses should be fairly equal. For the 3 and 4 legged topology in Table 10 the core and copper losses are essentially equal. In order to regulate the losses in the program, the inductance and frequency can be altered, but for the 1 and 2 legged converter the copper losses will be dominating, due to large currents.

In order to get the higher dependability that this converter topology can offer, more than two converters should be used. If the converter is based on a two legged topology and one leg fails the ripple is doubled, and the converter must be designed for a lot less ripple than necessary, or the capacitance needs to be dimensioned for a lot more ripple than necessary.

Table 8 and Table 9 shows that the 4 legged topology will weight generally less than the 3 legged topology, but the latter will have less power dissipation. The three legged topology will be simpler and less costly to utilize in the system, therefore a 3 converter topology will be utilized in this application. Among the 3 legged converter topologies, the 0.2 mH inductor is the best choice. It is almost the same size as the others, but has lower losses, and creates less ripple current.

Not all cores that are listed in the program are commercially available. The best commercially available core type was the AMCC 200 from METGLAS. The data for this core is presented

in appendix B. The preferred core listed by the program was the AMCC 3100S, but this was not available. These cores are C shaped and two will be used in order to make a complete magnetic circuit.

5.3 Inductor construction considerations

In order to be able to build the inductors properly, it is not enough to just use the simulation program. The practical realization of the inductors demands knowledge about the physics of the inductor. When the core is selected, the only way to alter the inductance is to change the number of windings and the length of the air gap. When the windings are wound, the air gap is the only factor that can be varied in order to obtain the right inductance. A copper foil is chosen for the windings, because of the better fill factor compared to Litz wire and good current carrying capabilities.

Imax =	100 A
Irms =	60 A
Frequency =	10 kHz
Inductance=	0.2 mH
Foil:	70 x 0.3 mm
Fill factor (FF) =	0.5
Acore=	0.00095 m^2

The copper area of the core is 83 * 25 mm. This is wider than the foil and the width will limit the number of turns. The maximum number of turns is given by (4.9) [19].

$$N = \frac{b_{core} * FF}{l_{foil}} = \frac{25mm * 0.5}{0.3mm} = 41 \tag{4.9}$$

The number of turns needed in order to get the calculated inductance is given by (4.10)[19].

$$N = \frac{L * \hat{I}}{A_{core} * \hat{B}} = 17.54 \tag{4.10}$$

In order to ensure that the rated inductance can be reached, 10 turns will be wound around each leg of the core. Figure 5.4 displays how large the air gap must be, for increasing number of turns, in order to get the rated flux density. The curve is made with the approximation that there are two equal air gaps. The air gap is calculated based on (4.11) [19], where the Agap is the area of the air gap and g is the length of the air gap.

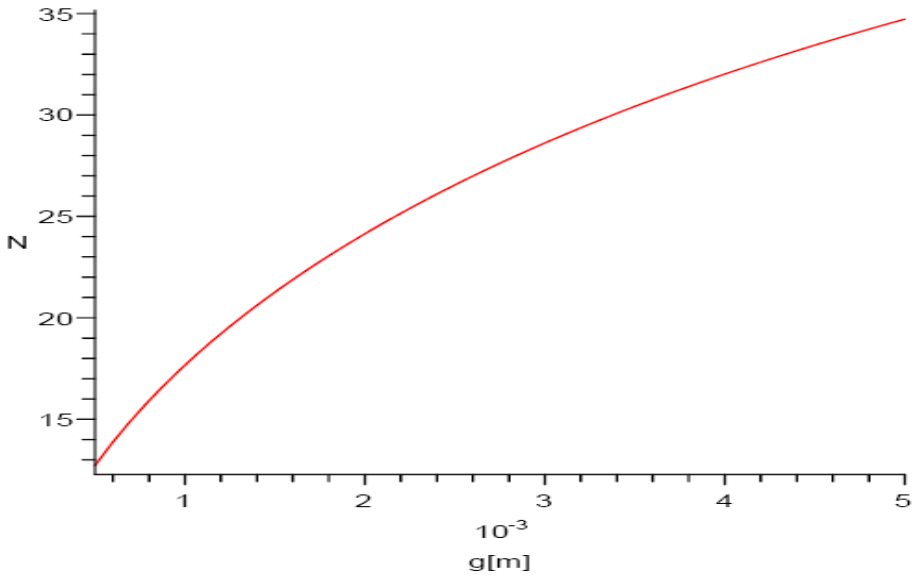

Figure 5.4: Length of each air gap dependant on the number of turns to achieve 1.2 Tesla

$$\hat{I}\,N = \hat{B}\,A_{core}\frac{2g}{\mu_0 A_{gap}} \tag{4.11}$$

For 20 windings each air gap should be 1.135 mm. The air gap area is assumed to be g/2 wider than Acore in all directions, due to the fringing effect, which is shown in Figure 5.5.

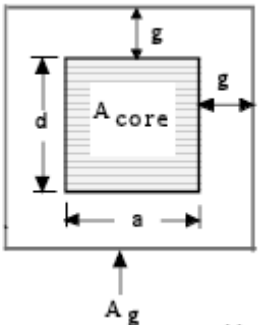

Figure 5.5: Air gap approximation

Losses are also important to consider when the inductors are made. If they are made without care for losses, the can easily be destroyed. The core losses are produced from the flux density ripple Bac, which is proportional to the current ripple (4.12) [16] (4.13) [26].

$$B_{ac} = \frac{0.4\pi N \Delta i_L * 10^{-4}}{l_g} \tag{4.12}$$

$$P_{core,W/kg} = 6.5 * f_{kHz}^{1.51} * B_{ac,T}^{1.74} \quad (4.13)$$

The electrical losses come from both resistance in the windings and induced currents and are harder to compute. In the foil used for the windings, some eddy currents can occur close to the air gaps. In the air gaps the flux is spread over a larger area, and some of it may enter the foil. Figure 5.6 shows the flux paths [27].

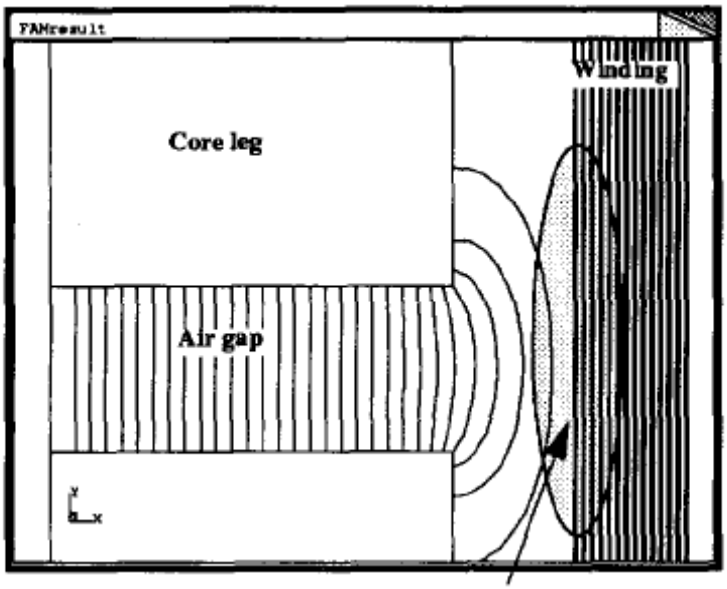

Figure 5.6: Induced currents because of fringing flux [27]

The amount of flux entering the coil is dependant on the distance between the windings and the core, and on the length of the air gap. When the flux enters the air gap circular currents will be induced in the foil. These currents will produce losses and can reduce the conduction capabilities of the foil. This effect can cause severe losses if not taken into account when designing. An alternative that will reduce losses is the use of Litz wire for the windings, but this has a poor fill factor.

In order to achieve a good design, these two strategies are suggested in [27]:

1. Consume the ampere-turns where they are generated. This is achieved by using many small air gaps.

2. Reduce the impact of the radial flux component. This is accomplished by increasing the distance between the core leg and the windings, i.e. increase the thickness of the bobbin.

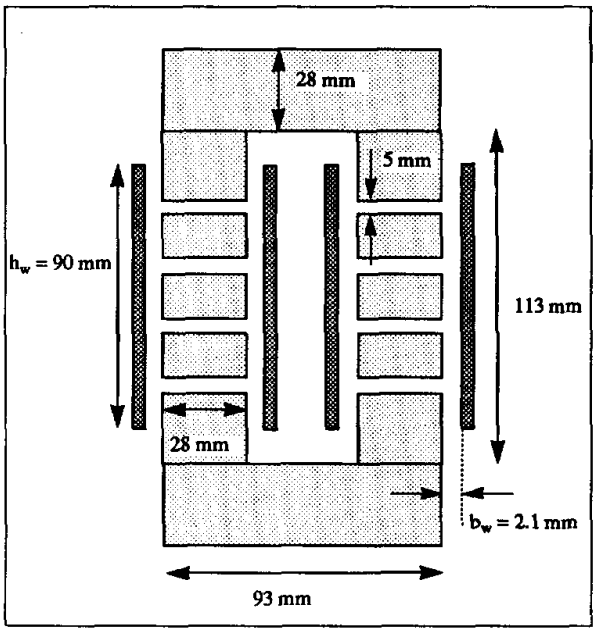

Figure 5.7: Core with several small air gaps [27]

The same strategies can also be applied for this application. The windings will be placed over the air gaps, in order to reduce the losses, but there will only be one air gap on each leg, because the air gap in this application is much smaller than the ones described in [27]. Placing the windings over the air gap will also reduce EMI from the inductor. The second strategy demands larger cores, so a trade off must be done between core size and losses. Another compromise that must be done is between the foil width and the width available for the foil in the core. At the edges of the foil there will be losses due to stronger fields [27]. By increasing the distance between the foil and the core, these losses will be reduced.

6 IPM selection

Since the With a three legged converter topology the maximum current can be calculated. The specifications for the converter are listed in Table 11.

Table 11: IPM specifications

Property	IPM
DC – link voltage	300 V
Maximum current	100 A
Average current	60 A
Frequency	10 kHz
Other	Certified for automotive applications

Based on the specifications Fuji electric and Mitsubishi electric, who manufacture IPMs was contacted. The companies were not fully stocked, and only Fuji could provide an IPM. The IPM was not the latest model and not certified for automotive applications. The IPM received was the Fuji 6MBP150RA-060. It can operate at up to 600 V and with 150 A current. The recommended ratings are listed in Table 12 [28].

Table 12: Recommended ratings of the IPM

Item		Symbol	Min.	Typ.	Max.	Unit
DC bus voltage		V_{DC}	200	-	400	V
Operating power supply voltage range of Pre-driver		V_{CC}	13.5	15	16.5	V
Switching frequency of IPM		fsw	1	-	20	kHz
Screw torque	Mounting (M5)	-	2.5	-	3.0	N·m
	Terminal (M5)	-	2.5	-	3.0	N·m

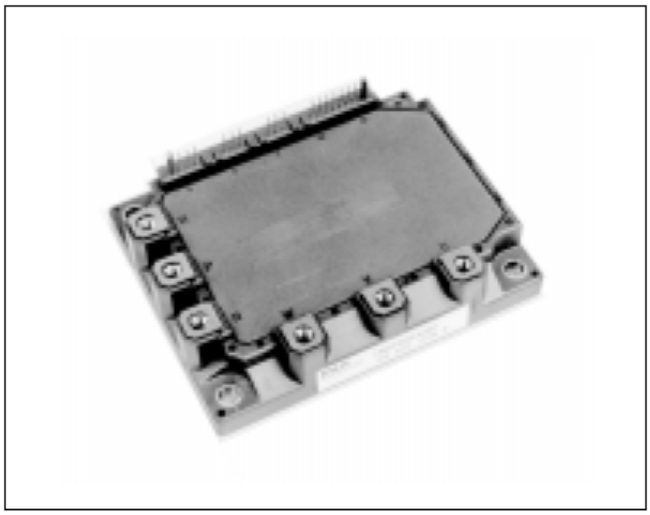

Figure 6.1: Intelligent power module from Fuji [28]

The IPM is originally made for DC to AC applications, and has the P – N connections to the DC link on the left side, and the three phases on long side. The upper connection is for braking resistors and is not connected in this application.

7 Thermal management

Thermal management of the power boost system is important in order to keep the components from deteriorating or being destroyed. The thermal management of a single component must be coordinated with that of the others, because the ambient temperature in the car is dependant on the power loss of all components. Both the converter and the supercapacitor are placed in a confined space, and the ambient temperature selected for the dimensioning is 45 °C. The thermal management must therefore be coordinated. There will be some natural convection from the components, but most likely the system needs to have a heat disposal unit, i.e. fan or water cooling. This will be finalized when the system is implemented in the car.

7.1 Thermal management of the IPM

The IPM will produce a lot of heat due to switching and conduction losses. The losses are shown in Figure 7.1.

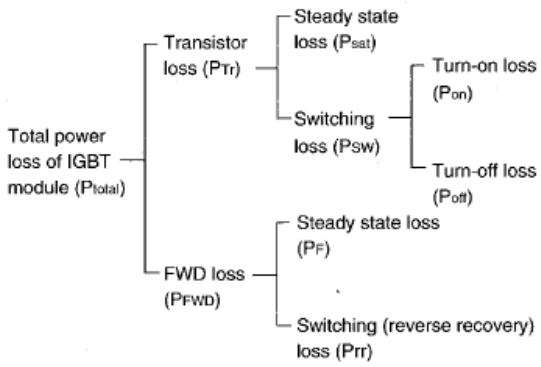

Figure 7.1: Power loss factors [29]

The losses in the IPM can be calculated using the characteristics in the datasheet [28]

$$P_{IGBT} = D*(V_{O,T}*I_C + I_C^2*R_T) + f*(E_{on} + E_{off}) \quad (6.1)$$

$V_{0,T}$ is the minimum conduction voltage across the IGBT and R_T is the ohmic losses in the IGBT.

$$P_{diode} = (1-D)*(I_C * V_{0,D} + I_C^2 * R_D) + f * E_{rr} \quad (6.2)$$

$V_{0,D}$ is the minimum conduction voltage across the diode and R_D is the ohmic losses in the diode.

As can be seen from (6.1) and (6.2) the loss is heavily dependant on the current and the switching frequency. The worst case scenario at 10 kHz gives an rms current of 57 A and a duty cycle of 0.5. The results are displayed in Table 13.

Table 13: IPM losses at 10 kHz, 57 A and 50 % duty cycle, VCC = 15 V

	Power loss (W) conduction + switching	Maximum power loss at maximum current = 100 A
IGBT	42.5 + 90	93 + 90
Diode	32.0 + 12	72 + 12
All transistors	397.5	549
All diodes	132	252
Total for the IPM	**529.5**	**801**

In the calculations above the following values were found in the datasheet [28]:

$V_{0,T}$ = 1 V
$V_{0,D}$ = 0.7 V
$R_{0,T}$ = 8.6 mΩ
$R_{0,D}$ = 7.4 mΩ
Err = 1.2 W/kHz
Eon = 4.5 W/kHz
Eoff = 4.5 W/kHz

7.2 Thermal equivalent circuit of the IPM

From the data in the datasheet [28][27], it is possible to build an equivalent electric circuit for the thermal resistances in the IPM. The circuit is shown in Figure 7.2.

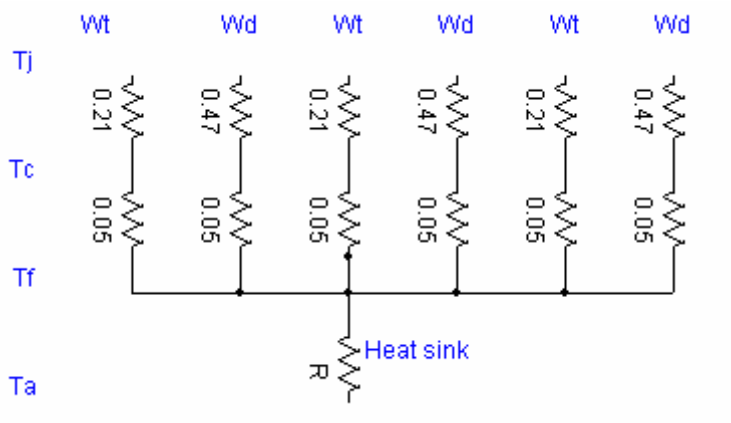

Figure 7.2: Equivalent thermal resistance for the IPM

The junction temperature for the transistors and diodes respectively is stated in (6.3):

$$\begin{aligned} Tj(t) &= W_T * (R_{(j-c)} + R_{(c-f)}) + (3W_T + 3W_D) * R_{(f-a)} + T_a \\ Tj(d) &= W_D * (R_{(j-c)} + R_{(c-f)}) + (3W_T + 3W_D) * R_{(f-a)} + T_a \end{aligned} \tag{6.3}$$

Where W_T is the power losses in a single IGBT and the WD is the power losses in the diode. Ta is the ambient temperature and $R_{(f-a)}$ is the thermal resistance between the heat sink and the surroundings.

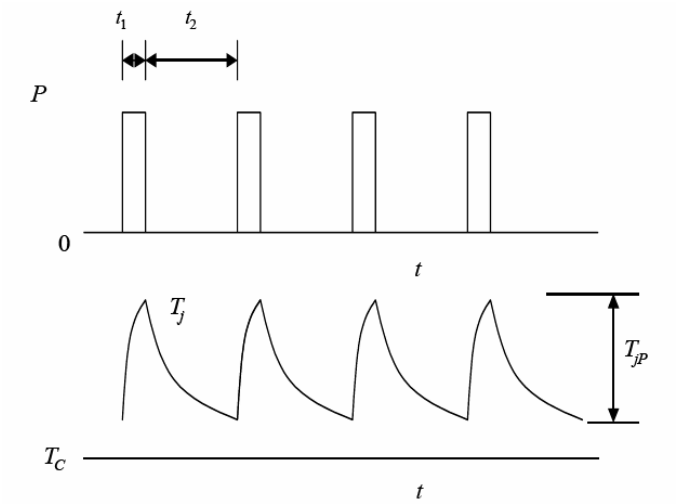

Figure 7.3: Thermal ripples [29]

Figure 7.3 shows how the junction temperature can vary with the power dissipation. In order to ensure that the IGBT is not overheated, the heat sink should be dimensioned for a maximum junction temperature of 120 °C, at maximum current. As can be seen from the results below, there heat sinks will have very different properties if it is not dimensioned for handling the thermal ripples.

Junction temperature 120, Pmax
IGBT max current: 0.034 °C/W
Diode max current: 0.039 °C/W

Junction temperature 150, Paverage
IGBT: 0.177 °C/W
Diode: 0.167 °C/W

Due to availability a heat sink of the type LA V 10 300 24 from Fisher Electronic is used to realize the cooling. Its dimensions are: Length = 300 mm, width = 160 mm, Height = 83 mm as shown in Figure 7.4. It has two fans running on 24 V DC, and a thermal resistance of 0.06 K/W. This heat sink does not meet the demands from the worst case scenario, but the best choice due to availability. Care must be taken when the converter is run, not to overheat the transistors. If the junction temperature is to be kept below 120 °C, the ambient temperature cannot be more than 25 °C.

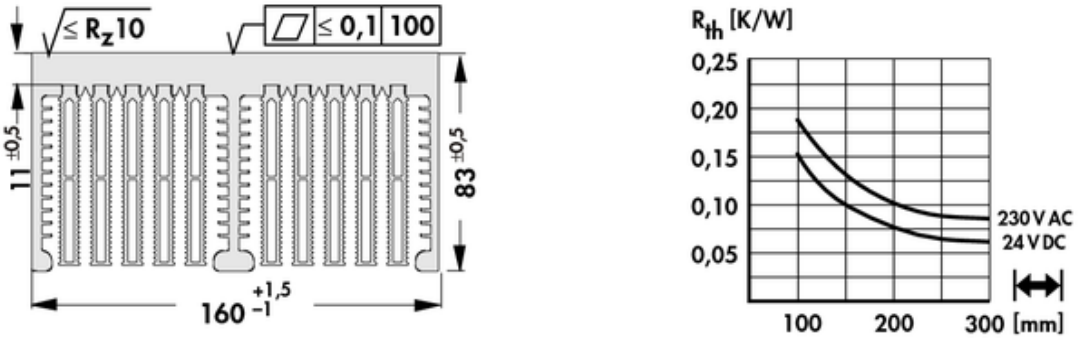

Figure 7.4: Heat sink properties [30]

7.3 Thermal management of the inductors

The inductors produce about 44 W of losses each. This number is theoretical and care should be taken when testing the inductors. There could be "hot spots" where the temperature could reach dangerous levels. Prototype testing has shown that the actual losses can have a large deviation from the theoretical values [27]. With three inductors, the power loss will be about 135 W. In still air the Metglas program estimate the temperature to reach 106 °C, and if this simulation is correct, the inductors will have adequate cooling with natural dissipation. However, tests should be run to verify these numbers. If the temperature increases too much, there is a danger that the bobbins or the isolation material between the windings catches fire or deteriorates. Temperature sensors should be implemented in order to keep the inductor form overheating, until more knowledge is gained about the thermal characteristics. The best places to place these sensors are on the foil, as close as possible to the air gap, on the edge of the foil, close to the core and on the core itself. With these three measurement points it is possible to measure the temperature satisfactory.

7.4 Thermal management of the supercapacitor bank

The thermal profile of the 1500 F cell is displayed in Figure 7.5. The worst case rms current will be 171 A during one discharge at 30 kW. The duty cycle will vary between 0.1 and 0.5.

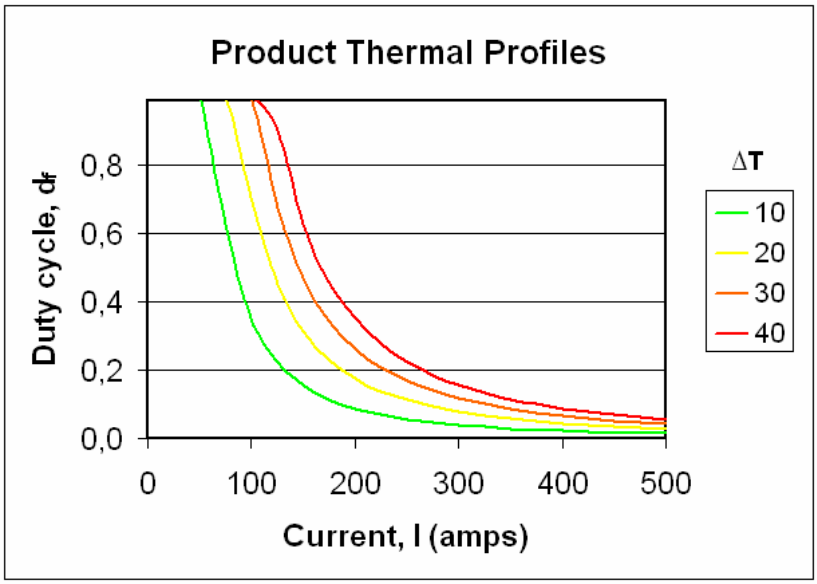

Figure 7.5: Thermal profile from Maxwell thermal charts

The maximum operating temperature of these supercapacitors is 65 °C, but the temperature should be lower in order to gain longer lifetimes for the supercapacitor bank. The ambient temperature is about 45 °C and this result in a maximum heat increase of 20 °C. The maximum power loss in each supercapacitor will be:

$$P_{SC,loss} = I_{rms}^2 * R_{DC} = 18.4W \tag{6.4}$$

Where Rdc = 0.63 mΩ. Total power dissipated from the supercapacitor bank will be 1660 W. Worst case calculations will give the temperature increase:

$$\Delta T_{sc} = I^2 R_{DC} R_{Th} = 82.9K \tag{6.5}$$

R_{Th} is the thermal resistance of the supercapacitor and is 4.5 °C/W. If this heat is not removed it might deteriorate and destroy the supercapacitors.

The actual thermal management design must be completed when the bank is installed in the Think car. An integrated solution is the best way of solving the total thermal management.

8 Voltage ripple management

The voltage ripples that are created by the converter are necessary to limit. If allowed in the system they will create a lot of EMI and losses, which could destroy parts of the system. The reduction is achieved by capturing the ripple current in the capacitors. A capacitor will be needed in parallel with both the supercapacitor bank and the output to the DC link.

8.1 Supercapacitor bank capacitor

The supercapacitor bank capacitor (Csc) will be dimensioned in order to handle the maximum ripple current that can occur. The characteristics needed for this is listed in Table 14.

Table 14: Csc characteristics

Property	Value
Current ripple	11.7 A
DC Voltage	240 V
Frequency	10 kHz
Ambient temperature	45 °C

At the rated voltage and ripple it is clear that electrolytic capacitors are the only type that can be utilized in such a system, and screw terminals are preferred because of the increased stability.

There are many companies that are manufacturing capacitors, and the difference in the capacitors they suggest is not very large. The voltage should be chosen to be higher than the maximum voltage listed in Table 14, in order to ensure the dependability. The PEH200 model rated 350 V and 2200 μF capacitor produced by Rifa will be used. This has a diameter of 50 mm and a height of 105 mm and a ripple capability of 24 Arms.

8.2 DC link capacitor

The DC-link capacitor (Cdc) must be dimensioned for the maximum ripple that can occur here, this ripple is a lot larger than that on the supercapacitor side of the converter.

The peak to peak ripple is given by (7.1).

$$\begin{aligned} \Delta i_{Peaktopeak} &= i_{dc,\max} - i_{dc,\min} \\ &= I_L + \Delta I_L \end{aligned} \tag{7.1}$$

The ripple for the dc link is a bit more complex than of the supercapacitor, due to the fact that for a part of the cycle the current goes through the IGBT and not the diode. Therefore the DC link will get current from 1, 2 or 3 legs of the converter at the time, depending on the duty cycle.

The worst case ripple is at the end of the discharge, when the duty cycle is 0.5. The rms value of this current can be calculated using a square wave approximation (7.2).

$$\begin{aligned} I_{C,rms} &= I_{Peaktopeak} * D \\ &= 50A \end{aligned} \tag{7.2}$$

The capacitor characteristics are displayed in Table 15.

Table 15: Cdc characteristics

Property	Value
Current ripple	50 A
DC Voltage	278 V
Frequency	10 kHz
Ambient temperature	45 °C

In order to ensure the lifetime of the capacitor, it will be dimensioned larger than the needed characteristics. Because of the properties of the commercially available capacitors, two will be mounted in parallel instead of one large one. The capacitors chosen were the PEH200 model rated 2200 μF, 450 V produced also by Rifa. It has a current filtering capability of 34.4 A each, a diameter of 75 mm and a height of 105 mm, which matches the height of the heat sink and IPM fairly well. In addition to these electrolytic capacitors, polypropylene or ceramic capacitors might be needed to filter high voltage transients.

9 Construction and testing of the power boost system

9.1 Construction and testing of the switches

For converter layouts it is necessary with a practical understanding of component placement. Important aspects include mechanical stability, which is ensured by a plate, and vertical alignment between the components. Figure 9.1 displays the converter layout. Only the heat sink, 450 V capacitors and current LEM modules are mounted on the plate, while the inductors are quite large and heavy, are attached with cables to have some flexibility in their placement. The 350 V capacitor is placed near the inductors in order to reduce EMI, while the DSP card will be mounted on top of the heat sink to ensure a stable platform, and elevated a from the heat sink to ensure that it is not heated by the IPM.

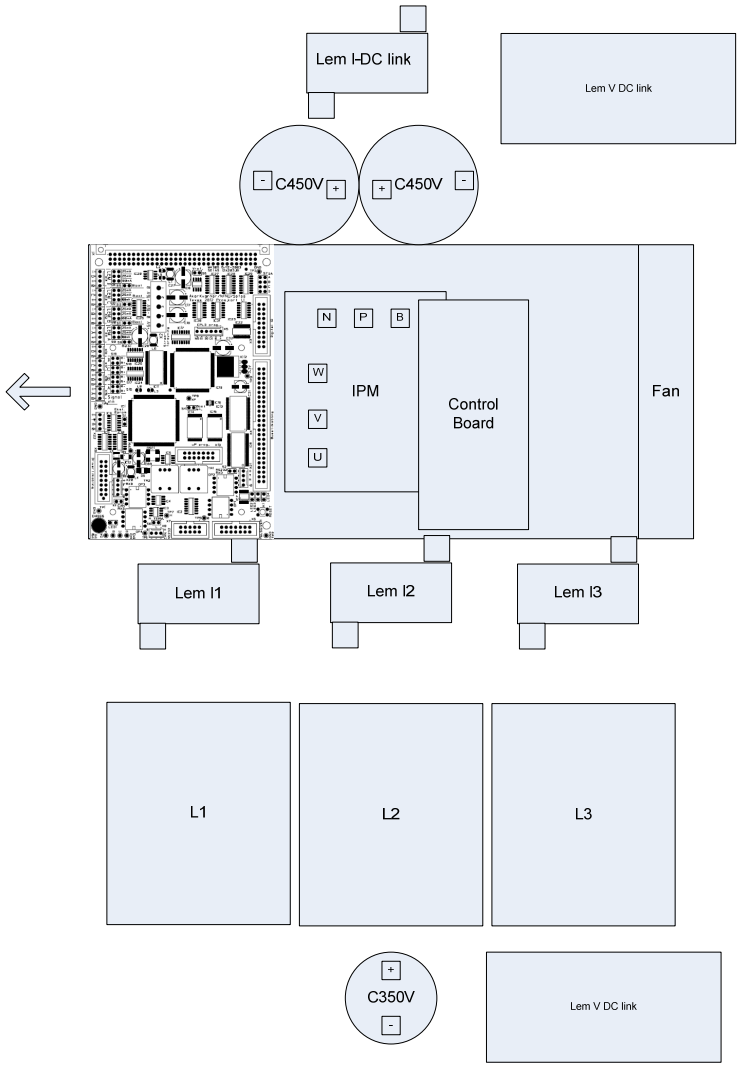

Figure 9.1: Outline of the converter

The components are placed on the long sides of the heat sink, to ensure sufficient cooling, where the air flow is represented by the large arrow in Figure 9.1 shows the direction of the air flow, and it should be allowed to flow freely in order to ensure sufficient cooling. The fans which are responsible for the forced air flow, are switched on and off by a thermal switch located on the heat sink next to the IPM. The fans run on 5 V DC, and will be supplied from the same source as the DSP.

9.1.1 Bus bar design and wire selection

The bus bars design is dictated by EMI (electromagnetic interference) considerations, where an effective design is to place the positive and negative bus bars on top of each other. If possible, the best solution is to let the bars cover 100 % of each other in a top-down view, except for holes needed for connection of components.

The wire between the U, V and W terminal of the IPM and the inductors is a 25 mm^2 wire, which can handle both the DC and AC component of the current. For a switching frequency of 10 kHz, the skin depth of the AC component is about 0.75 mm, and the wire size should be selected appropriately. Too large wire sizes should be avoided, not to encounter mounting problems due to wire stiffness and to reduce cost.

9.1.2 Testing of the IPM

To ensure that the IPM is working properly, the device needs to be tested. Each IGBT will be tested separately, gradually increased voltage level in order to avoid dangerous conditions. In its final application, the converter will be switching an inductive current, therefore, the IPM is tested with inductances.

The dual pulse method [31] is suitable for testing the IPM. It proposes a switching scheme where the IGBT is switched on and off twice at nominal frequency, and then the sequence is repeated once a second. This pattern will keep the device from potential overheating and ensures that the current goes to zero before the next switching starts. Increasing the voltage gradually, the current should reach the maximum value at the end of the second switching. This method will test the turn on / turn off capability of IGBT in the entire current range.

The IPM test circuit is displayed in Figure 9.2.

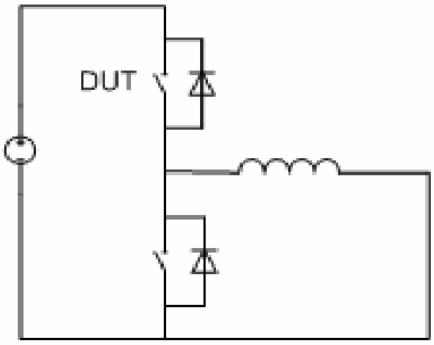

Figure 9.2: IPM test circuit

The switches are controlled using a card that is designed to help in the development of power electronics based on the TMS 320 F 2812 DSP from Texas Instruments. The program written in C++, was run on the processor using and embedded solution which communicated with the PC through the RS232 port. In order to capture the waveforms an oscilloscope with differential probes and an ampere meter was used.

The inductor chosen for this test was a 120 A, 40 µH ferrite inductor, which has low hysteresis losses and is well suited for the testing. The upper switches of the IPM have been tested in stages from 15 V up to 220 V.

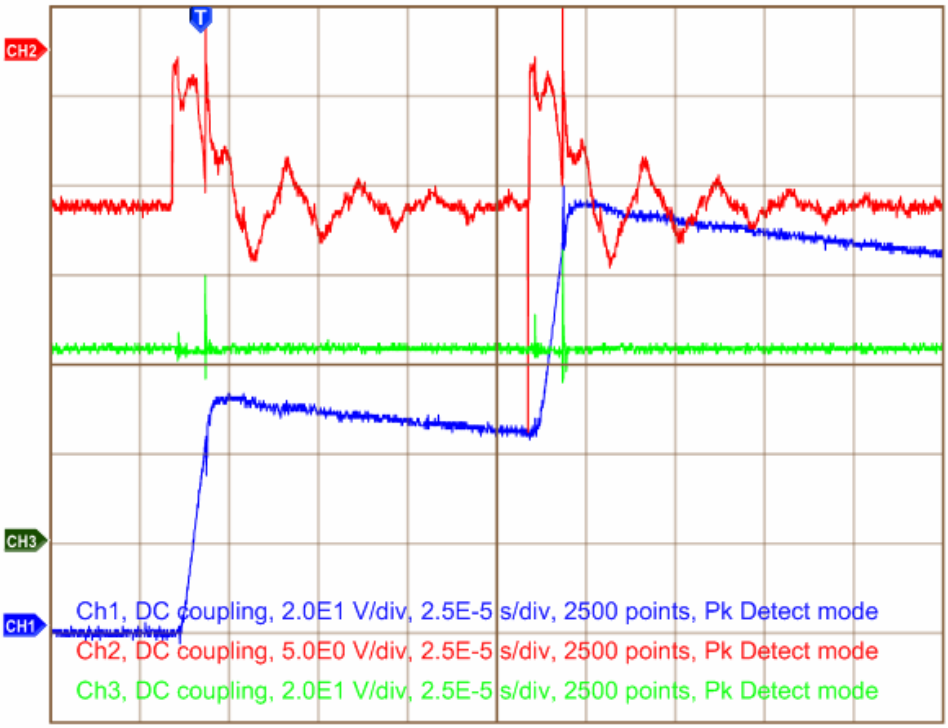

Figure 9.3: Testing of the U phase of the IPM, Ch1: Inductor current 20 A /div, Ch2: Gate signal D = 0.1, Ch 3: Input voltage 50 V/div

Figure 9.3 shows the test performed on phase U, with a source voltage of 220 V, supplied by a DC net. The current increases a bit after turn off from the gate signal, which is due the turn off time of the IGBT. The datasheet [28] states that the maximum turn off time is 3.6 µs. A lot of noise is measured in the gate signal, but the noise is less significant at lower voltages, implying that their origin is a large di/dt. If the circuit is run with just the capacitors as DC source, the disturbance in the gate signal is almost zero. Similar measurements are made for the V and W phase, and presented in appendix E. The disturbance in the gate signal varies between the gates. The W phase has the largest ripple, followed by the V phase, while the U phase has the smallest ripple.

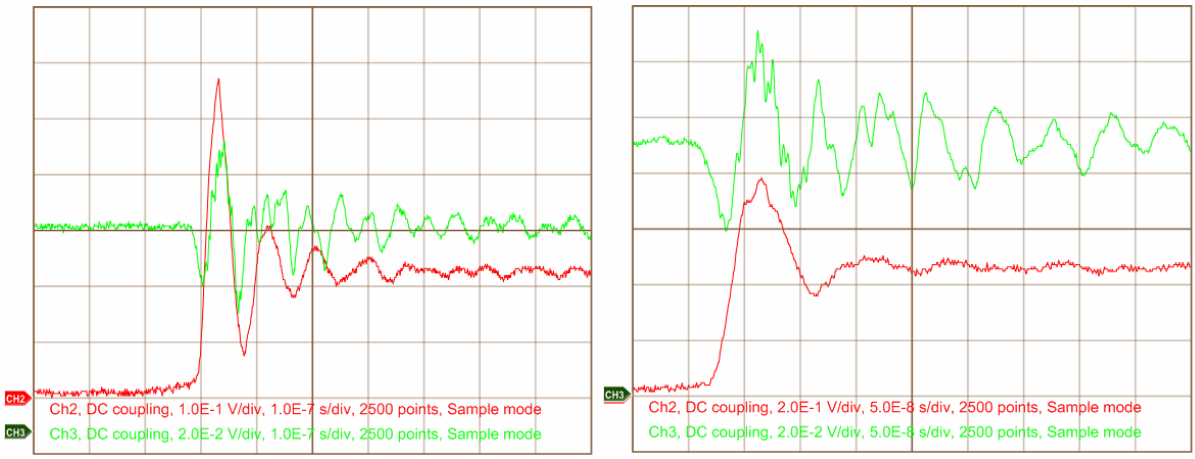

Figure 9.4: IPM input voltage measurements

Figure 9.4 shows the P – U voltage and the current through the IPM during turn on. The left shows the transients at 110 V and 60 A, with a voltage overshoot of approximately 180 V. The right shows the transient at 220 V and 90 A, which has an overshoot at a similar voltage level.

The IPM was destroyed due to a short circuit during testing of the lower switches. Because of the price for the IPM, no spare module was obtained and unfortunately new IPM was not possible to acquire in time to do a complete test of the system.

9.2 Construction of the inductors

The inductors were wound by the workshop at NTNU, where Figure 9.5 shows the principle of the design. The coils are series connected and have ten turns per leg, resulting in a total of 20 turns on each inductor. A 0.3 mm paper sheet is wound with the foil, in order to have electric insulation between the windings.

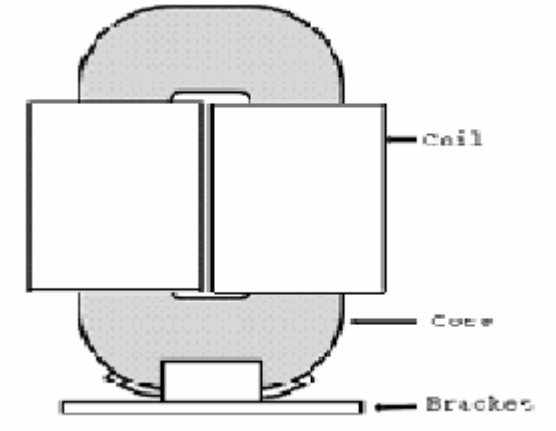

Figure 9.5: Inductor construction

The paper and foil is of the same thickness, resulting in a theoretical fill factor of 0.5. The effective fill factor is closer to 0.3, due to a wider core width than necessary and winding bobbins are filling some of the space. The extra space has some advantage in this application, because it reduces the copper losses considerably by reducing fields close to the air gap and on the sides of the foil.

The air gap length is created by the use of paper and a plate of plexiglass, achieving a total length of 1.1 mm. This is a bit less than the 1.135 mm calculated, and a larger inductance should be expected. In order to verify the inductor value, it was tested with voltage steps, with a voltage source of 36 V attached, and the current was increased until saturation was suspected. In order to obtain a correct inductance calculation, the lower and higher part of the current is discarded in order to calculate with the linear parts of the measurement. This is due to variations in di/dt at low currents and reduction of DC link voltage and saturation at high currents. Measurements between 40 and 50 A were used to determine the inductance using Equation (8.1), which shows the ohmic relation between inductance, current and voltage.

$$L = V\frac{\Delta t}{\Delta I} \tag{8.1}$$

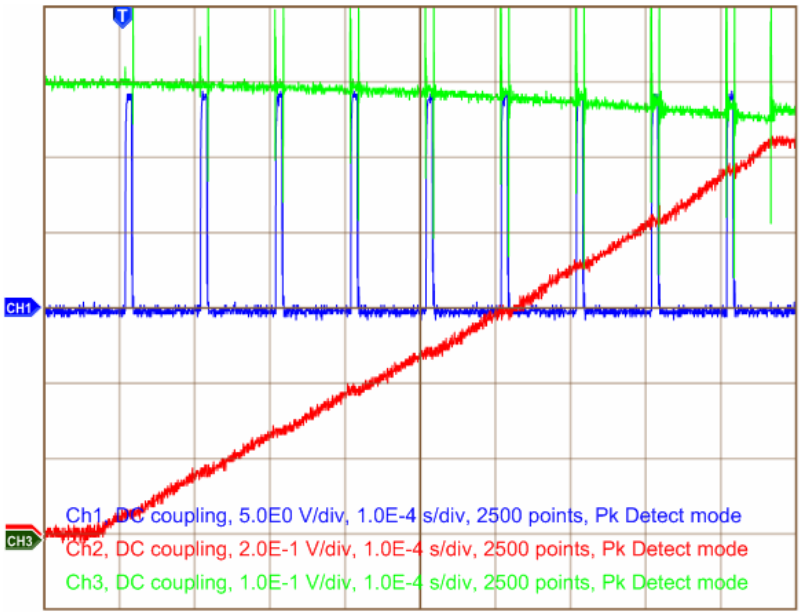

Figure 9.6: Inductance measurement Ch1: signal, Ch2: Current, 20 A/div, Ch3: Dc-link, 5V/div

Based on measurements displayed in Figure 9.6, the inductance is calculated to 0.25 mH. The current was achieved by switching a pre charged capacitor in parallel with a DC lab source as DC- link. With a duty cycle of 0.9 it was possible to increase the current with 12 A per pulse added. This test was done for all three inductors, and the results were almost identical.

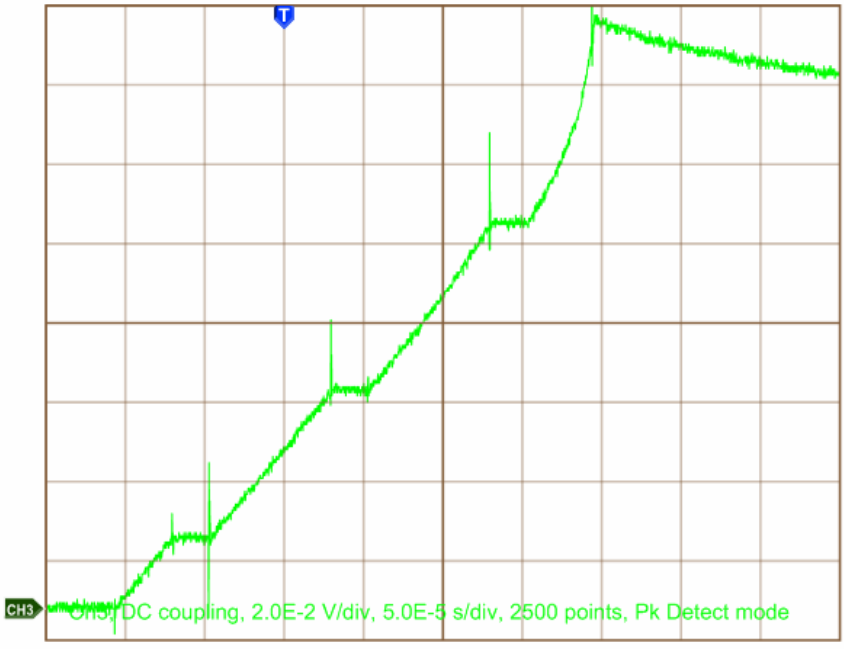

Figure 9.7: Inductor 1 current, 20 A/div at 36 V

Figure 9.7 displays the current through inductor 1. At currents above 80 A, the inductor starts to enter saturation. At 120 A, the inductor will enter heavy saturation and approaches short circuit behaviour. The data from the tests are presented in appendix E.

10 Power boost system results analysis

10.1 Sources of error and uncertainty factors

When working with converters, there is a mixture of high and low currents and voltages. The switching frequencies are high and the noise can be considerable. The measurements are gathered using probes and ampere meters, connected to an oscilloscope. There are many ways that the measurements can be affected by noise and transients in the system. The probes might work as antennas, thus sending a lot of noise into the system. The measurements will then indicate that the conditions are worse than the actual case. The noise can also travel into the oscilloscope, and reduce the dependability of the measurements. It was discovered that more ripple was measured by the ampere meter when the resolution was decreased. These effects were considered when the placing of the probes was decided, and a differential type of probe was used in order to get better measurements. These factors must be kept in mind when evaluating the scope images, where fast transients in particular must be considered as uncertain. However, not all measurements are regarded as uncertain. Most of them are consistent with the expected behaviour of the converter, indicating reliability.

10.2 The power boost system topology

Through the literature study, a topology that uses a supercapacitor bank in parallel with the battery of the EV, has been found as the best solution for the power boost system. Supercapacitors are chosen because of their ability to provide a lot of power in the seconds range with low losses. A converter that operates in an interleaved manner was found to give the best solution to interface between the supercapacitor bank and the DC - link. The current rating of the IGBTs and the necessary inductance was substantially reduced. Through overall system analysis, a topology using 3 legs has been found as the optimum, where the criteria are inductor size and losses together with current ratings of the switches and capacitors. The power boost system has been built to scale, but it has not been completely tested. The system is built for laboratory testing and modifications are necessary in order to do real life testing in the Think EV. The power boost system is based on three interrelated devices, the supercapacitor bank, switching part of the converter and the inductors, which are discussed in this chapter.

10.3 The supercapacitor bank

The supercapacitor bank has been dimensioned for a maximum voltage of 240 V, based on data from the battery, and is capable of delivering 30 kW for 12 seconds. The size is chosen based on availability of the supercapacitors and power requirement of the vehicle. The supercapacitors are connected in series, with voltage equalization circuits attached between each pair of capacitors, to obtain over voltage protection due to tolerances in the cells. The bank will also be equipped with a circuit breaker in order to prevent dangerous short circuits of the bank.

10.4 The switches

An IPM from Fuji with a rating of 600 V and 150 A has been chosen as switching device. This has been through preliminary testing of the switches at 220 V and up to 150 A. Some problems with the gate signal were discovered during the tests, where the following was observed:

- The disturbance increases with the voltage
- The disturbance is almost reduced to zero when the circuit is run from the capacitors and the DC net is disconnected
- The signal is worse for gate W than for gate V, and worse for gate V than for gate U

These observations imply that the inductance in the DC – net cables are causing a lot of noise when the di/dt is increased due to higher voltages. This effect should be reduced when the power boost system is installed in the car and the cable lengths are reduced. Another source of this noise is that the signal cable from the DSP had to pass over the IPM in order to connect to the control board, with possibility of noise induction in the signal cable due to large currents in the IPM wires.

The difference in gate noise between the phases implies a system design error. The most likely explanation is how the cables are connected to the converter. The cable between the W phase and the inductor passes over the IPM, which can cause a lot of disturbance in the gates. The V phase cable only passed over a part of the IPM, and the U phase cable did not pass over it at all.

The design of the converter should be altered in order to reduce these disturbances; the control parts of the system should be place on only one side of the IPM, and the U, V and W phase should be connected without crossing the IPM.

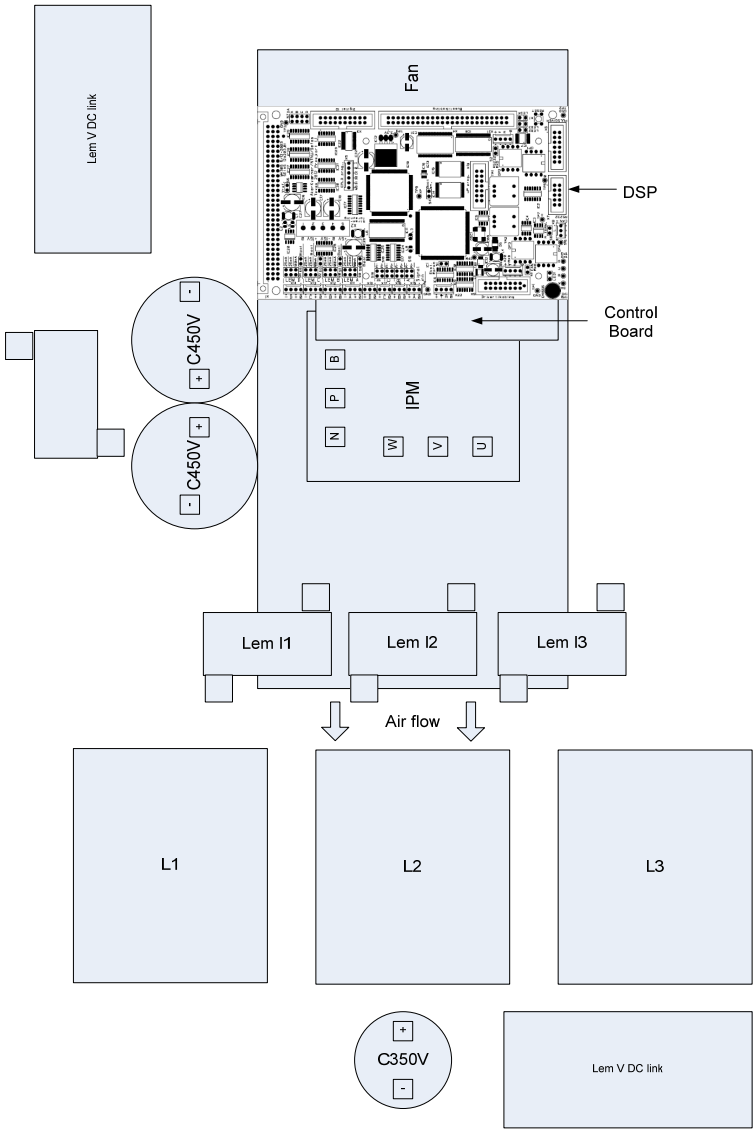

Figure 10.1: Redesigned converter for noise reduction

The design proposed in Figure 10.1 should reduce the gate noise. Inductors L1 to L3 will be placed in such a way that they have a minimum influence on the air flow through the heat sink. The DSP board will be elevated above the control board using spacers. In addition, the control board could be designed smaller than the design suggested in appendix D. The amount of noise induced in a circuit increases with the size, and a more compact design will work better. The redesigned circuit is shown in Figure 10.2.

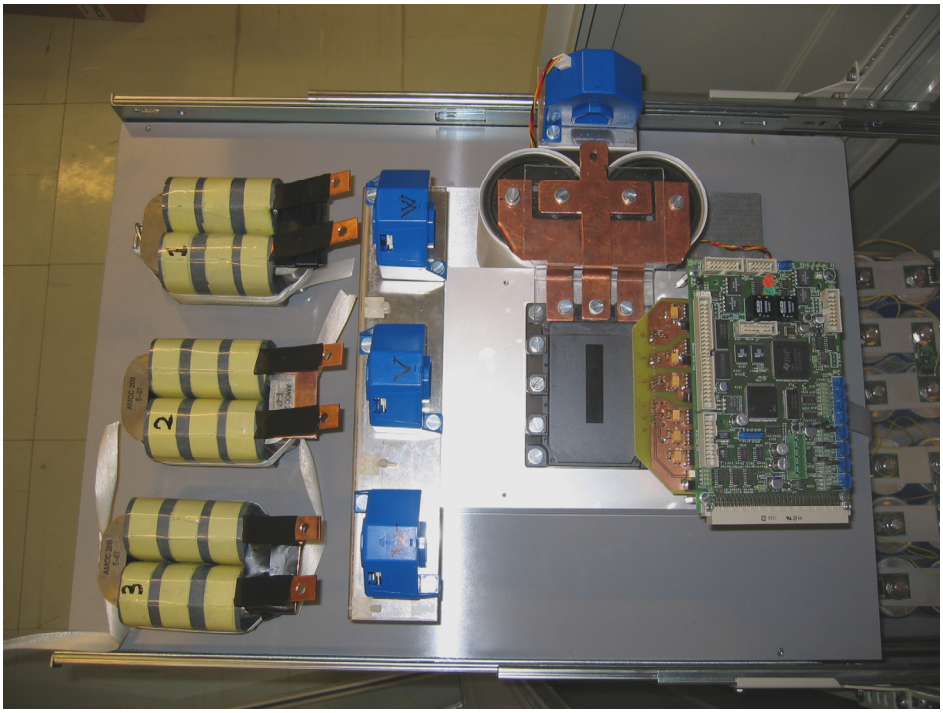

Figure 10.2: Redesigned converter

The input voltage measurements shows that for voltage conditions below recommended values, the voltage overshoot is relatively large. However, the overshoot does not increase with the voltage. The measurements done at 220 V dc voltage and 90 A indicate that operation around nominal voltage, will cause overshoots with a relatively large margin to the 600 V limit of the device.

10.5 The inductors

In order to realize the converter topology, three inductors had to be built. The construction goal was to achieve at least 0.2 mH, and a current capability of 100 A. The current rating is based on the maximum current when the supercapacitor bank is discharged at 30 kW. The inductors are based on an amorphous type core, produced by Metglas because of the saturation flux density of 1.56 T. The design will be several times smaller than its ferrite core counterpart. The AMCC 200 core is used and 10 turns of 70 x 0.3 mm foil is wound around each of the legs of the C cores.

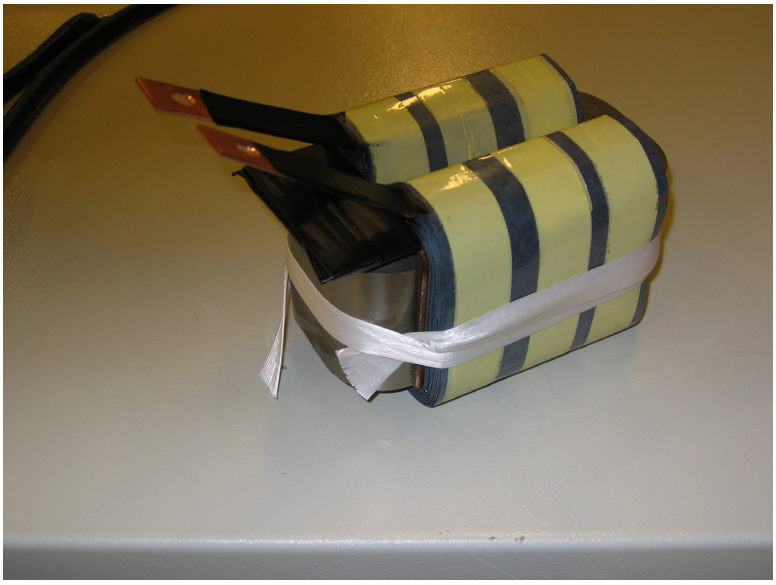

Figure 10.3: Inductor rated 100 A and 0.25 mH

Based on measurements the inductance was calculated to be 0.25 mH, which is 25 % above the design goal. A possible reason for this increase is the reduced air gap, where a 0.2 mH design had an air gap of 1.135 mm. The air gaps installed in the cores were measured to be 1.1 mm. In addition to this the air gaps could have been pressed together when the inductors were assembled. When currents flow in the foil some contraction forces will work on the air gap and further increase the pressure on the air gap material. These factors can have reduced the effective air gap to some extent. The shorter air gap in the core will reduce the saturation current of the inductor. The increased inductance will reduce the maximum current in the inductor to about 95 A. Figure 9.7 shows the current as the inductor enters saturation. For currents below 100 A, the saturation is not critical and the converter can still operate. Saturation is first experienced at 60 A, but it is barely noticeable until 80 - 90 A, while at 120 A the inductor must be regarded as a short circuit.

The inductance is increased above the design goal, thus reducing the core losses due to lower ripple. This implies that a smaller core could be selected and the number of turns reduced. However, the inductors should be thermally tested before any redesign is decided upon. The saturation flux decreases with temperature and if a smaller core is selected, the air gap must be increased and more losses will be produced in the inductor. The maximum flux density decreases with temperature, and an even larger air gap is necessary. If the air gap is too large the fringing effect might heat up the copper foil considerably. The thermal test will show how much losses that are produced in the inductor and if the redesign is preferable.

10.6 The power boost system

All parts of the system has been assembled and installed in a cabinet. The complete system is yet to be tested, but the tests of all components imply that the overall system will be able to operate as intended.

Figure 10.4: The power boost system

Figure 10.4 show the entire system installation. Before operation a protective cover will be mounted on the components in order to ensure that there will not be any short accidents.

11 Economical evaluation

The power boost system must also be analysed from a commercial point of view. It is to early in the process to evaluate the performance gained by implementing a power boost system, but the cost of it can be evaluated. It is important to consider that many of the components selected for the system built was selected out of availability. In order to limit the costs free samples were preferred for the first design. For series production, the cost of the components will decrease. Many manufacturers operate with different prices for different sizes of orders. The initial cost of this converter is listed in Table 16. Note that overall thermal management and implementation costs are not listed.

Table 16: Cost overview

Item	Number	Total NOK	Supplier	Comment
Supercapacitors	90	31300	OEM electronics	Produced by Maxwell
Integration kits	15	4200	OEM electronics	Produced by Maxwell
IPM	1	1200	Fuji Electronics	50 € extra for shipping and handling.
DSP platform	1	5000	Texas instruments +++	NTNU standard development platform
Electrolytic capacitors	3	1200	ELFA electronics	
Amorphous cores	3	1000	Hiatchi Metals / METGLAS	120 $ freight cost
Winding foil		0	EFD induction	Kindly provided free of charge
Heat sink	1	3000	Fisher Electronics	
Current LEM	4	2000	LEM	
Voltage LEM	2	700	LEM	
Small components		1000	Farnell and others	
Circuit Breakers	1	400		250 A
Total NOK:		**51000**		

For many of these products there are several possible suppliers. The companies listed here are chosen because they could provide the components in the time span of the master thesis and because they were usually used by the university, thus simplifying the ordering of components.

This is a considerable price for a car which has a market value of about 200000, and must be justified with increased battery lifetime, better energy recovery from regenerative breaking and reduced maintenance. In addition this supercapacitor bank provides increased performance by improving the acceleration.

12 Conclusion

The master thesis presents the dimensioning and construction of a power boost system capable of delivering and receiving 30 kW for 12 seconds to the DC link. The system consists of an energy storage based on supercapacitors and a bidirectional DC – DC converter based on an intelligent power module and amorphous core inductors. The converter is necessary in order to fully exploit the capability of the bank.

The supercapacitor bank is built from 90 series connected cells rated 1500 F each, and can be safely charged up to 240 V. The bank is regarded as discharged when the voltage is 120 V, because the currents must be limited. This setup allows a total of 100 Wh to be stored in the bank

The converter is connected between the supercapacitor bank and the DC link in the car. It has three parallel legs in a bridge configuration, and will be operated in an interleaved manner. This topology reduces the ripple in the supercapacitor bank and the current rating of the IGBTs. The intelligent power module has been tested at nominal current and at 80 % of nominal voltage. The tests demonstrate that it is well suited for this application, but all IGBTs should be tested at nominal voltage and current before installed in a car.

The converter topology reduces the current and increases the allowed ripple in each inductor. A reduction of the inductance was therefore possible, and three inductors measured to 0.25 mH and capable of carrying 100 A without experiencing heavy saturation, was constructed. The weight of the three inductors was only 6.6 kg in total. The inductors should be thermally tested in order to evaluate the efficiency and to locate possibly dangerous “hot spots”.

The boost power system should help the battery operate at a stable voltage during high power demands. This will decrease the strain on the battery, which will reduce losses due to high currents and increase the lifetime. During breaking the power boost system will collect the kinetic energy, which will further reduce losses. These effects will improve the overall performance of the electric vehicle and increase the maximum driving range.

13 Further work

There are several tasks that can be identified before the power boost system can be tested in an EV. All components must be tested at rated voltage and current. The IPM must be tested at least up to 350 V, and 120 A on the DC – link side. The thermal management of the IPM must also be verified. This can be done by cycling the IPM at rated conditions while measuring the temperature on the casing and heat sink.

The inductors must be thermally tested. It might be possible to utilize a smaller core size, if the inductor does not show a large temperature rise. The need for thermal management should be investigated as a part of this test. Temperature sensors must be placed on crucial parts of the inductor, i.e. at the end of the windings, on the core and on the windings, close to the air gaps. In addition to this, the organization of the air gaps should be investigated. Reducing the length of each air gap by increasing the number of air gaps can reduce the losses.

The supercapacitors should be tested, in order to make sure that all of them function properly. In total, about 1660 W is dissipated in the supercapacitors at maximum discharge current and the thermal management of this must be solved. The thermal management is dependant on available space and air flow in the compartment in the car, thus the car is necessary to do this. When a Zebra battery is acquired, the supercapacitor bank should be optimized in order to match the nominal operation voltage. When the car is available for testing, the energy content in the bank should be optimized. The price of the power boost system is closely related to the price of the bank, and it is a better chance of making a commercial product if the bank is optimized.

The whole system should also be tested at the rated power, to ensure that all components work satisfactory, and that the system functions as intended. For these tests a machine should be used as a load, in order to examine the system reaction to variable power demands. The frequency of the converter should also be varied and possible resonance frequencies should be found.

When the testing of the power boost system in the lab is finished, it should be implemented in a Think EV. In order to do this an interface with the power control unit already installed is necessary. A strategy for load sharing must also be developed and programmed. When this is done the performance of the power boost system can be evaluated. A cost performance analysis will give an indication on if this system can be commercialized. Another possibility for further development is to test the system with other kinds of energy sources, i.e. fuel cells.

14 References

[1] Micah E. Ortúzar, Design, implementation and evaluation of an auxiliary energy system for electric vehicles, based in ultracapacitors and buck-boost converter. Ph.D. thesis, Catholic University of Chile, 2005

[2] Juan Dixon, Miach Ortúzar, Eduardo Arcos, Ian Nakashima, "*Zebra plus ultracapacitors: A good match for energy efficient EVs*", EVS 21, 2005

[3] Frode Lium, "Supercapacitors as energy storage devices", Project NTNU, 2006

[4] Schneuwly, A., M. Bärtschi, V. Hermann, G. Sartorelli, R. Gallay, R. Koetz (2002): *BOOSTCAP® Double-Layer Capacitors for Peak Power Automotive Applications.* From: http://ecl.web.psi.ch/Publications/AABC_2002.pdf.

[5] MILLER, J., and SMITH, R. (2004) Ultracapacitor Assisted Electric Drives for Transportation. Maxwell technologies, White Papers. www.maxwell.com.

[6] Isola EM, Kyyrä J, Bergelin M, Keskinen J, "*Models of Supercapacitors and their charging behaviour",* ESSCAP 2006

[7] Kurzweil P, Chwistek M, Gallay R, "*Electrochemical and spectroscopic studies on rated capacitance and aging mechanisms of supercapacitors based on acetonitrile*", ESSCAP 2006

[8] R. L. Spyker, R. M. Nelms, and S. A. Merryman, "Evaluation of Double-layer Capacitors for Power Electronic Applications",*Proc IEEE APEC, Vol. 2*, 1996, pp. 725-730.

[9] P. Barrade, S. Pittet, A. Rufer, "Series connection of supercapacitors, with an active device for equalizing the voltages", *Proceeding Power Conversion PCIM2000,* Nürnberg, 2000

[10] Yasser Diab, Pascal Venet, Gerard Rojat, "*Comparison of the Different Circuits Used for Balancing the Voltage of Supercapacitors: Studying Performance and Lifetime of Supercapacitors*", ESSCAP, Lausanne, Switzerland, November 2006

[11] Verhaeven E., Knorr R., Gallay R., Van Mierlo J., *Hybrid high energy electrical storage (HyHEELS)*, ESSCAP 2006

[12] Steiner M., Klohr M., *Energy storage on board of railway vehicles,* ESSCAP 2006

[13] Sartorelli G, Schneuwly A, *Role and utilization of voltage balancing fro EDLC stacks,* ESSCAP 2006

[14] Kim, Sang-Min, Sul, Seung-Ki, "*Control of rubber tyred gantry crane with energy storage based on supercapacitor bank",* IEEE Transactions on power electronics, vol. 21, No. 5, September 2006

[15] J. A. Oliver, P. Zumel, O. García, J.A. Cobos, J. Uceda, *"Passive component analysis in interleaved buck converters"*, Applied Power Electronics Conference and Exposition, 2004

[16] Colonel Wm. T. McLyman, *Magnetic core selection for transformers and inductors*, Marcel Dekker, Inc, 1982

[17] Traction motor key requirements A306 MY2007_V0_5, technical specification from Think

[18] O'sullivan, T. M., Bingham, C. M., Clark, R. E., "Zebra Battery Technologies for the All Electric Smart Car" SPEEDAM 2006

[19] Mohan, N., Undeland, T. M., Robbins, W. P, *Power Electronics,* 3rd ed. Wiley, 2003.

[20] Maxwell Technologies BCAP1500 Ultracapacitors. From: http://www.maxwell.com/pdf/uc/datasheets/MC_Cell_Energy_1009323_rev4.pdf

[21] Maxwell technologies, BOOSTCAP Integration Kit. From: http://www.maxwell.com/pdf/uc/integration_kit_manual_1008233_rev2.pdf

[22] Tetrais, F., Caumont, O., Brégeon, L., *Supercapacitor abuse testing*, ESSCAP' 2006

[23] Ortúzar, M., Moreno, J., Dixon, J. W. "*Report on fire event originated by ultracapacitors in an experimental electric vehicle",* IEEE Vehicular Power Propulsion, VPP-2004, 6-8 October 2004, Paris, Franc

[24] Chin Chang, Mike A. Knights, "*Interleaving Technique in Distributed Power Conversion Systems",* IEEE transactions on circuits and systems, vol. 42, No 5, May 1995

[25] O. Garcia, P. Zumel, A. de Castro, J. A. Cobos, *"Effect of the tolerances in multi-phase DC-DC converters"*, Power Electronics Specialists Conference, 2005. PESC '05. IEEE 36th

[26] Metglas webpage, http://www.metglas.com, 27.02.07

[27] A. Nysveen, M. Hernes, ”*Minimum losses design of a100 kHz inductor with foil windings*”, EPE 1993

[28] Fuji electric 6MBP 150RA-060 IPM Datasheet

[29] Fuji electric N-series IGBT-modules Application manual, REH982

[30] Fisher elektronik web page: www.fischerelektronik.de, 02.05.07

[31] Richard Lund, Multilevel Power Electronic Converters for Electrical Motor Drives, Ph.D. NTNU 2005

Appendices

A Matlab scripts

A.1 SC current ripple dependant on duty cycles

This programs display a graph over the SC current ripple for 1 – 4 converter legs

```
Vbatt = 278;%Battery Voltage
Ts=0.0001;  %Switching time
L=0.1e-3;   %Inductance
Isc0=108;    %Current at battery voltage

for i= 1:100;

    D(i)=0.005*i;
    Vsc=Vbatt*(1-D(i));
    Vscplot(i)=Vsc;
    deltai=Vsc*Ts/L*D(i);
    Isc(i)=Isc0*1/(1-D(i));
    Peaktopeak2(i)=deltai*(2-1/(1-D(i)));

    if (D(i) <= 0.25)

        Peaktopeak3(i)=(3*deltai-2*deltai/(1-D(i)));
        Peaktopeak4(i)=deltai*(4-3/(1-D(i)));

    elseif (D(i) >= 0.25) & (D(i) <= 0.3333)

        Peaktopeak3(i)=(3*deltai-2*deltai/(1-D(i)));
        Peaktopeak4(i)=deltai*(4-1.5/(1-D(i))-1/(2*D(i)));

    else

        Peaktopeak3(i)=deltai*(1-2/(3*(1-D(i)))+2*(D(i)-1/3)/D(i));
        Peaktopeak4(i)=deltai*(4-1.5/(1-D(i))-1/(2*D(i)));

   end

    DIsc(i)=deltai;
end
%plot properties
subplot(2,1,1);plot(D,DIsc,D,Peaktopeak2,D,Peaktopeak3,D,Peaktopeak4)
title (['SC Ripple Current, L = ',num2str(L),'H'])
```

```
legend ('1 converter','2 converters','3 converters','4 converters',2)
xlabel ('D')
ylabel ('Ampere')
grid on

Subplot(2,1,2);plot(D,Vscplot,D,Isc)
title ('SC Voltage and current')
legend ('Vsc','Isc',1)
xlabel ('D')
ylabel ('Volts and Ampere')
```

A.2 SC discharge simulation

This script simulates the discharge of the supercapacitor bank, with a variable number of converters.

```
Currents and voltages as a function of time
%Initial conditions
P=30000;
Conv=2;             %Number of converters in parallel
C=16.9;
f=10000;
N=1000;          %iteration steps pr second
k=12*N;         %Number of measuring points for a 12 s cycle
Vbatt = 278;     %Battery Voltage
Ts=1/f;          %Switching time
L=0.15e-3;        %Inductance
Isc0=108;        %Current at battery voltage
counter=1;

%Initial conditions for iterations
tid(1)=0;
V(1)=240;
I(1)=P/V(1);
Il(1)=I(1)/Conv;
Il2(1)=Il(1)^2;
D(1)=1-V(1)/Vbatt;
deltai(1)=V(1)*Ts/L*D(1)/2;
Ilripple(1)=Il(1)+deltai(1);
Il2ripple(1)=2/N*((Il(1)^2)+(deltai(1)^2)/3);
Irmsripple(1)=sqrt(Il2ripple(1)/(2/N));

%Calculations
for t=1:k;

    I(t+1)=P/V(t);
    V(t+1)=V(t)-I(t)/(N*C);     %1/N is the length of the iteration step
```

```
    tid(t+1)=t/N;                %Time counter
    Il(t+1)=I(t+1)/Conv;
    Il2(t+1)=Il(t+1)^2;

    D(t+1)=1-V(t+1)/Vbatt;
    deltai(t+1)=V(t+1)*Ts/L*D(t+1)/2; %half of peak to peak

    Ilripple(t+1)=Il(t+1)+((-1)^(t))*deltai(t+1);

    %Calculation for one period of the current with ripple
    if (counter==1)
        counter = 0;
    else
        Il2ripple(t+1)=2/N*((Il(t+1)^2)+(deltai(t+1)^2)/3);
        counter = 1;
        Irmsripple(t+1)=sqrt(sum(Il2ripple)/((t+2)/N));
        Irmsripple(t)=Irmsripple(t+1);
    end

end


Ilmax = max(Ilripple)
Irms=max(Irmsripple)
Ripplemax=max(deltai)


%plot
plot(tid,V,tid,Ilripple,tid,Il,tid,Irmsripple)
title (['SC discharge at 30 kW using ',num2str(Conv),' converters'])
legend ('Vsc','IL ripple','IL','Irms current')
ylabel ('Volts and Ampere')
xlabel ('Time')
grid on
```

B Inductor core data

Metglas®, Inc.

Inputs to DC Reactor Core Design Tool

Inductance	Ipeak	DC Current	High Freq Ripple	Frequency	Insulator Thickness	Former Thickness	Ambient Temp	Air Flow	Number of Gaps	Core Size
henries	Amps	Amps	Amps	Hz	cm	cm	°C	cfm		
0,0002	100	60	35	10000	0,013	0,2	55	0	2	AMCC200

Core size selected by Designer AMCC200

Summary of DC Reactor Design

No.of Turns	Copper Area	Copper Thknss	Copper Width	Total Gap	Spacer Per Leg	Copper Loss	Core Loss	Total Temp
.	sq.cm	cm	cm	mm	mm	watts	watts	°C
22	0,15	0,02	6,7	2,4	1,2	22,64	22,09	116

CORE DETAILS

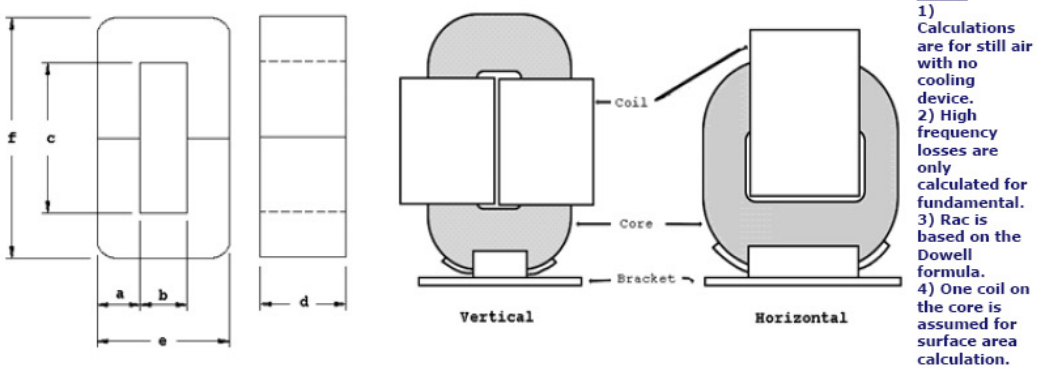

NOTE:
1) Calculations are for still air with no cooling device.
2) High frequency losses are only calculated for fundamental.
3) Rac is based on the Dowell formula.
4) One coil on the core is assumed for surface area calculation.

Core Data

Part No.	A mm	B mm	C mm	D mm	E mm	F mm	Lm cm	Ac sq.cm	Mass kg	Wa sq.cm	WaAc cm4
AMCC200	19	25	83	50	63	121	29,8	7,8	1,67	20,8	162,2
AMCC200 * 1	19	25	83	50	63	121	29,8	7,8	1,67	20,8	162,2

METGLAS ALLOY2605SA1 MASS +(-) 3%

C Inductor testing data

C.1 Inductor 1

Inductance test:

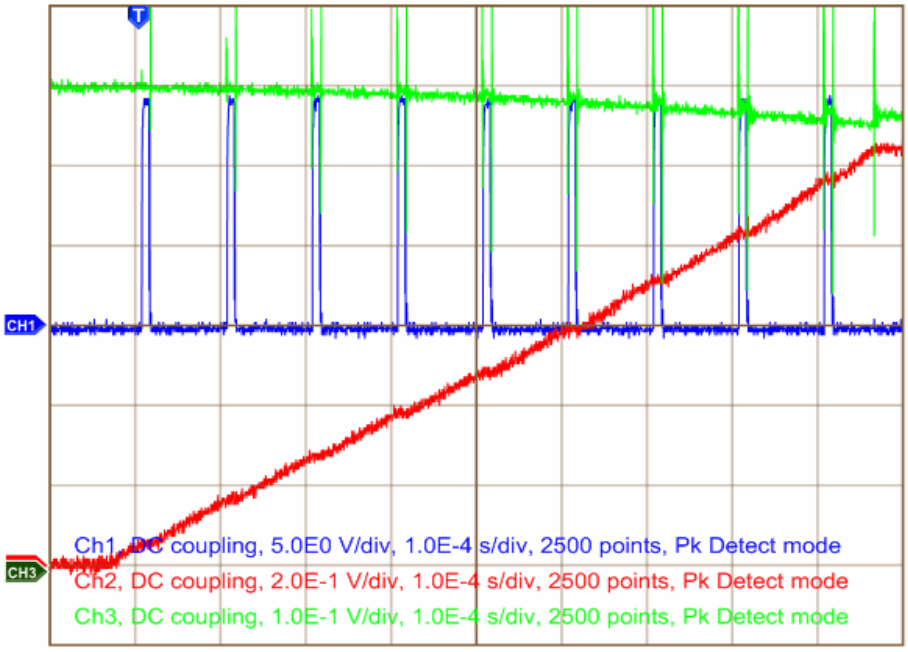

Ch1: Gate signal, Inverted
Ch2: Inductor current, 20 A/div
Ch3: DC link voltage

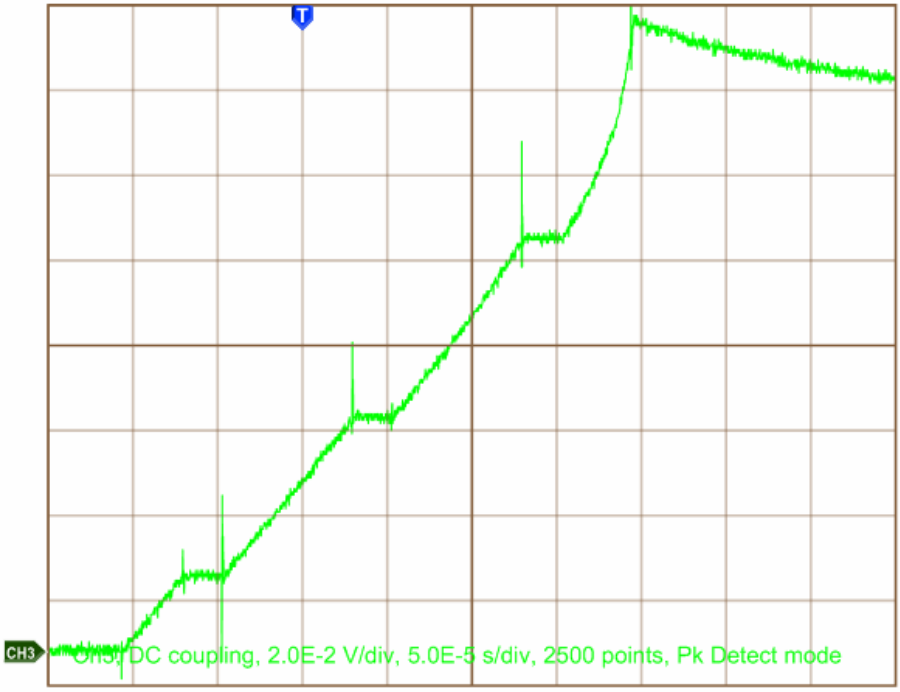

Ch3: 20 A/div

Saturation current measurement

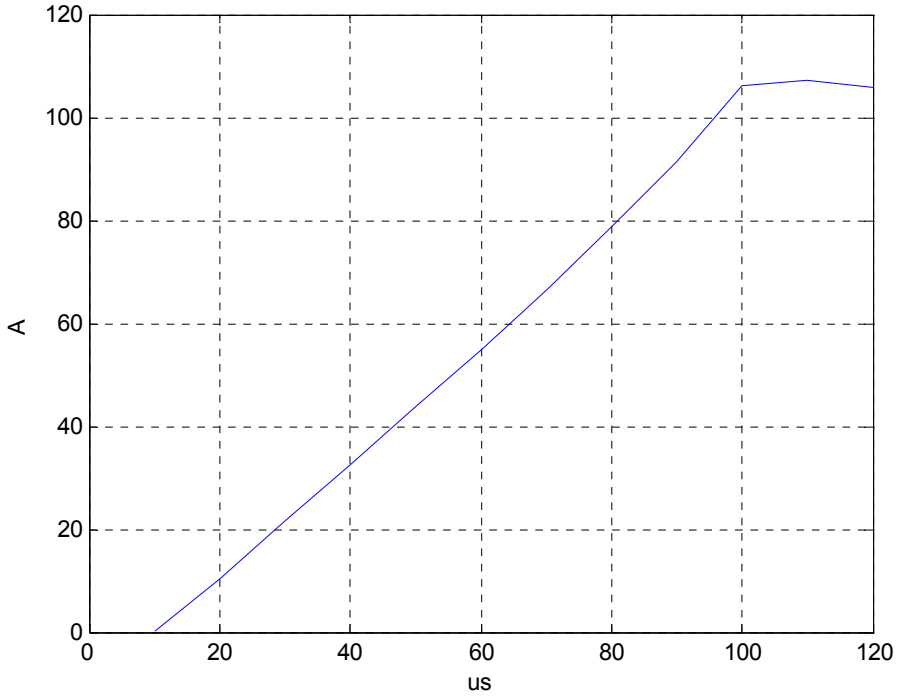

Saturation current measurement using the LEM module and DSP board

C.2 Inductor 2

Inductance test:

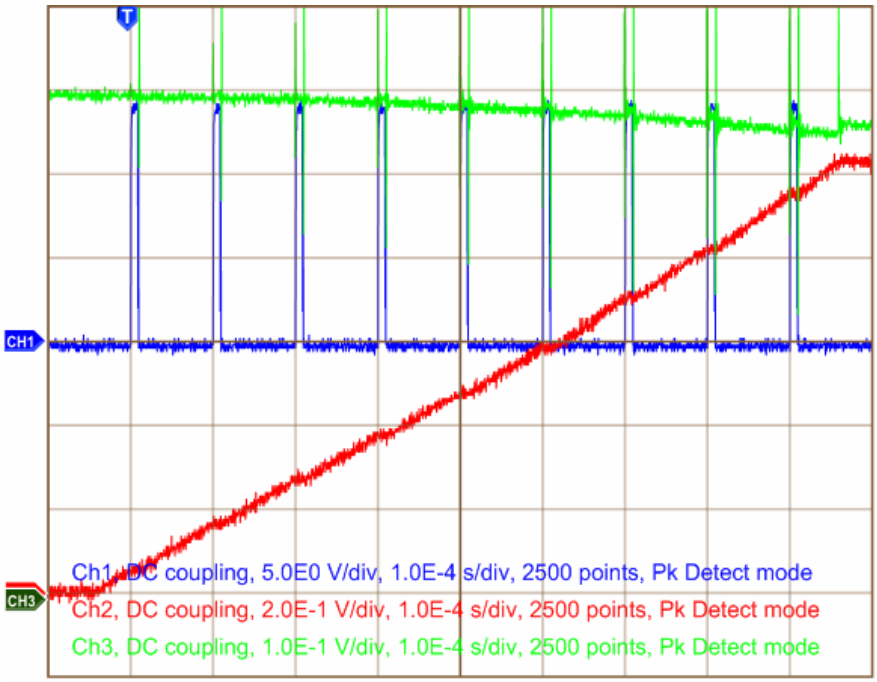

Ch1: Gate signal, Inverted
Ch2: Inductor current, 20 A/div
Ch3: DC link voltage

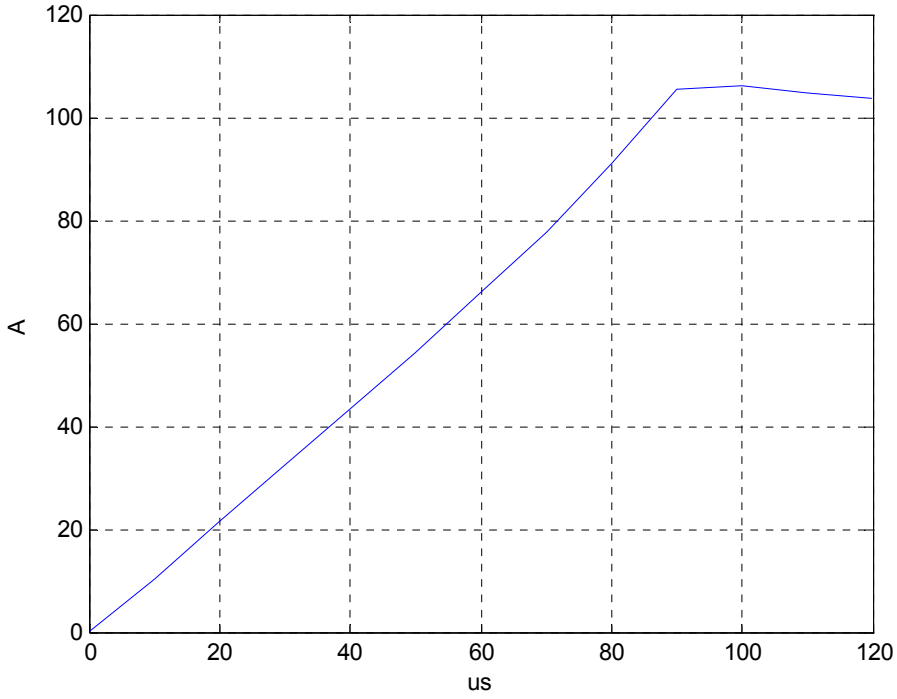

Saturation current measurement using the LEM module and DSP board

C.3 Inductor 3

Inductance test:

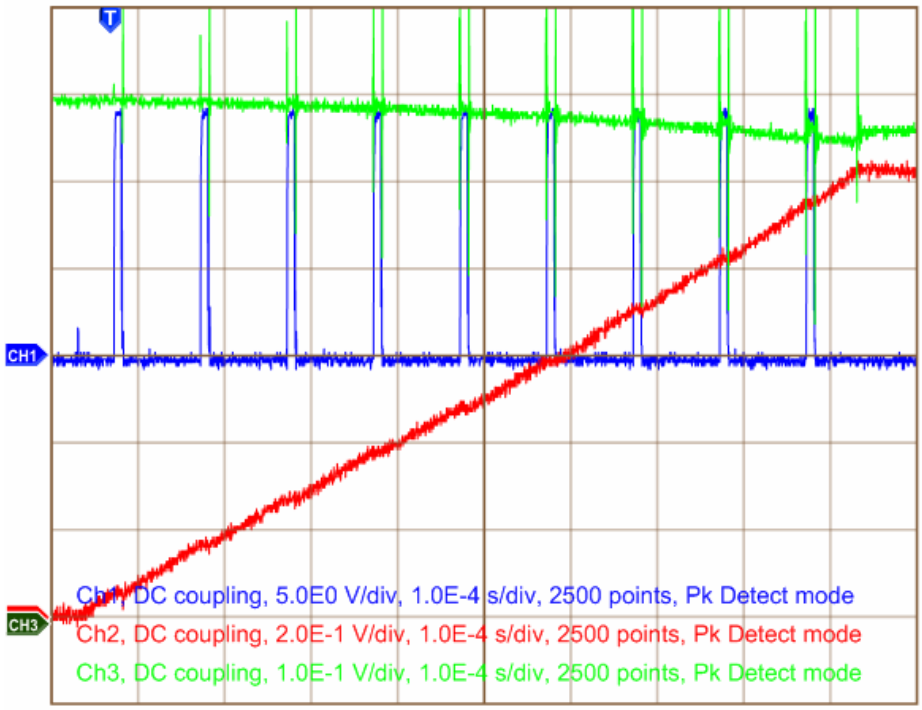

Ch1: Gate signal, Inverted
Ch2: Inductor current, 20 A/div
Ch3: DC link voltage

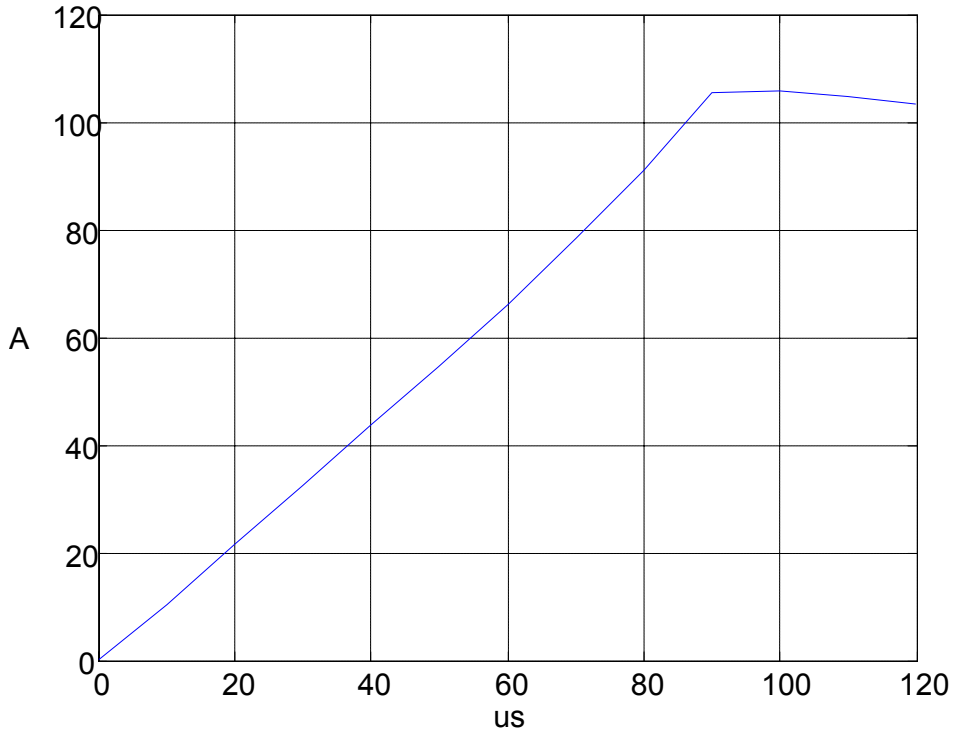

Saturation current measurement using the LEM module and DSP board

D Control circuit for the IPM

In order to drive the IPM, a control circuit is needed between the DSP and the IPM. The application manual [29] provides a possible solution of how to build this control circuit. The figure below shows this diagram. In accordance with the application manual the opto-couplers used is the HCPL – 4506 for the driver signals, and TLP521-1 GR for the alarm circuit. It is important to know that the gate signal is clamped at 8 V by a zener diode internal in the IPM. In order to limit the size and get better components, surface mounted components were chosen for the resistors and capacitances.

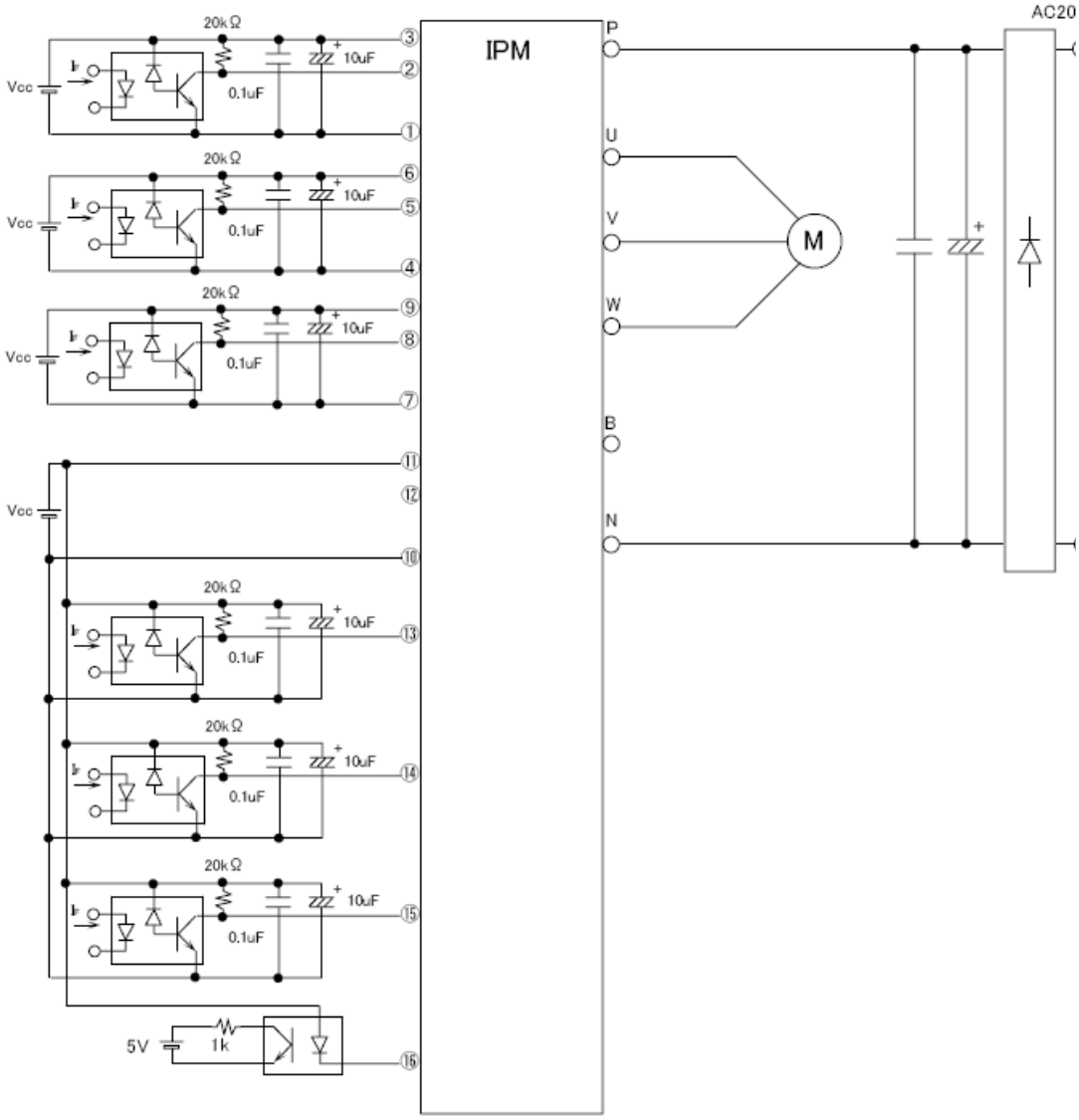

The Vcc in the circuit needs to be an isolated voltage source. This is done with a 1 W DC - DC converter connected between the 5 V output from the DSP and the 15 V input of the IPM. Additional capacitance is recommended in order to achieve electrical separation between the high and low of the input and output of the DC-DC converter. The circuit was constructed by

using an etching technique on a board with copper on both sides. This board is covered with a varnish that can be removed with spirit, after it has been illuminated with ultra violet light. First the circuit needed must be drawn. The figure below shows this circuit.

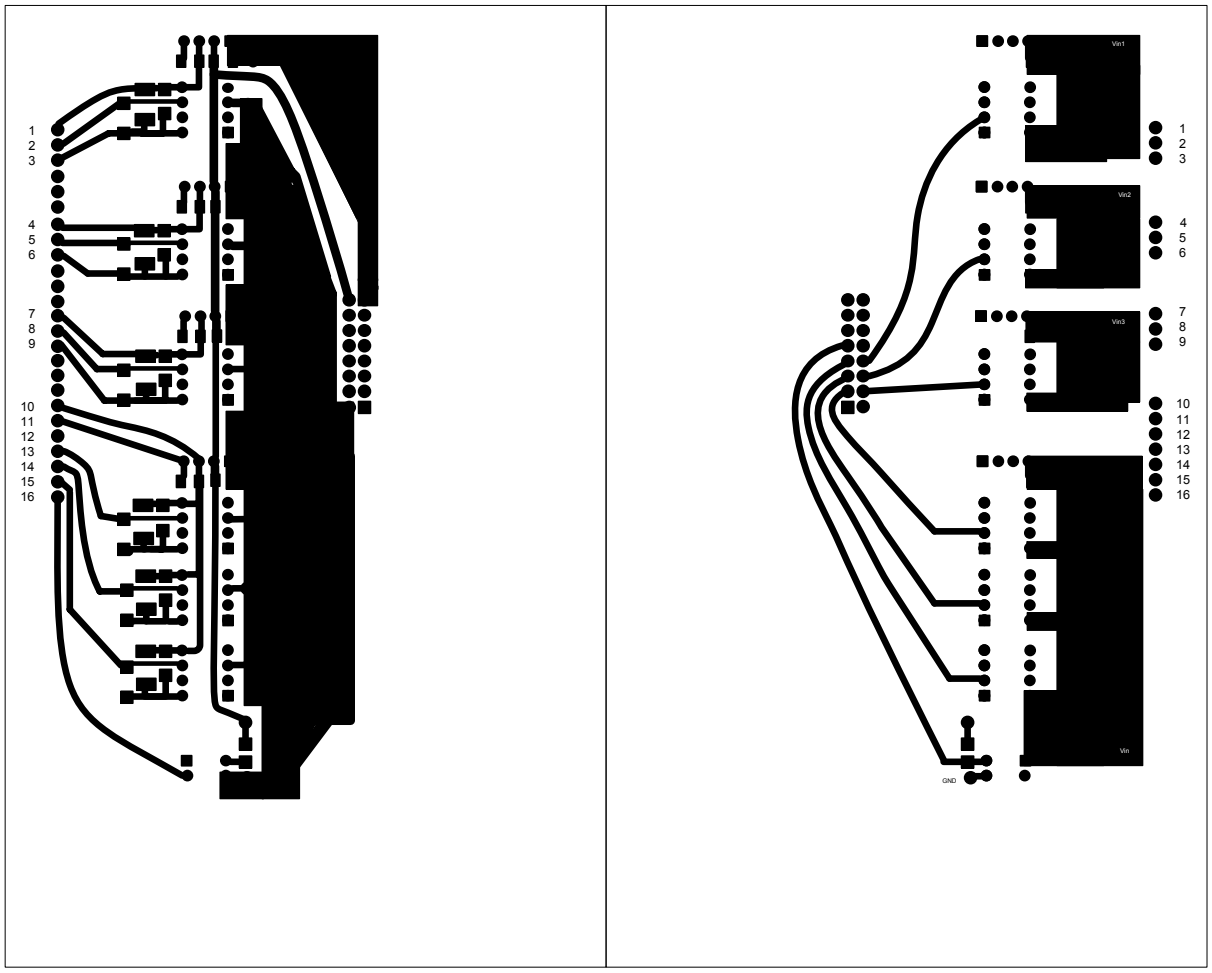

There are several important things to be aware of. The black areas are the areas that will be conductive when the process is finished. Holes are usually placed where there is a need to drill through the board, and should be on both sides of the board. This is important for the soldering of the components. The solder will only stick to the copper and for automotive applications it might be necessary to solder on both sides, to ensure that none of the components may loosen. The sizes and placement of the components must be exact. 0.5 mm error is enough to make the circuit unusable. For surface mounted components, square copper areas are normally used. It is preferable to make the tracks as wide as possible to reduce the losses. In order to reduce noise, 90 ° turns should be avoided and the ground should cover a large area. It is important to put in measurement points in the design for the prototype, in order to simplify the testing of the converter.

When the circuit is drawn, it must be printed on a special type of sheet and placed on the copper plate. The sides need be placed exact according to each other. When the sides are attached, the copper plates are illuminated with ultra violet light for 2 min 40 sec on each side. During this phase the copper plates should be shaded from other light. The next step is to remove the varnish from the all the copper that was not covered by the circuit. This is done by laying the board into a pan with spirits for 10 – 15 seconds, until the varnish is gone. This reveals the copper that should be removed from the board. This copper is etched away by iron(III)chloride foam. The board should be soaked in this for 10 – 15 minutes, until the copper is gone. Because of the varnish covering the circuit, this copper will not be removed. The final phase is to illuminate the board again with no cover, and remove the rest of the varnish. The board is now ready for drilling and soldering. These parts are straight forward, and will not be dealt with in this master thesis.

E IPM switching test

The tests were run gradually from low voltage and up to 220 V. The plots presented here have a duty cycle of 0.1 and the DC link voltage is 220 V.

E.1 Phase U switching characteristics

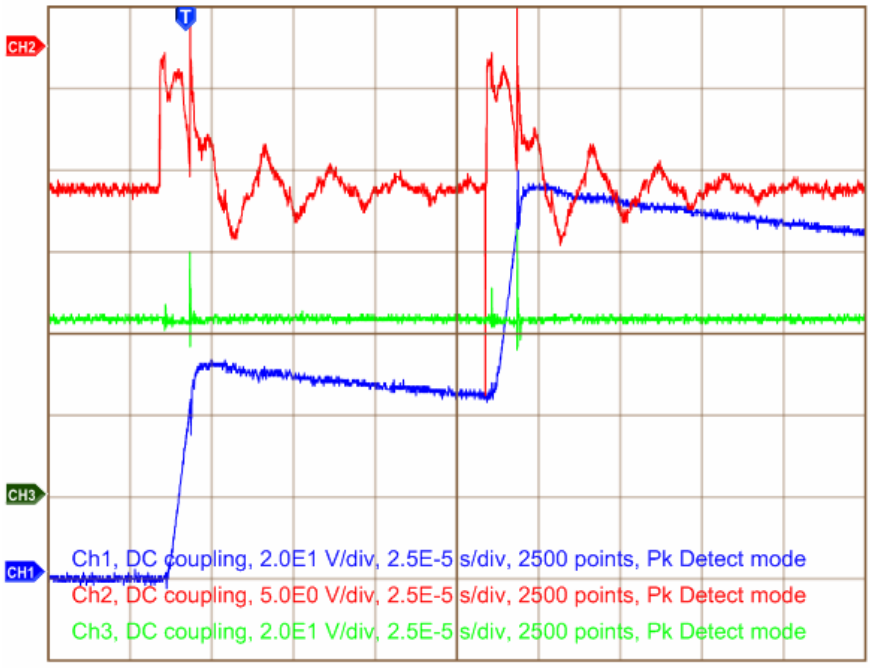

Ch1: Inductor current, 20 A/ div
Ch2: Switching signal
Ch3: P-N Input voltage, 100 V / div

E.2 Phase V switching characteristics

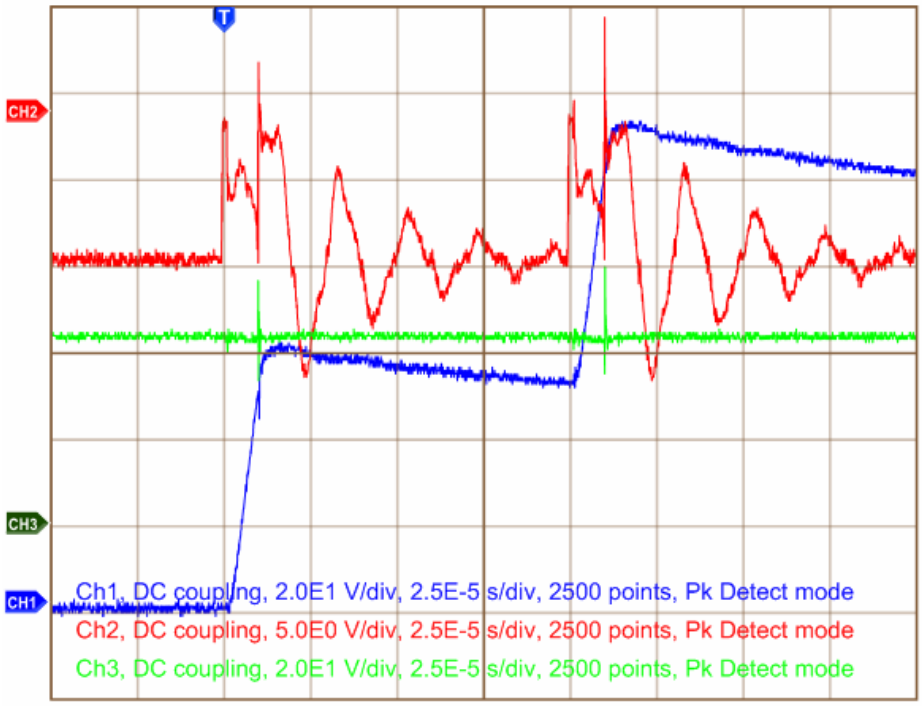

Ch1: Inductor current, 20 A/ div
Ch2: Switching signal
Ch3: P-N Input voltage, 100 V / div

E.3 Phase W testing

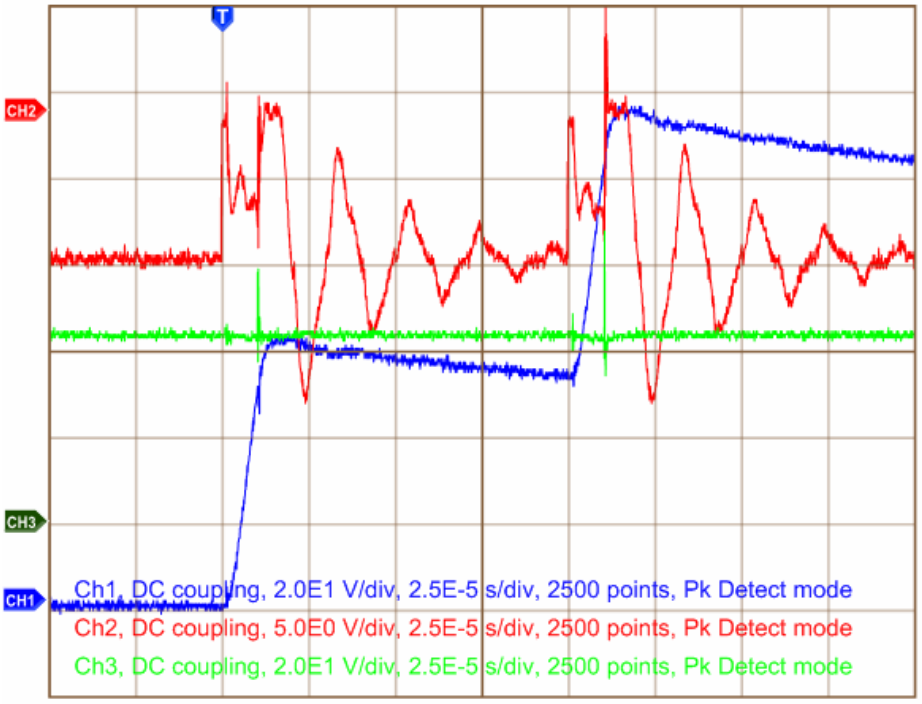

Ch1: Inductor current, 20 A/ div
Ch2: Switching signal
Ch3: P-N Input voltage, 100 V / div

E.4 Input voltage testing

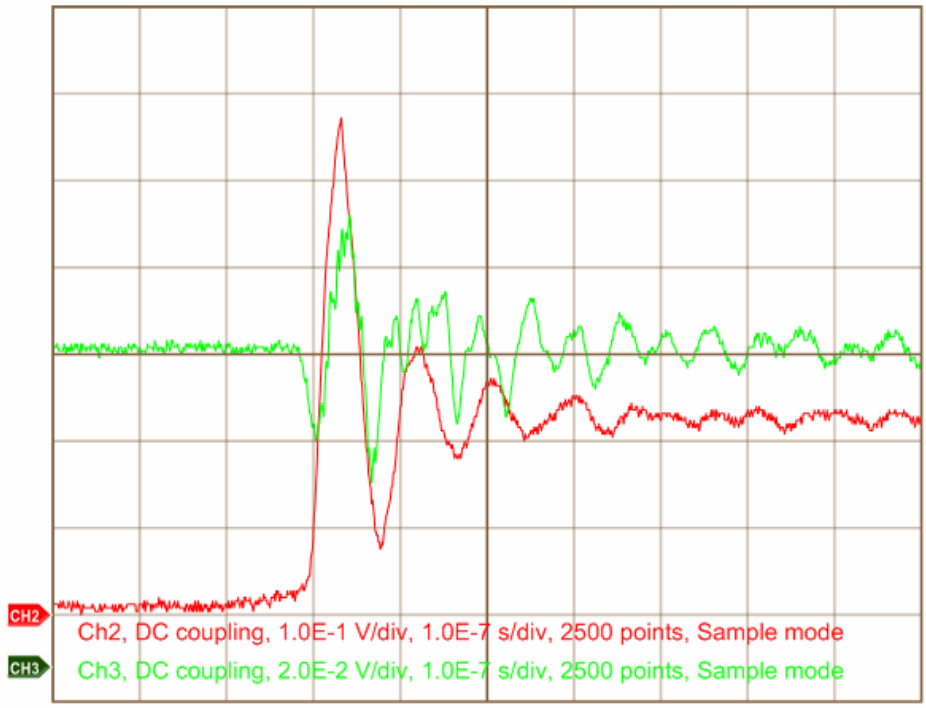

Ch.2 50 V /div
Ch3: 20A/div

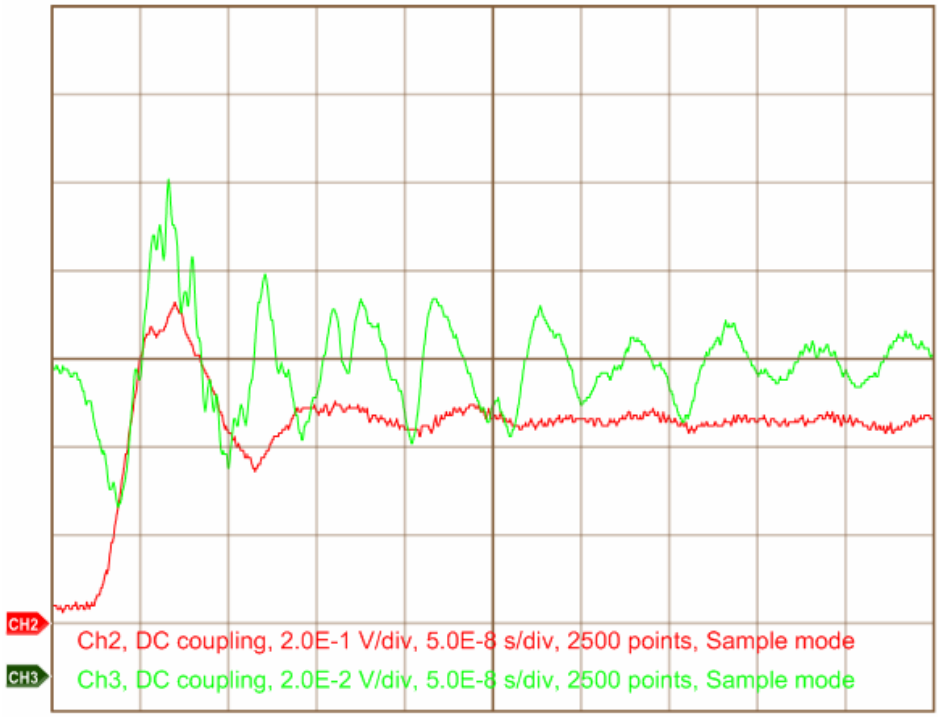

Ch2: P-U input voltage, 100 V/ div
Ch3: Inductor current, 20 A /div

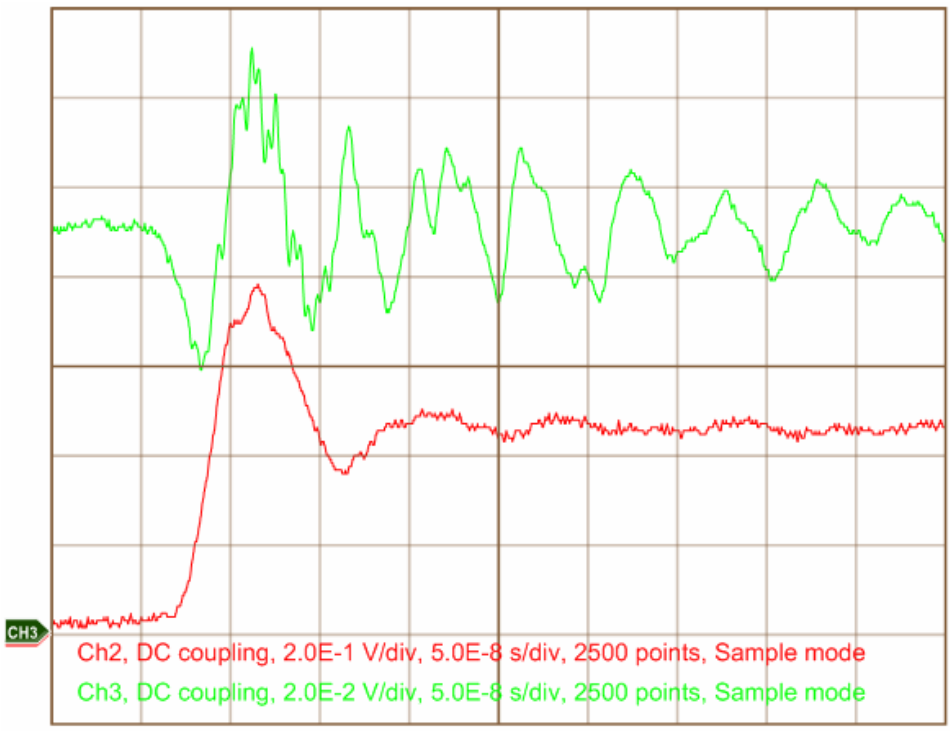

Ch2: P-U Voltage, 100 V/div
Ch3: Inductor current, 20 A/div